Low Power, Low Area, Monolithic Oversampling Digital to Analog Conversion

by

Edward A. Keehr

Submitted to the Department of Electrical Engineering and Computer Science
in partial fulfillment of the requirements for the degree of
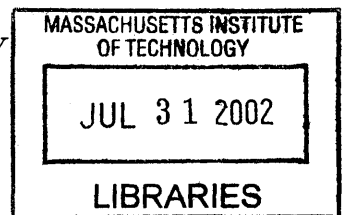
Master of Engineering in Electrical Engineering and Computer Science

at the

MASSACHUSETTS INSTITUTE OF TECHNOLOGY

September 2002

© Edward A. Keehr, MMII. All rights reserved.

The author hereby grants to MIT permission to reproduce and
distribute publicly paper and electronic copies of this thesis document
in whole or in part.

Author ....
Department of Electrical Engineering and Computer Science
June 19, 2002

Certified by......................
James K. Roberge
Professor of Electrical Engineering
Thesis Supervisor

Certified by.......................
Sean J. Wang
Senior Engineer, Qualcomm, Inc.
Thesis Supervisor

Accepted by ....
Arthur C. Smith
Chairman, Department Committee on Graduate Students

Low Power, Low Area, Monolithic Oversampling Digital to Analog Conversion

by

Edward A. Keehr

Abstract

This thesis project examines the design of a monolithic audio-band digital-to-analog (D/A) converter with the objective of achieving a high signal-to-noise ratio, low analog die area consumption, and low static power dissipation. Issues relating to system design, digital signal processing, sigma-delta modulation, D/A topology selection, and switched-capacitor filter design are covered. The Direct Charge Transfer filtering technique in particular is analyzed in detail, confirming its suitability and superiority over traditional switched-capacitor filtering techinques for the given project requirements. The end result of this project was the design of a D/A converter that achieved an SNR of 92dB with an analog die area consumption of 0.187mm^2 and a static power dissipation of 2.2mW in a 0.25μm CMOS process with a 2.5V supply voltage.

Thesis Supervisor: James K. Roberge
Title: Professor of Electrical Engineering

Thesis Supervisor: Sean J. Wang
Title: Senior Engineer, Qualcomm, Inc.

Acknowledgments

I wish to acknowledge the support and the assistance of the many people both at Qualcomm, Inc. and the Massachusetts Institute of Technology that contributed to this thesis and made this project a professional and academic experience beyond compare.

First, I would like to acknowledge the support of my friend and direct project supervisor Sean Wang, who provided countless hours of mentoring in order to help me make the leap from the textbook to real world design. As a supervisor, Sean struck a keen balance between pointing my project in the right direction and providing key design hints where necessary, while constantly forcing me to question my work such that I obtained a deeper understanding of what I was doing than would have otherwise been the case.

I would like to acknowledge the support of Seyfi Bazarjani, who took a chance by selecting me to run this project and who provided invaluable assistance in helping me surmount my initial hurdles in understanding sigma-delta modulation and simulation of sigma-delta modulators.

I would like to acknowledge the support of Levent Aydin, who explained the system-level aspects of D/A converters and whose sigma-delta modulator simulation I built upon to produce the system-level simulation of my choice of D/A architecture. Levent also provided invaluable advice with respect to the postfilter droop compensation technique used in the interpolation filtering chain.

I would like to acknowledge Samir Gupta's keen and well-timed interjection that the number of interpolation filter taps was "not an issue".

Finally, I would like to acknowledge Professor James Roberge, who accepted the

duty of reading this report and who provided the final word on several debates surrounding this project.

Contents

6

List of Figures

10

List of Tables

Chapter 1

Introduction

1.1 Motivation

During the course of the last two decades, digital systems have found their way into every corner of human civilization. The speed and robustness of digital technology has led to its replacement of analog technologies and to the development of wholly digital systems. Of current relevance to today's economy is the prevalence of digital mobile communications systems. Digital signal processing techniques allow us to compress and encode the human voice in such a way as to vastly increase the capacity of our communication networks. The robustness of digital signal transmissions allows us to reduce the power requirements of such systems, resulting in ever smaller and cheaper mobile communications systems.

Despite the power of digital systems, the fact remains that the world around us is analog in nature, and thus signals between the two domains must be converted from one to another. Hence, at the endpoints of any digital system, we find either an analog-to-digital (A/D) or a digital-to-analog (D/A) converter providing the interface from the analog world to the digital domain. Although the bulk of the processing performed in today's systems is done in the digital domain, the performance of such

systems is largely dominated by the performance of the A/D and the D/A converters. While a digital system can be made arbitrarily precise by changing the number of bits, the A/D and D/A converters must limit the noise and distortion that they introduce to the incoming and outgoing signals to acceptable levels through careful circuit design.

It can be said in general that to improve the analog noise performance of an A/D or a D/A converter, the power consumption and die area of the converter analog circuitry must increase. However, today's telecommunication markets demand chipsets that are ever more efficient in terms of power and area consumption. In addition to dominating the noise performance of a system, A/D and D/A conversion circuitry often contribute significantly to these metrics. Thus, designing A/D and D/A converters with optimal power and area consumption for a given noise figure can help maximize the profit margin and marketability for a chipset.

1.2 Objective

The design of contemporary data converters is a nontrivial one because of the constraints placed upon the designer. Cost and reliability considerations often require the monolithic integration of the converter onto a single mixed-signal die, precluding the use of off-chip components and filters. Furthermore, the A/D and D/A converters are often integrated onto the same die as some of the digital signal processing circuitry. The CMOS silicon processes used for such dies are optimized for speed and component density in digital designs, rather than the component matching and noise performance needed for robust analog performance. Typical CMOS processes provide device matching precision on the order of 8-10 bits, far less than the 16-20 bits required in most DSP A/D and D/A converter applications.

Oversampling converters using sigma-delta ($\Sigma\Delta$) modulation do not necessarily require the use of matched elements to produce a linear output. By increasing the speed of the analog circuitry operation, the incoming signal can be quantized to an arbitrarily low number of output bits while pushing the added quantization noise to higher frequencies. With a low number of quantization bits, analog component matching problems become much easier to deal with. This tradeoff between operating speed and resolution is attractive for applications requiring a relatively small bandwidth, such as digital audio.

The goal of this project was to research and design a power and area efficient monolithic oversampling D/A converter. The project specifications were to accept a 16-bit Nyquist-sampled digital PCM signal and to deliver an output signal for a differential voltage swing of 3.25Vpp with a peak SNR of 90dB in a 0.25μm CMOS technology with a supply voltage of 2.5V. Digital interpolation filtering is to be performed off-chip in DSP software, and hence its area and power dissipation are negligible for this design. An additional requirement for this design was that the entire D/A chain have a variable bandwidth, although the key specifications are those for the widest bandwidth (24kHz). The final analog design design delivered an output signal with an SNR of 91.71dB, a power consumption of 2.2mW, and an area consumption of 0.187mm^2.

Chapter 2

D/A Conversion Overview

According to Nyquist's sampling theorem, a continuous-time signal can be exactly reconstructed from its samples, provided that the signal is bandlimited and that the continuous-time signal is sampled at twice the bandlimiting frequency [1]. Therefore, an ideal discrete-to-continuous time (DT-CT) converter would convert discrete-time samples into continuous-time impulses which would then be passed through an ideal sinc reconstruction filter to obtain the desired output waveform. Unfortunately, neither of these processes exist in an ideal sense, and we are forced to engineer another solution to perform discrete-to-continuous time conversion.

A physically realizable approximation to the ideal DT-CT converter is the digital-to-analog (D/A) converter. A D/A converter takes as its input a sequence of digital code words and, based on each binary word, generates an analog voltage or current level proportional to the value of the code word. This voltage or current level is typically held constant between sampling instants and is then passed through a lowpass reconstruction filter to reject spectral images arising as a result of the interpolation, smoothing the output waveform in the time domain.

2.1 General D/A Conversion Procedure
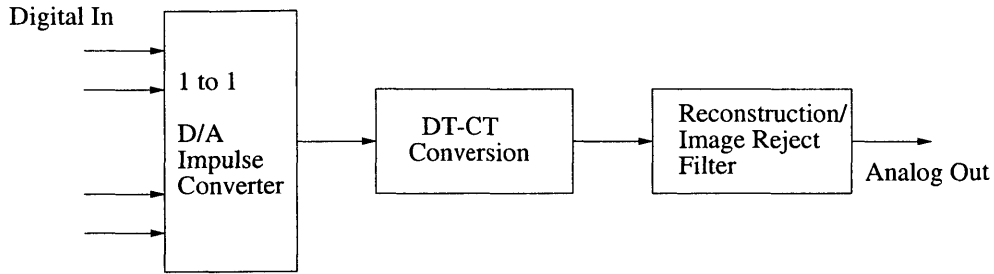
Figure 2-1: Block Diagram of Generic D/A Converter

Shown above is a block diagram of a generic D/A converter illustrating the D/A procedure described in the preceding paragraph. Inherent in the operation of the D/A converter is the DT-CT conversion process, although because it most often occurs implicitly, it is not often modeled.

2.1.1 D/A Code Topologies

The actual D/A conversion can be performed in a number of ways, but it is almost always done by subdividing a voltage or current reference with an array of passive elements. In addition, the digital code that is processed by the D/A converter can be one of a number of forms.

Perhaps the most intuitive digital code representation is that of a binary weighted D/A architecture. Since the signal representation in a digital system is typically in binary format, the digital signal can interface directly with the analog reference division circuitry. Binary reference division circuitry uses a number of binarily weighted reference elements and ideally generates an output signal of the form:

$$X_a = A_{os} + A_0(b_o(nT) + 2b_1(nT) + ... + 2^{N-1}b_{N-1}(nT)) \qquad (2.1)$$

17

Decimal	Binary			Thermometer Code						
	b_0	b_1	b_2	d_0	d_1	d_2	d_3	d_4	d_5	d_6
0	0	0	0	0	0	0	0	0	0	0
1	0	0	1	0	0	0	0	0	0	1
2	0	1	0	0	0	0	0	0	1	1
3	0	1	1	0	0	0	0	1	1	1
4	1	0	0	0	0	0	1	1	1	1
5	1	0	1	0	0	1	1	1	1	1
6	1	1	0	0	1	1	1	1	1	1
7	1	1	1	1	1	1	1	1	1	1

Table 2.1: Binary and Thermometer Digital Code Representations

where A_0 is the reference voltage or current, A_{os} is the DC offset, $[b_i(nT)]_{i=0}^{N-1}$ are the input bits at time interval nT, and T is the sampling period of the D/A. Binary architectures minimize the number of switches, digital encoding circuitry, and number of output elements [2]. However, because there exists a significant size disparity between the largest and smallest elements, this scheme suffers a disadvantage in terms of element matching. For example, if the largest element in the array is mismatched from its nominal value by an amount greater than the size of the smallest element, the converter may not have an output characteristic that increases monotonically with the value of the digital input code. This drawback of binary scaled converters also causes them to suffer from glitches and other large nonlinearity errors [3].

Another method for realizing a D/A converter is to subdivide an analog reference based on the thermometer-encoded version of the binary input word. Thermometer code representation, as shown above in Table 2.1, differs from binary representation in that it requires $2^N - 1$ unit sized reference elements, as opposed to the N elements of a binary converter, where N is the number of incoming digital bits. The analog output at the time nT is given by:

$$X_a(nT) = A_{os} + A_0 \sum_{i=1}^{M} c_i(nT) \tag{2.2}$$

Although the number of elements is greater, a quick inspection of the two schemes shows that their D/A converter sizes are equal. For example, a 3-bit switched capacitor has $7C$ unit elements for a thermometer decoding scheme, while a binary coding scheme also has the equivalent of $7C$ unit elements $(C + 2C + 4C = 7C)$.

Although the analog area of the two schemes is equal, the digital circuitry responsible for performing the thermometer decoding can be large depending of the number of bits being decoded, even in modern CMOS processes [5]. However, thermometer encoding confers several benefits. Since the ratio of the largest to smallest element is unity, matching between elements in the array improves over the binary weighted case. Monotonicity in the D/A converter is guaranteed because an increment in the digital code results in approximately a unit increase in the output current, voltage, or charge, regardless of mismatch. Lastly, a thermometer-encoded D/A significantly reduces glitching errors, since there are no large banks of unit elements that can be changed at slightly different times due to unequal control logic propagation, as in a binary converter [3].

2.1.2   D/A Medium Topologies

For a given code representation, a D/A converter can subdivide different types of analog references based on the binary input code. For example, switched-resistor (SR) topologies divide a voltage reference along a string of equal-sized resistors or along an R-2R ladder network. However, SR topologies are in general not suitable for implementation in CMOS topologies due to the poor matching properties of resistors and their nonlinearity with respect to the input voltage.

Switched-current (SI) topologies are quite suitable for implementation in CMOS topologies, as current source arrays that are relatively insensitive to mismatch are easy to design therein. In addition, the reference and summing elements (current source references and I-V opamps) can be implemented in a robust manner. SI topologies can be designed to operate at high frequencies and are often used in large-bandwidth applications where very high speed in the D/A converter is required [2] [5]. Typically, this class of D/A converter operates as a bank of thermometer or mixed (binary and thermometer) encoded elements that are switched to the output summing node via CMOS switches.

Switched-capacitor (SC) topologies subdivide an analog voltage reference by operating on a two-phase system. On the first phase, the bits of the binary input word determine which capacitors of the capacitor array will be charged to the reference voltage V_{ref} and which will be charged to ground such that the total charge on the capacitors is proportional to the digital input word. On the second phase of operation, the charges on the capacitors are combined, usually by discharging them to an opamp virtual ground, where the total charge is integrated onto the opamp feedback capacitor. Although the speed of the SC D/A is limited by the achievable opamp bandwidth and the on resistance of the switches, it can present an attractive design option in that the D/A converter will integrate nicely into an analog switched-capacitor postfilter.

2.1.3   Discrete Time - Continuous Time Interface

The most common DT-CT interface that is realized in D/A converters is a zero-order hold. Zero-order hold (ZOH) operation occurs implicitly when the output of the D/A converter is maintained at a constant level between sampling intervals. Although ZOH operation is easily overlooked, it results in several nonidealities that affect the

operation of the overall D/A converter. For example, the continuous time frequency response of the ZOH operation can be shown to be:

$$H_0(f) = \frac{\sin(\frac{\pi f}{f_s})}{(\pi f)/f_s} e^{\frac{-j\pi f}{f_s}} \tag{2.3}$$

For sampling frequencies near the Nyquist rate, the rolloff of this transfer function severely attenuates in-band signal frequencies and must be compensated for in the analog postfiltering scheme, posing an additional burden.

In addition, sampling time noise, commonly known as *clock jitter*, introduces distortion directly into the signal path by causing slight time displacements at the output samples [6]. Although jitter-induced distortion is not technically noise, its effects are often modeled as such, contributing to the overall signal-band noise performance of the D/A converter [7].

2.1.4 Analog Postfiltering

The analog postfilter in the generic D/A converter compensates for the droop in the zero-order-hold transfer function and rejects any out-of-band spectral images. Ideally, the transfer function of this postfilter should be the inverse of the zero-order-hold transfer function within the signal band and zero elsewhere [4]:

$$\tilde{H}_r(f) = \frac{\frac{\pi f}{f_s}}{\sin(\frac{\pi f}{f_s})} e^{\frac{j\pi f}{f_s}}, |f| < \frac{f_s}{2} \tag{2.4}$$

$$\tilde{H}_r(f) = 0, |f| > \frac{f_s}{2} \tag{2.5}$$

Of course, a filter with such a sharp cutoff is difficult to obtain in practice, a limitation inherent in the design of Nyquist converters.

21

2.2 Nyquist Converters

Contrary to its namesake, a Nyquist D/A converter does not actually operate at the Nyquist rate, but typically at a rate 1.5 to 10 times greater than required by the Nyquist criterion in order to ease postfiltering requirements. The key characteristic of a Nyquist converter, however, is that it generates a series of output analog values in which each analog value has a one-to-one correspondence with a single digital input value. The advantage of this setup is that the D/A conversion process is intuitive and that the converter has a low speed of operation, reducing bandwidth requirements on active devices that act as charge or current summers, as in the SC and SI topologies.

While Nyquist-rate converters can be implemented in an SR, SI, or SC topology, they all generally require that the one-to-one digital-to-analog conversion be performed to the overall precision of the converter. Since these one-to-one converters almost invariably use matched elements to subdivide a reference voltage or current, the overall precision of the converter is determined by the quality of the matching in the available CMOS process. In general, this is no greater than 8-12 bits [8], but can be improved through laser trimming of elements or error-correcting circuitry, the first of which incurs a direct dollar cost, and the second of which can be expensive in terms of power, area, and design time.

It was stated earlier that a Nyquist converter is typically operated at a sampling rate 1.5 to 10 times greater than the Nyquist rate. To gain some appreciation as to why this is done, Fig. 2-2 shows graphically that for a Nyquist converter operating at the Nyquist rate, spectral images of the signal of interest appear immediately adjacent to the signal band. As shown on the lower set of axes, a very sharp analog postfilter is necessary to attenuate this image while ensuring a flat filter frequency response over the signal band.
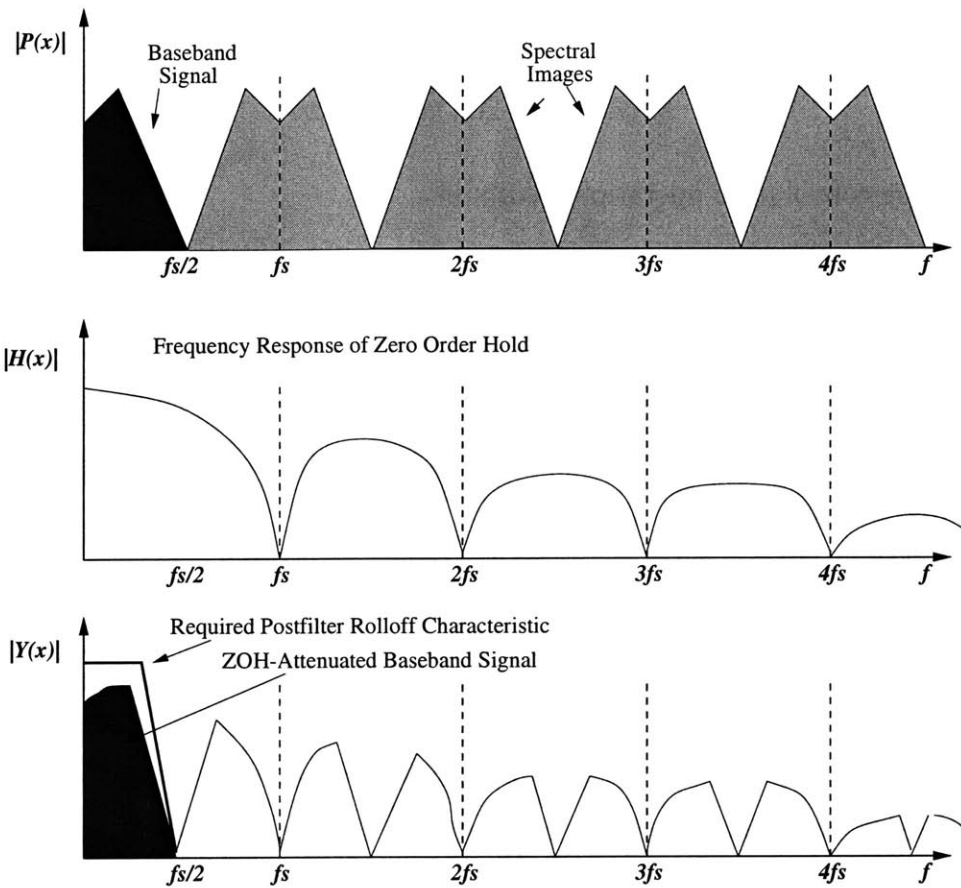
Figure 2-2: Signal Spectra of Nyquist Converter after DT-CT Conversion

In a DT-CT conversion that is performed at the Nyquist rate, spectral images are spaced at every multiple of the sampling frequency f_s, or equivalently, $\frac{2\pi}{T}$, where T is the sampling period. We find that this is true because a continuous-time signal with frequency response $X_c(j\omega)$, when sampled by an ideal periodic impulse train with frequency response:

$$S(j\omega) = \frac{2\pi}{T} \sum_{k=-\infty}^{\infty} \delta(\omega - k\omega_s) \qquad (2.6)$$

has its frequency response convolved with that of the above frequency-domain

23

impulse train, resulting in a sampled signal with frequency response:

$$X_s(j\omega) = \frac{1}{2\pi} X_c(j\omega) * S(j\omega) \qquad (2.7)$$

where the convolution operation results in:

$$X_s(j\omega) = \frac{1}{T} \sum_{k=-\infty}^{\infty} X_c(j(\omega - k\omega_s)) \qquad (2.8)$$

We note that, if the bandwidth of signal is denoted as ω_N, the spectral images of baseband signal do not overlap if the sampling frequency ω_s is greater than twice the bandlimited frequency ω_N.

$$\omega_s - \omega_N > \omega_N, \quad \omega_s > 2\omega_N \qquad (2.9)$$

If ω_s is even greater, these spectral images are spaced even farther apart. When this is the case, the requirements on the rolloff of the analog reconstruction filter are relaxed, as the attenuation of a lowpass filter increases at higher frequencies. In general, a 40-60 dB attenuation of the spectral images is considered sufficient in digital audio applications [9].

2.3 Oversampling D/A Converters

While Nyquist converters are suitable for applications in which the signal bandwidth to be processed is on the same order of magnitude as the achievable clocking frequency, contemporary CMOS processes are capable of operating at clock frequencies much greater than many classes of analog signal, digital audio in particular. This affords the analog designer the attractive design option to clock the D/A converter much faster than the Nyquist rate, placing much of the filtering and element matching

burdens in the digital domain [3]. Oversampling converters commonly employ digital noise shaping, also known as sigma-delta modulation, in order to reduce the number of quantization bits at the D/A interface while shifting the majority of the additional quantization noise out of the signal band. Reducing the number of D/A elements can greatly ease the matching requirements for the D/A converter.

Oversampling converters are qualified according to their *oversampling ratio*, or OSR. The oversampling ratio is defined as the ratio between the sampling frequency and the Nyquist frequency corresponding to the signal bandwidth of interest. Mathematically,

$$OSR = \frac{f_s}{f_N} = \frac{f_s}{2f_0} \tag{2.10}$$
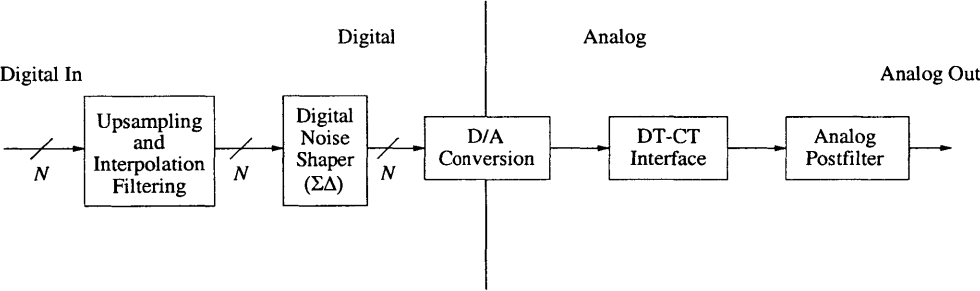
Figure 2-3: Oversampling D/A Converter Block Diagram

Shown in Fig. 2-3 is a block diagram for a generic oversampling D/A converter. The input to the oversampling D/A converter is a digital pulse code modulated (PCM) waveform sampled at the Nyquist rate. In order to create an oversampled signal, the digital waveform is upsampled by a factor L and interpolated by a digital image rejection filter that removes any spectral images. The frequency domain view of this process is shown in Fig. 2-4.
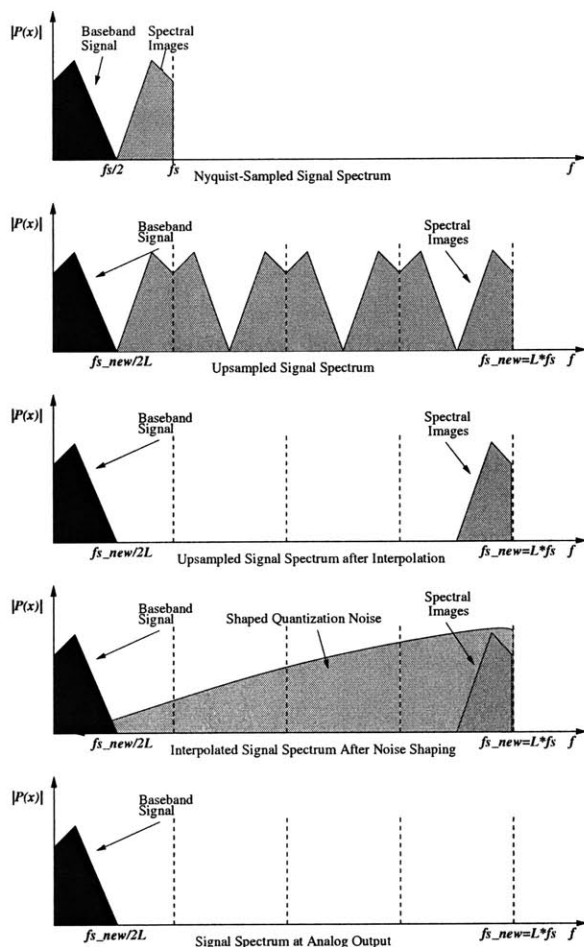
Figure 2-4: Signal Spectra at Various Points in the Oversampling D/A Converter

The first set of axes contains the one-sided frequency response for the Nyquist-sampled PCM input to the oversampling D/A. After upsampling by an arbitrary integer L, the frequency response is as shown on the set of second axes. The resultant spectral images are rejected by a digital interpolation filter that follows the upsampling register, as shown on the third set of axes. Note that the cutoff of this first interpolation filter must be relatively sharp, however, use of the oversampling D/A converter topology assumes that implementing such a digital filter is less expensive in terms of power and area dissipation than a comparable analog image-reject filter. Shown on the fourth set of axes is the result of sigma-delta modulation, the

addition of out-of-band shaped quantization noise to the signal, and on the fifth set of axes is the signal spectrum at the output of the analog postfilter.

The upsampling that is followed by interpolation filtering may take place across one or more stages, but typically does not increase the sampling rate of the incoming signal greater than a factor of 16. The remainder of the upsampling process is followed by a digital zero order hold (ZOH) register. Although ZOH interpolation does not entirely attenuate spectral images, as shown in the bottom half of Fig. 2-5, these images are typically far enough away from the baseband signal that they will be easily attenuated by the analog postfilter. Following the digital zero order hold, the signal is processed by a digital sigma-delta noise shaper, which reduces the number of bits used to represent the signal while shifting the additional quantization noise out of band. Doing so can reduce the matching requirements of the D/A converter in two ways.
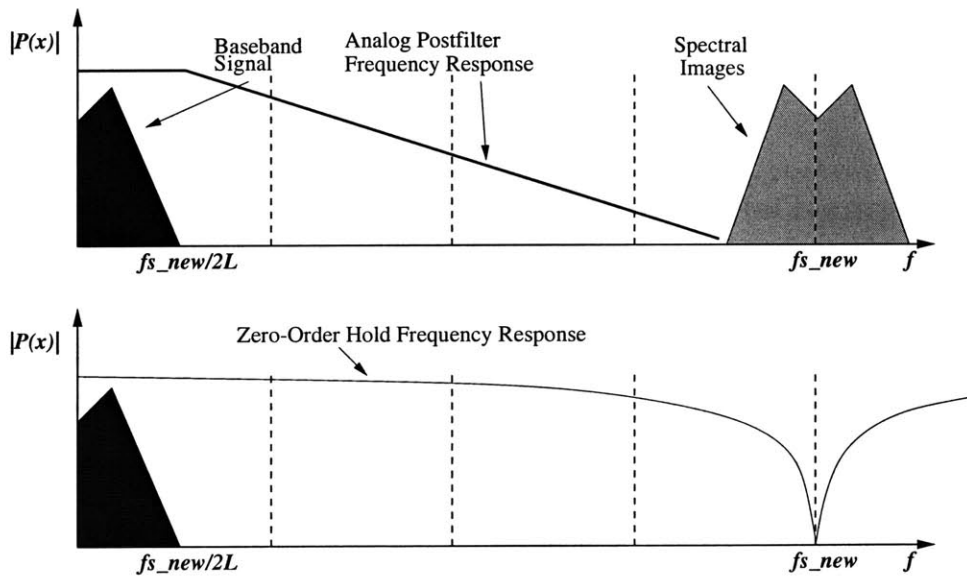
Figure 2-5: Analog Postfilter Image Reject Requirements for Oversampling Converters

The first of these is to reduce the number of quantizer bits at the sigma-delta output to one, thus reducing the D/A converter to a two level output. Provided that the two levels of the D/A converter are time invariant, the D/A converter is precisely linear, containing only a gain error. Although linearity is guaranteed in this scheme, quantizing the digital signal down to 1 bit introduces a large amount of quantization noise, some of which may remain in the signal band if the oversampling ratio is not large.

The second method of reducing the element matching burden is to use a multibit D/A converter with a small (3-6) number of output bits. This reduces quantization noise over the entire frequency range from the 1-bit case, but still keeps the number of output elements relatively low such that D/A array linearization schemes become feasible. To alleviate mismatch problems, the D/A converter elements are either calibrated [5] or swapped in a general class of pseudo random switching techniques known as dynamic element matching (DEM) [12]. Although these techniques can make the effects of element mismatch negligible, they become exponentially more costly to implement as the number of sigma-delta output bits increases linearly.

2.3.1 Sigma-Delta Modulator Concepts

A conceptual block diagram of a sigma-delta modulation scheme is shown below in Fig. 2-6 for the case of a 1-bit quantizer. The signal is passed through a transfer function $A(z)$ and through a quantizer that can be modeled as a unity gain block that introduces white noise as a by-product of the quantization process. Since the quantization noise is introduced at a location different than that of the input signal, it is possible to choose $A(z)$ such that the transfer function from the input to the output is unity in the signal band, while the transfer function from the quantizer to the output is high pass in nature. Given that the quantizer injects an effective

28

noise signal $e(n)$ into the modulator and that a signal $x(n)$ enters the modulator at its input, we can derive a signal transfer function $S(z)$ and a noise transfer function $N(z)$.

$$S(z) = \frac{Y(z)}{X(z)} = \frac{A(z)}{A(z)b_1 + 1} \tag{2.11}$$

$$N(z) = \frac{Y(z)}{E(z)} = \frac{1}{A(z)b_1 + 1} \tag{2.12}$$

we also have by superposition

$$Y(z) = S(z)X(z) + N(z)E(z) \tag{2.13}$$
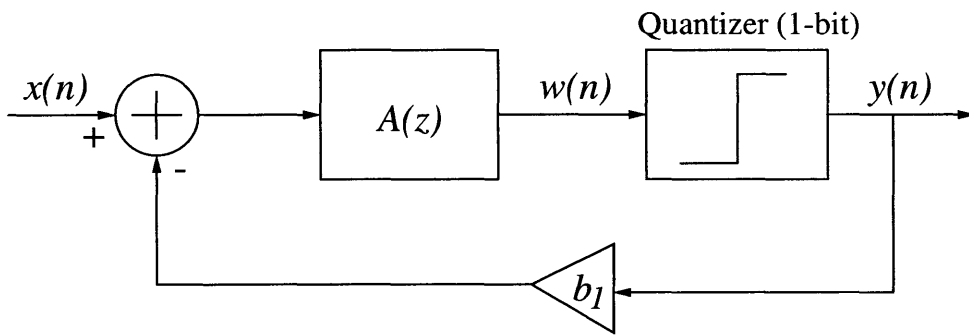
Figure 2-6: Sigma-Delta Modulator Concept

We thus would like to choose $A(z)$ such that it is large in the signal band $|f| < f_0$ such that $S(z)$ approximates unity within this range and that $N(z)$ approximates zero in the same region, maximizing the inband signal-to-noise ratio. One such transfer function that is easily implemented in digital circuitry is that of a discrete-time integrator, specifically:

$$A(z) = \frac{z^{-1}}{1 + z^{-1}} \tag{2.14}$$

Note that the transfer function has a pole at dc (z=1) and decreases in magnitude

29

as z moves across the unit circle to z=-1. This implementation is shown in Fig. 2-7.
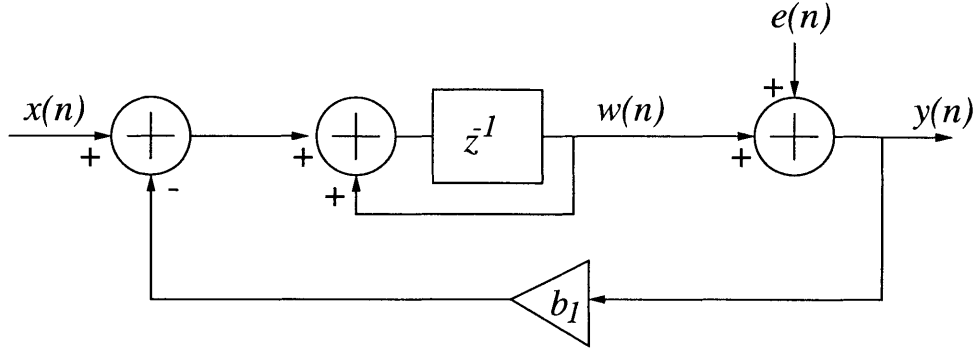
Figure 2-7: Sigma-Delta Modulator Block Diagram

Substituting in for $A(z)$ and setting b_1 to unity to simplify the analysis, we obtain the transfer functions for this sigma-delta modulator.

$$S(z) = \frac{Y(z)}{X(z)} = \frac{\frac{z^{-1}}{1+z^{-1}}}{\frac{z^{-1}}{1+z^{-1}+1}} = z^{-1} \tag{2.15}$$

$$N(z) = \frac{Y(z)}{E(z)} = \frac{1}{\frac{z^{-1}}{1+z^{-1}+1}} = (1 - z^{-1}) \tag{2.16}$$

We see that the transfer function from the signal input to the output is merely a delay, while the transfer function from the quantizer to the output is a discrete-time differentiation, which is high-pass in nature. In the frequency domain, the transfer function seen at the quantizer input is:

$$N(f) = 1 - e^{\frac{-2j\pi f}{f_s}} = \frac{e^{\frac{j\pi f}{f_s}} - e^{\frac{-j\pi f}{f_s}}}{2j} \cdot 2j \cdot e^{\frac{-j\pi f}{f_s}} \tag{2.17}$$

Taking the magnitude of both sides, we obtain:

$$|N(f)| = 2\sin\left(\frac{\pi f}{f_s}\right) \tag{2.18}$$

Equation 2.18 represents a high-pass transfer function. It follows that since the

30

transfer function from the quantizer to the output is high-pass in nature, the larger the oversampling ratio is made, the more confined the signal bandwidth f_0 will be to the frequencies where the magnitude of the noise transfer function is very low. This concept, illustrated below in Fig. 2-8 introduces one of the key design tradeoffs inherent in low power, low area D/A converter design. Although increasing the OSR decreases the amount of in-band quantization noise, the increased operating speed imposes an additional burden on the analog postfilter, the burden depending on the type of D/A converter and postfilter used.
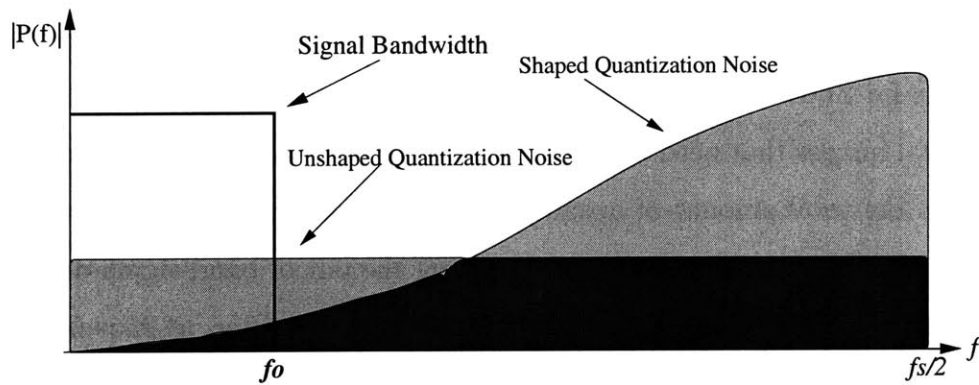
Figure 2-8: Oversampling Advantage

2.3.2   Analog Postfilter

Although the sigma-delta modulator ensures that most of the noise introduced by its quantizer lies outside of the signal band, it is often to great advantage to filter out this noise regardless of its effect (or lack thereof) on the signal. For example, unfiltered D/A converter quantization noise could corrupt intermediate frequency (IF) signal processing in adjacent RF circuitry. In addition, this noise could mix with a high-frequency clock signal, resulting in intermodulation products that are mixed down to baseband before reaching the output of the analog chip. Finally, in the case

31

of a discrete-time postfilter (some postfilters can be discrete-time and analog), the reduction of out-of-band quantization noise improves the jitter performance of the D/A converter [17] [40]. Therefore, a general rule of thumb is that the analog post-filter for an oversampling converter must be of the same order or higher than that of the sigma delta modulator. This ensures that the sigma-delta quantization noise as a function of frequency does not rise faster than the increase in postfilter attenuation as a function of frequency.

For typical values of oversampling ratios, which range from 64 to 512, the effect of the zero order hold droop arising from the DT-CT conversion is negligible across the signal band, as shown in Fig. 2-5. Thus, the analog postfilter does not need to compensate for ZOH droop, as is required in the Nyquist converter. In addition, the only spectral images that need to be suppressed by the analog postfilter occur at Kf_o where K is the total amount of upsampling that is followed by digital interpolation filtering. However, it is typical that attenuating the out of band sigma-delta quantization noise is the more stringent requirement on the postfilter, as K is usually close to an order of magnitude greater than unity.

Analog postfilters are either implemented in active-RC fashion or as a switched-capacitor topology. The former are preferred in current-mode converters, as an active-RC filter can also double as an I-V converter provided that the input resistor is removed. Switched-capacitor postfilters are convenient to implement when the D/A converter is already a switched-capacitor topology.

2.4 D/A Converter Metrics

2.4.1 Static Metrics

Due to mismatch between elements of the D/A converter, the transition points of the transfer function will be altered as illustrated in Fig. 2-9
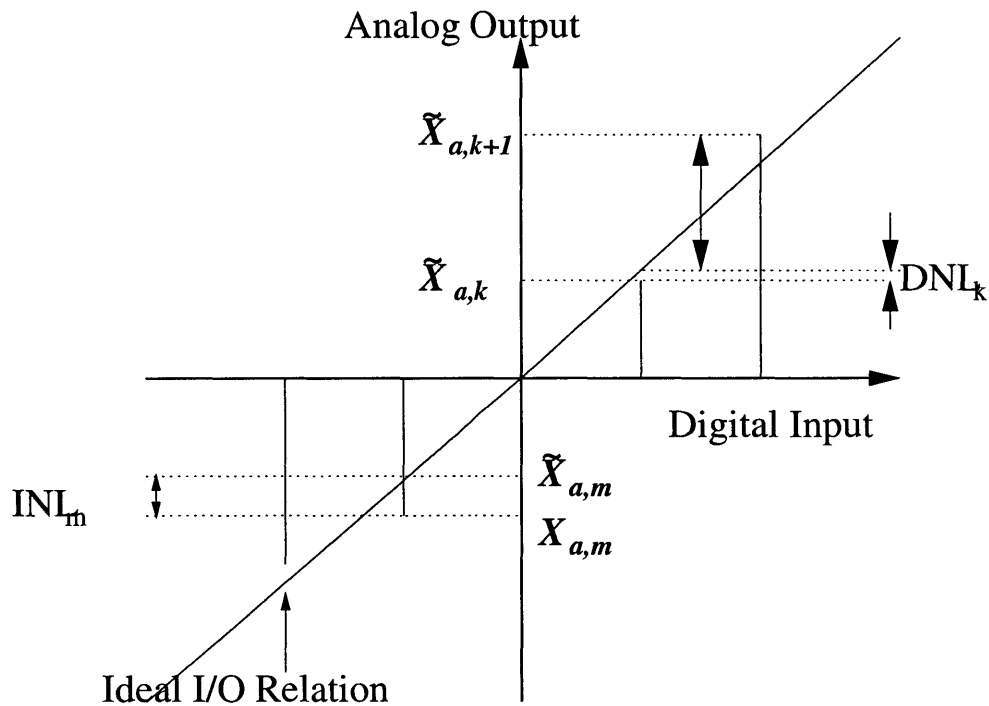
Figure 2-9: Non-ideal D/A Converter Transfer Function

In the plot above, actual DAC transfer function values are denoted with a tilde ~over the value of interest. Thus $\tilde{X}_{a,k}$ corresponds to the actual analog output of the D/A converter for a given digital input $\tilde{X}_{d,k}$, while $X_{a,k}$ corresponds to the ideal analog output value [2].

Offset and Gain Error

In a D/A converter, the offset error is defined to be the output that occurs for the input code that should produce a zero input, or mathematically,

$$E_{offset} = \tilde{X}_{a,0} \tag{2.19}$$

The gain error is defined as the deviation at the full scale digital input code from the actual and ideal D/A characteristics after the offset error has been removed. This can be expressed mathematically as:

$$E_{gain} = \tilde{X}_{a,N} - X_{a,N} - \tilde{X}_{a,0} \tag{2.20}$$

Differential Nonlinearity (DNL)

An ideal D/A converter increases its output by a uniform step size Δ for each increment of the digital input code. Any deviation from this uniform step size is referred to as a differential nonlinearity (DNL). Differential nonlinearities are defined for each digital input code, however, this metric is usually quantified as the maximum DNL for a given D/A converter.

Differential nonlinearities are illustrated above in Fig. 2-9 and are expressed mathematically as:

$$DNL_k = \tilde{X}_{a,k+1} - \tilde{X}_{a,k} - \Delta \tag{2.21}$$

Integral Nonlinearity (INL)

After removing the gain and offset errors, the integral nonlinearity error, or INL, can be defined at a given digital input code to be the deviation of the actual D/A transfer function from a straight line. A conservative measure for nonlinearity is to define the

34

straight line to be the line connecting the analog output values $\tilde{X}_{a,N}, \tilde{X}_{a,0}$. Another measure chooses the straight line to be the linear best-fit to the actual D/A transfer function. The relationship between INL and DNL is given by:

$$INL_k = \sum_{l-1}^{k} DNL_l \qquad (2.22)$$

Monotonicity

A monotonic D/A converter is one in which the analog output level always increases with an increment in the digital input code. In order words, the slope of the digital/analog characteristic is always positive or negative, but never both.

2.4.2 Frequency Domain Metrics

Although static D/A converter metrics are useful in quantifying the performance of Nyquist-rate converters, most contemporary oversampling converters are quantified using frequency domain metrics. This is because most oversampling converters employ calibration, DEM, or a two-level D/A to either significantly reduce or to eliminate D/A nonlinearities altogether.

Since the dominant nonidealities of the oversampling converter are typically the remaining in-band quantization noise, analog postfilter component noise, and analog postfilter harmonic distortion, more useful metrics of performance include signal-to-noise ratio (SNR) and total harmonic distortion. This performance is often determined by using a single-tone input sinusoid, but two-tone and multi-tone tests may yield more useful information if intermodulation distortion is considered relevant to the converter's operation.

Signal to Noise Ratio

Typically, the noise in an oversampling D/A converter is determined by applying a sinusoidal signal at the input, then integrating the resultant output noise across the signal bandwidth. For audio D/A converters, this integration is often performed taking the characteristics of the human ear into account, a process known as A-weighting. The ratio between the rms power of the output sinusoid to this integrated noise power is thus the signal to noise ratio, and is usually expressed in terms of decibels. In this project, the SNR will be measured by integrating the unweighted noise from 20Hz to 20000kHz as an approximation to the A-weighting method.

$$SNR = 10 \log_{10} \left(\frac{\text{Signal Power}}{\text{Integrated Noise Power}} \right) \qquad (2.23)$$

Total Harmonic Distortion

The total harmonic distortion (THD) is the ratio of the rms sum of the powers of the single-tone harmonics to the power of the input fundamental tone.

$$\text{THD} = 10 \log_{10} \left(\frac{\text{Sum of Harmonic Powers}}{\text{Signal (Fundamental Tone) Power}} \right) \qquad (2.24)$$

$$\text{THD} = 10 \log_{10} \left(\sum_{k=2}^{\infty} \frac{X_k^2}{X_1^2} \right) \qquad (2.25)$$

where X_1 is the voltage level of the fundamental tone and X_k the rms voltage of the kth harmonic component.

Other Measures

In addition to these two measurements, combinations or qualifications thereof are also common metrics in oversampling D/A design.

36

Signal-to-quantization noise ratio, or SQNR, is computed the same as the signal-to-noise ratio, except only digital quantization noise is included in the computation.

Signal-to-noise-and-distortion ratio (SNDR) is computed as the ratio between the signal power and the sums of the integrated noise and the total distortion power over a given signal bandwidth.

Dynamic range is defined as the ratio between the largest signal output magnitude available from the D/A converter to the smallest signal that is resolvable above the noise floor.

2.5   Oversampling D/A Optimization Strategies

Even without a priori knowledge of the performance of the individual blocks of the oversampling D/A converter, a general strategy for optimizing the output-referred SNR from a system level perspective can be described.

2.5.1   Gain and Noise

As the signal passes through each of the blocks described above, some amount of noise is added to the signal, whether it be from digital truncation effects or thermal noise from analog components. It can be seen quite readily that it is not optimal to place a large gain after a dominant noise source, as this results in subsequent amplification of the noise. Rather, if the gain, or part of it, can be placed before the dominant noise source, the overall performance of the system will improve, as the signal is amplified before the noise is added to it.
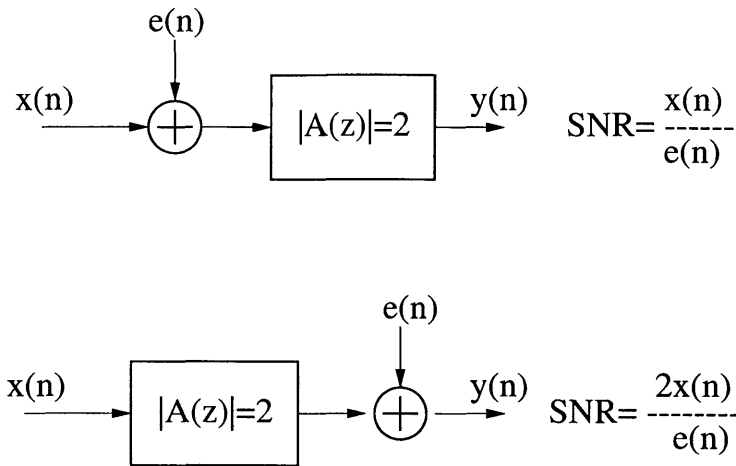
Figure 2-10: Effect of Gain Positioning on System Noise Performance

2.5.2 Linearity and Overload

In an ideal setup, therefore, we would be able to shift all of our system gain to the front of the D/A converter chain. However, each of these blocks has a soft limit on the size of the signal that it can process without introducing severe distortion. For example, a signal within the interpolation filters is constrained to be a digital PCM signal of magnitude no greater than N bits. If a gain greater than unity is introduced anywhere in this chain, the resultant signal may exceed the PCM bitwidth of N bits for a full scale input tone, causing severe distortion by saturating the signal at N bits.

Since we know that distortion in the analog portions of the D/A converter is unavoidable, we will design our digital system blocks such that as much gain as possible is placed up front in the chain while guaranteeing that distortion is kept to a minimum. This will maximize the noise budget available to the analog circuitry, allowing a reduction in its size and power dissipation. In addition, where possible, the gains

38

present in the analog blocks will be minimized to the extent that the signal does not incur significant distortion within the analog circuitry.

Chapter 3

Digital Interpolation and Noise Shaping

Unlike analog circuitry, whose accuracy is limited by physical factors such as thermal noise and finite supply voltage, digital circuitry can be made arbitrarily precise, assuming that an infinite number of bits are available to represent a digital signal. Advances in process technology over the last twenty years have scaled down the dimensions of digital circuitry, enabling the implementation of large bit width signal paths without incurring a severe cost in terms of circuit speed and die area [10]. In order to achieve low power and area consumption in the analog portion of the D/A converter, it is thus desirable to shift as much of the noise burden to the digital portion as possible, inasmuch as it can be easily absorbed.

Furthermore, in many industry applications, part of the digital D/A converter circuitry is implemented in a digital signal processing (DSP) core where specialized digital architectures optimized for polyphase filtering handle a number of signal processing operations. Although the digital filtering requirements of the D/A are likely to only form a small fraction of the filtering load performed by the DSP, the bus bit widths available to the outputs of the digital interpolation filters are usually de-

termined by system architecture considerations rather than D/A converter digital accuracy requirements, resulting in an upper bound on the SNR available from the digital portion of the converter.

3.1 Digital Quantization Noise

Because the quantization process is highly nonlinear, its exact analysis, although necessary to precisely predict the performance of the D/A converter, is particularly troublesome. When quantization is incorporated into a multiple feedback loop, as in a sigma-delta modulator, the analysis becomes even more difficult. In order to make this analysis tractable, various methods based on certain assumptions and approximations have been introduced and applied with successful results [14]. Even in very practical circumstances where the simplifying assumptions regarding quantization have been completely violated, useful results can still be obtained, especially given that a more precise analysis is either prohibitively difficult or impossible.

3.1.1 Uniform Quantization

Fortunately for purposes of simplifying the analysis, the most common form of quantization present in D/A converter systems is that in which the quantizer has an even number 2^N of levels each spaced exactly by a distance Δ known as the *bin width*. The quantizer can accommodate input signals up to a level X_m above which the quantizer gives as its output $X_m = \Delta \cdot 2^{N-1}$, as shown in Fig. 3-1.

These levels may be represented by a number of binary weighted coding schemes depending on which is most suitable for the application at hand. Two's complement binary notation is commonly used in microprocessors and computers due to the fact
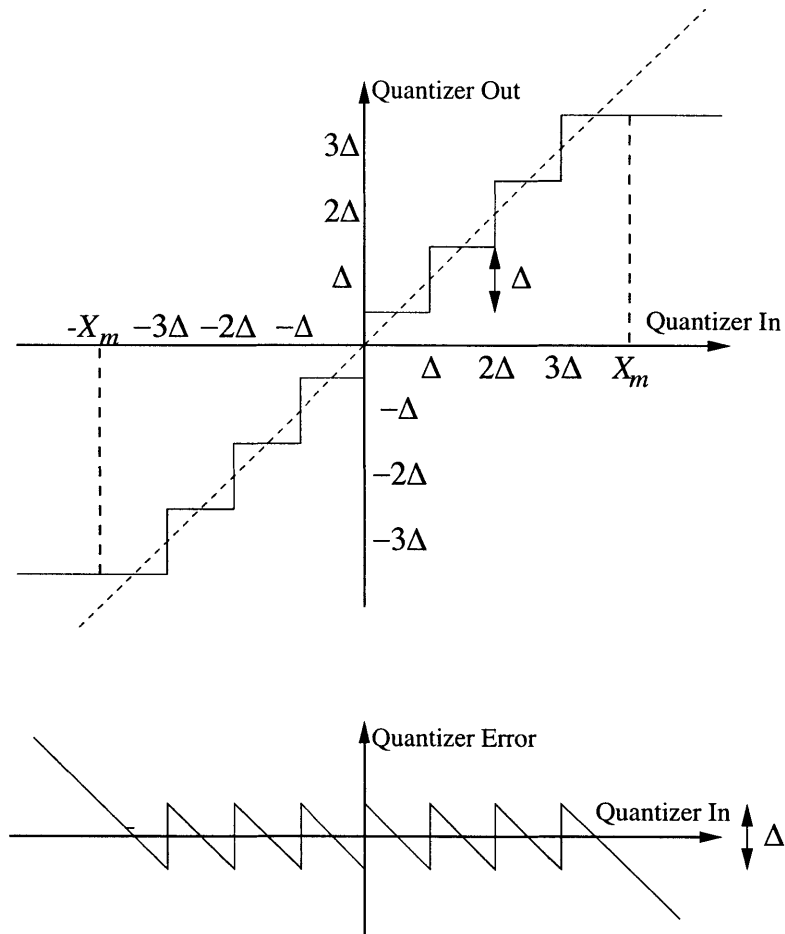
Figure 3-1: Input/Output Relation and Input/Error Relation for a Uniform Quantizer

that addition of positive and negative numbers can be performed by straightforward addition without the use of specialized arithmetic blocks. Also, the subtraction of two numbers is easily performed by complementing the bits of the number to be subtracted, adding one LSB to create the two's complement of the number to be subtracted, then finally adding the first of the two numbers in the subtraction operation [3]. For the same reason, this representation is also commonly used in DSP processors. As shown in Table 3.1, in the two's complement notation, the leftmost bit is taken as the sign bit, where "0" denotes a positive integer, while a "1" denotes a negative integer. The remaining binary digits denote the specific number or fraction

42

Number	Normalized Number	Sign Magnitude	2's Complement
+7	+7/8	0111	0111
+6	+6/8	0110	0110
+5	+5/8	0101	0101
+4	+4/8	0100	0100
+3	+3/8	0011	0011
+2	+2/8	0010	0010
+1	+1/8	0001	0001
+0	+0	0000	0000
(-0)	(-0)	(1000)	
-1	-1/8	1001	1111
-2	-2/8	1010	1110
-3	-3/8	1011	1101
-4	-4/8	1100	1100
-5	-5/8	1101	1011
-6	-6/8	1110	1010
-7	-7/8	1111	1001
-8	-8/8		1000

Table 3.1: Common Signal Digital Number Representations

to be represented.

The output of the quantizer $y[n]$ differs from the value of the input sample $x[n]$ by an amount $e[n]$ which is termed the *quantization error*. As long as the magnitude of the input is bounded between $\pm X_m$, the error $e[n]$ takes on a value anywhere between $-\frac{\Delta}{2}$ and $\frac{\Delta}{2}$. However, if the magnitude of the input is greater than X_m, the quantizer is said to be in *overload* and the error magnitude $|e[n]|$ is given by $|x[n]| - X_m$. In general, it is desirable to avoid operating the quantizer in the overload region, as it leads to signal clipping which results in severe harmonic distortion.

3.1.2 Quantization Noise Linearization Approximation

Although a uniform quantizer inherently introduces signal-dependent nonlinear errors into the signal path, the classic study conducted by Bennett [11] developed a set of conditions by which the quantization operation can be approximated by an additive white noise source.

Bennett's theorem postulates that if the following conditions are met:

I. That the quantizer input is not in the overload region.

II. That the number of levels in the quantizer is asymptotically large.

III. That the spacing Δ between quantizer levels is asymptotically small.

IV. That the joint probability density function (pdf) of the input signal is smooth at different sample times.

Then the quantization error sequence $e[n]$ has the following properties:

Property 1. $e[n]$ is statistically independent of the input signal $u[n]$.

Property 2. The pdf of e[n] is uniformly distributed in $[-\frac{\Delta}{2}, \frac{\Delta}{2}]$. It is an unbiased estimator of the input signal, that is to say, $E[y[n]] \approx E[x[n]]$, as shown in Fig. 3-2.

Property 3. $e[n]$ has a flat power spectral density (i.e. is "white").

The ability to replace a nonlinear quantizer with a linear noise source considerably simplifies the analysis involved because the well-developed body of linear systems theory can now be applied to digital blocks in a mixed-signal system. As shown in Fig. 3-3, quantization of a full scale sinusoid to 16 bits in MATLAB yields a power

44
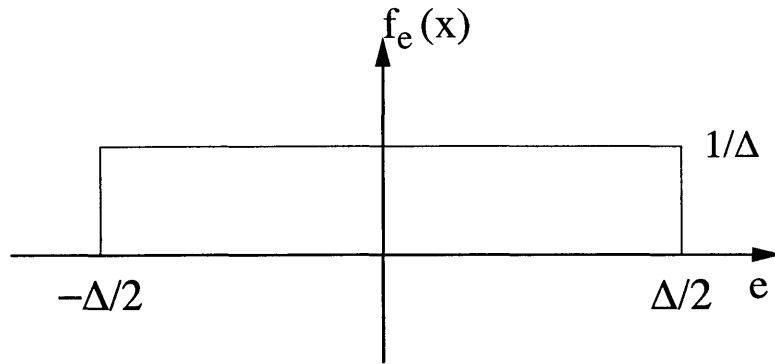
Figure 3-2: Theoretical Quantizer Output Error Probability Density Function

spectral density that can be well approximated as being "white".

Although the approximations noted above yield good results in most cases, it should be noted that in a wide variety of commercial quantizer applications, the conditions required by Bennett's condition are compromised and in some cases violated entirely, as in the example of the oversampling D/A with a two-level quantizer. Despite these limitations, the assumptions held by Bennett's theorem still provide many useful insights and yield reasonably good predictions of system behavior [14]. For example, a sigma-delta noise shaper based on a two-level quantizer generates a noise spectrum that is shaped much as theory predicts, but also contains in-band tones due to idle sequences generated by the 1-bit sigma-delta operation.

An important example in which Properties 2 and 3 above hold exactly is the case for an input signal that is itself an independent identically distributed random signal situated within the no-overload range of the quantizer. It is easy to see that the pdf of the quantization error is then uniformly distributed over the range $[-\frac{\Delta}{2}, \frac{\Delta}{2}]$.
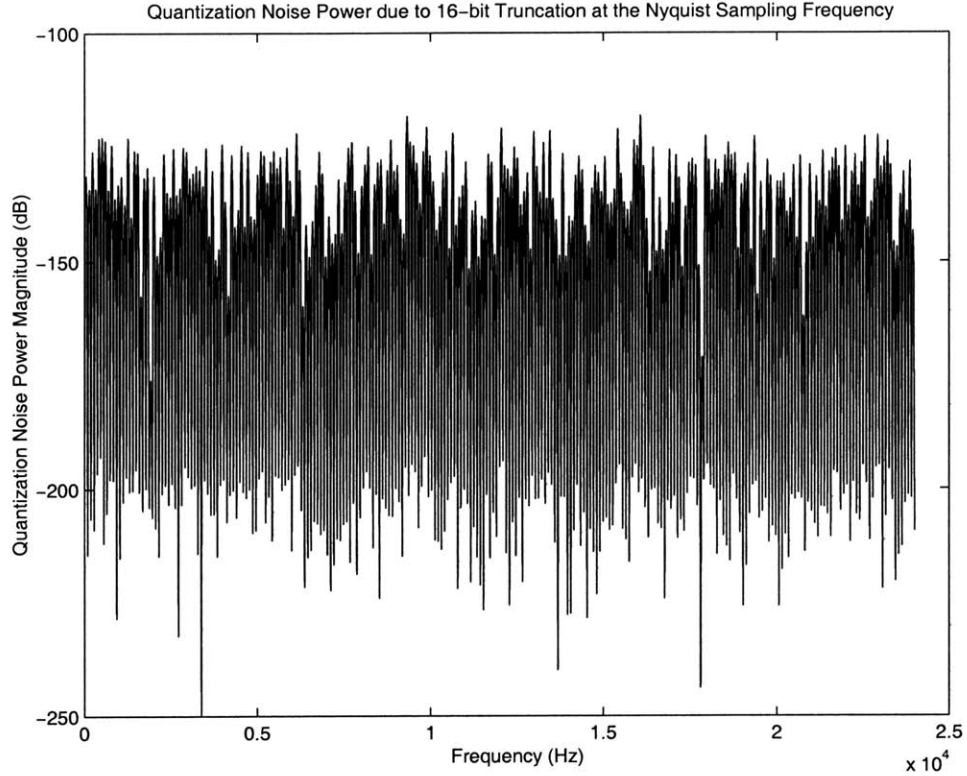
Figure 3-3: 16 Bit Quantization Error Power Spectral Density for Sinusoidal Input

3.1.3 Calculation of Quantization Noise Power

Proceeding with the assumptions noted in the above section, it is seen that an approximated white-noise process with a uniform pdf extending from $[-\frac{\Delta}{2}, \frac{\Delta}{2}]$ and having height $\frac{1}{\Delta}$ has a variance of:

$$\sigma_e^2 = V_{noise}^2 = \int_{-\frac{\Delta}{2}}^{\frac{\Delta}{2}} e^2 \frac{1}{\Delta} de = \frac{\Delta^2}{12} = \frac{2^{-2N}(2X_m)^2}{12} \tag{3.1}$$

Since the variance of the quantization noise process must equal its total power, we can then develop expressions relating the power of the input signal to the noise power generated by the quantization process. A common metric of particular interest to mixed-signal engineers is the peak signal to noise ratio SNR_{max}, where the maximum amplitude of the input signal is X_m. A randomly distributed input signal in the no-

46

overload range thus has a signal power of:

$$V_{signal}^2 = \frac{(2X_m)^2}{12} \tag{3.2}$$

which gives an SNR of:

$$10\log_{10}\left(\frac{V_{signal}^2}{V_{noise}^2}\right) = 10\log_{10}(2^{2N}) = 6.02N \text{ dB} \tag{3.3}$$

A sinusoidal signal can be analyzed the same way. A full-scale sinusoidal signal has a power of:

$$V_{signal}^2 = \frac{X_m^2}{2} \tag{3.4}$$

which gives a peak SNR of:

$$SNR_{max} = 10\log_{10}\left(\frac{V_{signal}^2}{V_{noise}^2}\right) = 10\log_{10}\left(\frac{3}{2}2^{2N}\right) = 6.02N + 1.76 \text{ dB} \tag{3.5}$$

Since a full-scale sinusoid results in the maximum SNR for a quantizer, we denote this quantity as SNR_{max}.

3.1.4 Quantization Noise Power with Oversampling

Continuing to assume that the quantization process yields an error sequence $e[n]$ that can be modeled as white noise, for an oversampled system, the quantization error power is spread uniformly across the frequency range $[-\frac{f_s}{2}, \frac{f_s}{2}]$, where f_s is a sampling frequency much greater than the Nyquist rate. Since the resultant power spectral density is equal to the variance of the error sequence $e[n]$, the quantization noise power per unit Hz frequency must be given by:

$$S_e(f) = \frac{\Delta^2}{12}\frac{1}{f_s} \tag{3.6}$$

47

In an oversampled D/A converter, the primary parameter of interest is not the SNR per se, but the SNR across the signal bandwidth f_0. Thus, to calculate the in-band SNR, we first integrate the noise power spectral density across the signal band. Remembering to integrate across both sides of the two-sided power spectral density, we obtain:

$$\sigma_e^2 = \frac{\Delta^2}{12} \frac{2f_0}{f_s} = \frac{\Delta^2}{12} \frac{1}{OSR} \tag{3.7}$$

Again, assuming a sinusoidal input signal, which is commonly used to characterize the noise performance of a D/A converter,

$$\sigma_s^2 = \frac{\Delta^2 2^{2N}}{8} = \frac{(2X_m)^2}{8} \tag{3.8}$$

Taking the logarithm ratio of the signal power to the error power yields:

$$SNR_{max} = 10 \log_{10}\left(\frac{3}{2}2^{2N}\right) + 10 \log_{10} OSR = 6.02N + 1.76 + 10 \log_{10} OSR \text{ dB} \tag{3.9}$$

Thus, as the signal of interest is oversampled, the SNR increases by about 10dB for every additional decade of oversampling. Equivalently, for each factor of four increase in OSR, an additional bit of resolution is obtained. While this improvement seems impressive, increasing the effective bit resolution through straight oversampling quickly becomes expensive. For example, consider a 5-bit quantizer that we would like to use to convert an oversampled signal with 16 bits of audio signal band resolution. This requires an oversampling ratio of 4,200,000, corresponding to a sampling frequency of 201GHz, a rate not currently attainable with modern CMOS processes. Fortunately, the use of sigma-delta modulation helps to achieve the desired signal resolution without such a dramatic increase in sampling rate.

The reason for the improvement in SNR with the oversampling ratio is that more

samples are taken per unit time. Prior to the point where the system SNR is measured, these samples are averaged out via low-pass filtering to reconstruct the baseband signal. During this averaging, the baseband signal components add linearly because they are self-correlated. However, the quasi-random quantization error has an impulse autocorrelation function and thus adds as the square root of the sum of the squares [3].

3.2   Digital Interpolation Filtering

3.2.1   Upsampling

The process by which the sampling frequency is increased in an oversampling converter is colloquially referred to as *interpolation* but more accurately should be referred to as upsampling followed by image-reject filtering. When a discrete-time signal is upsampled by a factor L, each sample of the original signal is mapped to every L^{th} sample in the new signal sequence, which runs at a sampling rate L times greater than that of the original. The remainder of the samples retain a value of zero. Obviously, the upsampling process produces some unwanted modification to the input signal. This modification is best viewed in the frequency domain and is derived as follows:

The upsampling process can be expressed in the discrete time domain as:

$$x_u[n] = \begin{cases} x[n/L] & \text{if } n = 0, \pm L, \pm 2L, \dots \\ 0 & \text{otherwise} \end{cases} \tag{3.10}$$

equivalently, we can express the above case statement as:

$$x_u[n] = \sum_{k=-\infty}^{\infty} x[k]\delta[n - kL] \tag{3.11}$$

Given the discrete-time Fourier transform

$$X(e^{j\omega}) = \sum_{n=-\infty}^{\infty} x[n]e^{-j\omega n} \tag{3.12}$$

We obtain the frequency domain response of the upsampled signal

$$X_u(e^{j\omega}) = \sum_{n=-\infty}^{\infty} (\sum_{k=-\infty}^{\infty} x[k]\delta[n - kL])e^{-j\omega n} \tag{3.13}$$

Exchanging summations yields:

$$X_u(e^{j\omega}) = \sum_{k=-\infty}^{\infty} (\sum_{n=-\infty}^{\infty} x[k]\delta[n - kL]e^{-j\omega n}) \tag{3.14}$$

Since the term in the inner summation has a nonzero value only at $n = kL$, the expression contracts to:

$$X_u(e^{j\omega}) = \sum_{k=-\infty}^{\infty} x[k]e^{-j\omega kL} \tag{3.15}$$

$$X_u(e^{j\omega}) = X(e^{j\omega L}) \tag{3.16}$$

Thus, the Fourier transform of the upsampled signal is just the same as that of the Fourier transform of the old signal, only compressed by a factor of L along the discrete time frequency axis. In other terms, the discrete time frequency axis was normalized before as: $\omega = 2\pi f/f_{s,old}$, where f is the continuous-time frequency axis, and $f_{s,old}$ is the original sampling period. After upsampling, the discrete time frequency axis is now normalized as: $\omega = 2\pi f/(Lf_{s,old})$ where $Lf_{s,old} = f_{s,new}$. As shown in Fig. 3-4, this contraction of the discrete time frequency axis results in the introduction of undesired spectral images adjacent to the signal band.

Digital filters commonly known as *image-reject filters* or *interpolation filters* are used to remove the undesired spectral images introduced by upsampling. The interpolation filter required to remove the images from the first upsampling must typically be of considerable length, as the transition band required to attenuate the adjacent
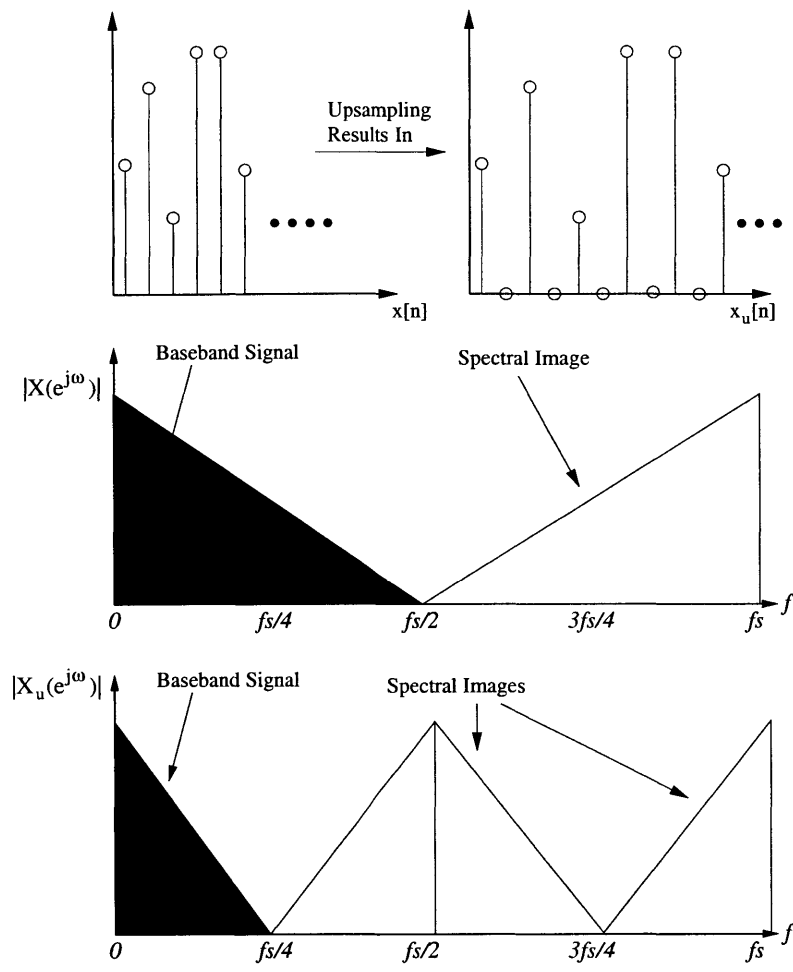
Figure 3-4: Discrete-Time and Frequency Domain Depictions of Upsampling

spectral image is very narrow. As a low-pass interpolation filter in effect performs an averaging operation on the upsampled signal, the signal magnitude is reduced by a factor of L for a filter with 0dB gain. In order to maintain the filtered upsampled signal at its original magnitude, the filter must have a gain of L associated with it.

3.2.2 FIR Image-Reject Filtering

In audio D/A converters, the digital interpolation filters are commonly realized by finite impulse response (FIR) filters [4]. FIR filters are filters that, as their name

implies, have impulse responses that are bounded in time. In general, they are implemented as shown in Fig. 3-5 as a bank of digital multipliers whose inputs are separated by delay registers and whose outputs are summed to generate the filter output.
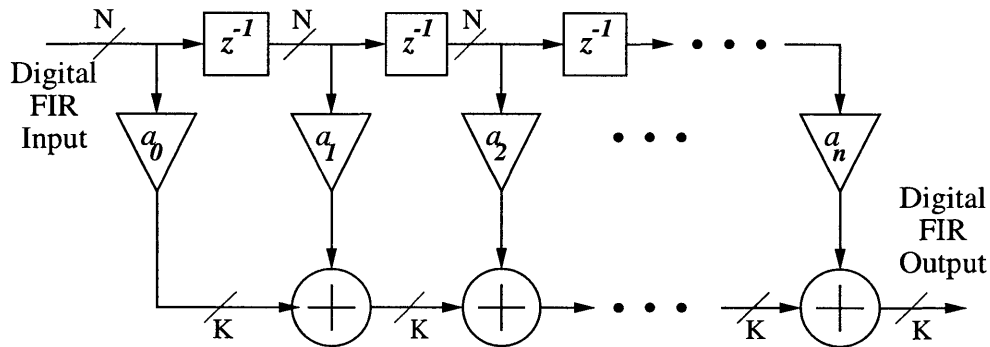
Figure 3-5: Digital Implementation of FIR Interpolation Filter

FIR filters are frequently used in audio applications because an FIR filter can be easily designed to have linear phase, and thus constant group delay, which minimizes phase distortion of the audio signal. To see how this can be accomplished, consider a time-bounded filter of length M such that:

$$h_e[n] = h_e[-n] \tag{3.17}$$

Taking its discrete-time Fourier transform yields:

$$H_e(e^{j\omega}) = \sum_{n=-M/2}^{n=M/2} h_e[n]e^{-j\omega n} = h_e[0] + \sum_{n=1}^{M/2} 2h_e[n]cos(\omega n) \tag{3.18}$$

Since the filter is time-bounded and even, its discrete-time frequency response is purely real and thus has zero phase. Of course, such a filter is not causal and is hence impossible to implement. However, adding a time delay to the filter such as to make it purely causal only has the effect of adding a linear phase to the frequency response:

$$h[n] = h_e[n - M/2] \tag{3.19}$$

$$H(e^{j\omega}) = H_e(e^{j\omega})e^{j\omega M/2} \tag{3.20}$$

$$|H(e^{j\omega})| = |H_e(e^{j\omega})| \tag{3.21}$$

$$\angle H(e^{j\omega}) = -j\omega M/2 \tag{3.22}$$

Contemporary design of optimal FIR filters is greatly aided by the use of filter design software algorithms. One particularly effective and ubiquitous FIR design algorithm was developed by Parks and McClellan[19] , which takes as its arguments the desired filter passband edge ω_p, the desired filter stopband edge ω_s, the number of filter taps M, and the desired passband and stopband errors, denoted δ_1 and δ_2 respectively. The Parks and McClellan algorithm fixes ω_p, ω_s, and M while letting δ_1 and δ_2 vary. The resulting optimal lowpass filter has an equiripple response in both the passband and the stopband. Kaiser [20] performed a computational study of this method and subsequently obtained a relation between the parameters of the filters, with gives the number of taps as:

$$M = \frac{-10\log_{10}(\delta_1\delta_2) - 13}{2.324\Delta\omega} \tag{3.23}$$

where

$$\Delta\omega = \omega_s - \omega_p \tag{3.24}$$

for a lowpass filter.

Thus, for a given error specification in the passband and stopband, there exists a tradeoff between the sharpness of the filter transition band and the number of the taps in the filter. It is also evident that if a signal is interpolated by a large factor L, the transition band of the interpolation filter must be incredibly sharp in order to

reject the spectral image immediately adjacent to the baseband signal.

3.2.3 Multistage Interpolation

A common approach to reducing the number of filter taps required in the first interpolation filter that must be used to reject the spectral image adjacent to the signal band is to break up a large interpolation factor into a multistage interpolation scheme, as shown in Fig. 3-6. Instead of performing all of the required upsampling in one step, the upsampling is done by a factor of 2 at a time in order to ease the transition band requirements as much as possible. To see how this might work, consider a mathematical example, partially illustrated below in Fig. 3-7

FIR Interpolation and Image Reject Stages   Interpolation and Digital ZOH
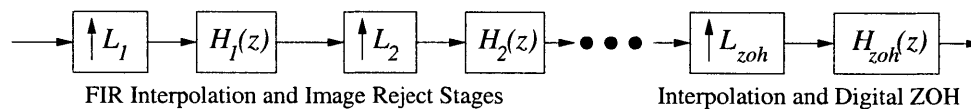
Figure 3-6: Multistage Interpolation Block Diagram

Given that we require $\delta_1 = 0.001$ (guaranteeing a stopband image rejection of -60dB), $\delta_2 = 0.001$ (to minimize ripple within the passband) over a transition band that spans from 20kHz to 26kHz for an upsampling factor of $L = 8$, plugging these values into Equation 3.23 yields a required number of taps M equal to 206.

If the required upsampling were broken up into three stages of $L = 2$ the transition bandwidth in radians would be approximately 4 times larger for the first interpolation filter. This results in a reduction of the number of filter taps by approximately the same factor, resulting in $M = 52$. As shown in Fig. 3-7, during the next upsampling by 2, the next spectral image is not adjacent to the signal band, and thus the transition bandwidth requirements are significantly relaxed, resulting in the requirement of a filter with only 12 taps. Subsequent calculation will show that a further upsampling
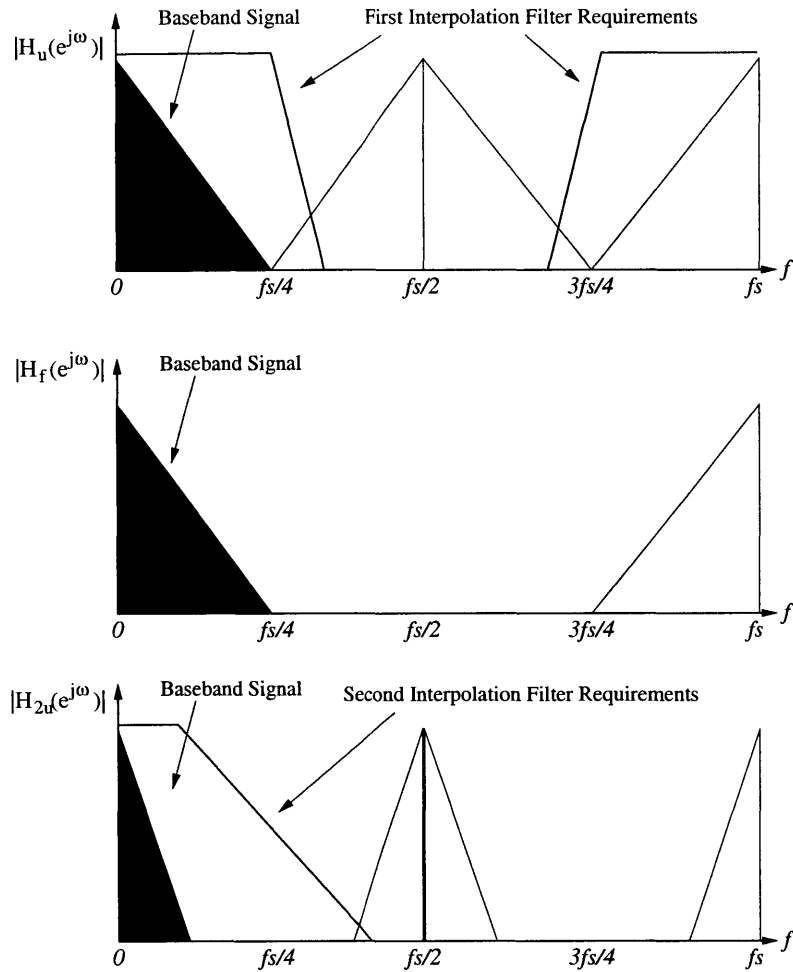
Figure 3-7: Generic PSD for Consecutive Upsamplings by 2 and Interpolation

by two will require a final interpolation filter with 9 taps. Thus, the total number of taps required in the multistage implementation is 73, compared to the 209 taps required for the single stage interpolation.

When dedicated circuitry for oversampling D/A converter interpolation filtering was expensive in terms of area and power dissipation, the savings realized above were a powerful motivator for a multistage interpolation scheme. However, the cost of digital circuitry has dropped dramatically in recent years due to the scaling of

CMOS technologies. Whereas such digital circuitry might have dominated the D/A converter power and area dissipation in years past, its contribution to the power-area product of a D/A converter in a modern process pales in comparison to that of the analog postfilter. However, in a practical implementation, digital filtering introduces quantization noise into the signal band that can severely degrade the in-band SNR. If possible, we would like to trade the number of taps in the interpolation filtering scheme for an improved SNR.

To see how multistage interpolation filtering introduces additional quantization noise into the signal, consider the following: The incoming digital signal of bit width N is convolved with an FIR filter in which the values of the filter taps add up to K bits. The result of the convolution is a filtered signal that is held as an intermediate result in a register of $N + K$ bits. Normally K is chosen to be as small as possible to provide sufficient filter tap resolution while minimizing the size of the intermediate value holding register. Although the holding register can be chosen to be large, if the interpolation filters are realized as part of a multipurpose DSP processor, the data bus widths are likely to be limited to the signal bit width N. Thus, before propagating through the data bus, the filtered upsampled signal at the holding register must be requantized back to N bits, introducing additional quantization noise.

An intuitive grasp of the magnitude of this problem is best illustrated by a simple mathematical example, as described below:

The in-band SQNR is dominated by the initial quantization of the incoming signal to N bits at the Nyquist sampling rate. Assuming that the signal bandwidth of interest is exactly half of this initial sampling rate, the amount of this initial quantization noise power can be calculated as:

$$\sigma^2_{e_{initial}} = \frac{2^{-2N}}{12} \frac{1}{OSR} \tag{3.25}$$

but since OSR=1 for the Nyquist-sampled case

$$\sigma^2_{e_{initial}} = \frac{2^{-2N}}{12} \tag{3.26}$$

For the case of the multistage interpolation architecture, quantization noise is added after each of the upsampling and filtering operations, and thus at each subsequent upsampling stage, the quantization noise is spread over a higher bandwidth. Hence, the additional quantization noise due to requantization can be calculated as:

$$\sigma^2_{e_{stage1}} = \frac{2^{-2N}}{12} \frac{1}{2} \tag{3.27}$$

$$+\sigma^2_{e_{stage2}} = \frac{2^{-2N}}{12} \frac{1}{4} \tag{3.28}$$

$$+\sigma^2_{e_{stage3}} = \frac{2^{-2N}}{12} \frac{1}{8} \tag{3.29}$$

$$= \sigma^2_{e_{total}} = \frac{2^{-2N}}{12} \frac{7}{8} \tag{3.30}$$

The single stage interpolation scheme upsamples the signal by a factor of 8 prior to filtering and quantization. It thus introduces a noise power of only

$$\sigma^2_{e_{total}} = \frac{2^{-2N}}{12} \frac{1}{8} \tag{3.31}$$

These two techniques were evaluated in MATLAB for both the multistage and single stage architectures. The single stage filter was derived by interpolating and convolving the three filters in the multistage architecture. Thus, the two filter chains perform exactly the same filtering operations. The results of the MATLAB simulation are shown in Fig. 3-8 for a 16 bit sinusoidal input at 1171.875 kHz.

SNR=98.41dB for full scale input

SNR=96.41dB   SNR=96.05dB   SNR=96.01dB

SNR=98.17dB
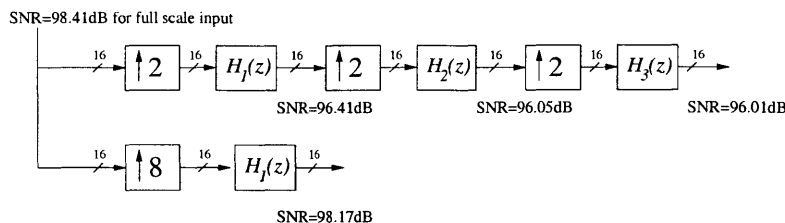
Figure 3-8: SNR Degradation in Multistage Interpolation Filtering

3.2.4 Postfilter Droop Correction

Because they are implemented in digital hardware, interpolation filters have an inherently robust frequency response, that is to say, the frequency response of the digital filter will always be exactly the same regardless of any non-critical process variations within the digital circuitry. Thus, it is often desirable to correct any imperfections in the analog domain of the D/A converter with compensatory filtering in the digital domain. Our goal of keeping the analog postfilter circuitry as simple as possible serves to underscore this point. Although digital interpolation filtering has been proposed to correct for zero order hold droop in D/A converters [18], discussed below is a compensation technique that is more aggressive and is intended to compensate for the passband droop induced by the cascade of two first-order filters.

A digital interpolation filter designed using an optimizing algorithm such as the ones mentioned above produces a filter with a flat passband response containing a negligible amount of ripple. In order to correct droop in the postfilter, which occurs primarily in the 10-20kHz region of the passband, it is desirable to have the passband response of the digital interpolation filter to slope upwards at at approximately the same rate at which the magnitude of the analog postfilter droops in the passband.

This passband droop compensation can be done in an interactive fashion by first generating the appropriate interpolation filter taps using one of the exchange al-

gorithms discussed above. The filter taps actually represent the coefficients of a $\mathcal{Z}$-domain polynomial which can be factored using numerical manipulation software such as MATLAB. Once obtained through factoring, the roots of this polynomial represent the zeros of the FIR filter, as shown in Fig. 3-9.

FIR Passband Response Droop Correction Technique
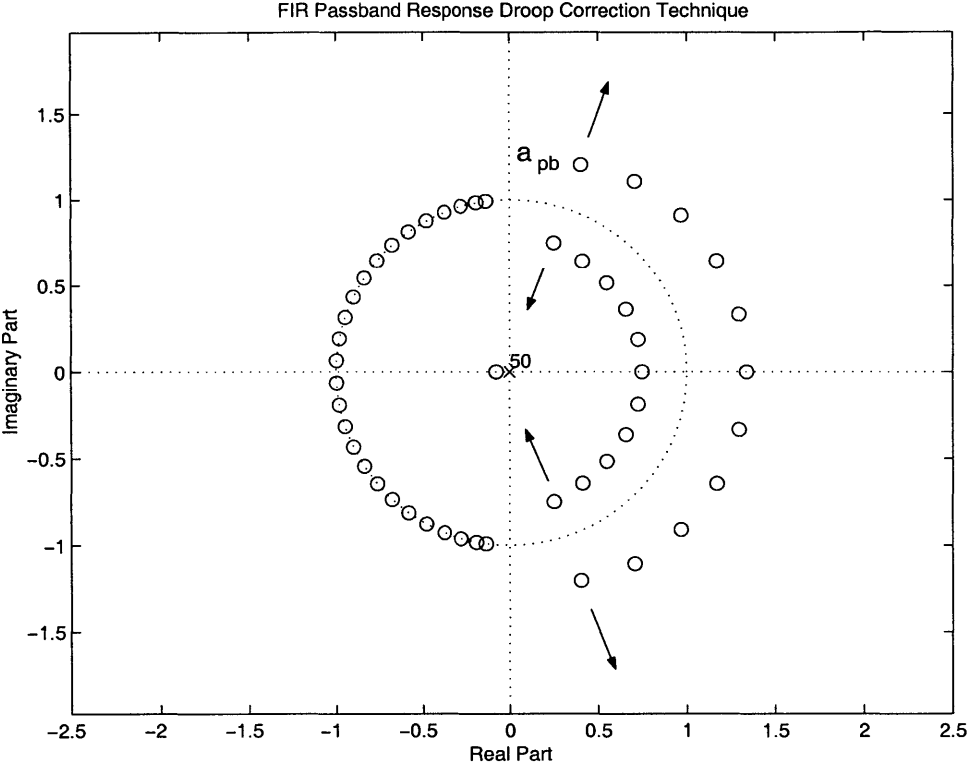
Figure 3-9: Filter Droop Compensation on the Complex Z-Plane

Note that as shown in Fig. 3-9, the passband area is denoted by the region in which the zeros are located off of the unit circle, while the stopband region is denoted by the region in which the zeros are located directly on the unit circle. A careful inspection of the pole-zero plot reveals that each zero z_0 on the plot is joined by its inverse z_0^{-1}, and its conjugate z_0^*. To see why this is the case, consider the fact that the FIR interpolation filter is symmetric around $n = M/2$ where $n = M$ is the last

sample of the filter.

$$H(z) = \sum_{n=0}^{M} h[n] \tag{3.32}$$

but since the filter is symmetric, it is possible to also write

$$h[n] = h[M - n] \tag{3.33}$$

and to substitute into the $\mathcal{Z}$-transform equation

$$H(z) = \sum_{n=0}^{M} h[M - n]z^{-n} \tag{3.34}$$

substituting $k = M - n$ yields

$$H(z) = \sum_{k=M}^{0} h[k]z^{k}z^{-M} = z^{-M}H(z^{-1}) \tag{3.35}$$

Therefore, if z_0 is a zero, that is, $H(z_0) = 0$, then the above relation holds that:

$$H(z_0) = z_0^{-M}H(z_0^{-1}) = 0 \tag{3.36}$$

Which means that if z_0 is nonzero, then z_0^{-1} must also be a zero.

One property of z-transforms holds that in general [4]:

$$h^*[n] = H^*(z^*) \tag{3.37}$$

However, since the FIR filter taps are all real,

$$h[n] = h^*[n] \tag{3.38}$$

and since the FIR filter is designed to have generalized linear phase, it is also true that

$$H(z) = H_{real}(z) \cdot z^{M/2} \tag{3.39}$$

$$H^*(z) = H_{real}(z) \cdot z^{M/2} = H(z) \tag{3.40}$$

Thus, it holds that the z-transform of the FIR filter also yields:

$$H(z^*) = H(z) \tag{3.41}$$

Equation 3.41 implies that if z_0 is a zero, then z_0^* also is a zero of the FIR filter polynomial.

In order to perform the postfilter droop compensation, it is necessary to increase the magnitude of the filter frequency response gradually starting from 10kHz and peaking at approximately 17.5kHz. In order to do this, it is helpful to examine an expression for the magnitude of the frequency response as a function of ω as the position of the frequency on the unit circle. This is given by:

$$|H(e^{j\omega})|^2 = H(e^{j\omega})H^*(e^{j\omega}) = H(z)H^*(1/z^*)|_{z=e^{j\omega}} \tag{3.42}$$

Given the discussion above regarding the properties of the frequency response of a generalized linear phase FIR filter, it is possible to write:

$$|H(e^{j\omega})|^2 = H(z)H(1/z) = |H(z)|^2 \cdot z^M = \prod_{k=1}^{M}(z - a_k)^2|_{z=e^{j\omega}} \tag{3.43}$$

Equation 3.43 implies that the magnitude of the FIR frequency response at a given frequency is equal to the product of the position of that frequency mapped onto the unit circle to each of the zeros in the $\mathcal{Z}$-plane. In a system that has a frequency response such as that of an FIR filter, the magnitude at any given frequency is largely determined by those zeros closest to that frequency. For example, while moving along the unit circle near the zero denoted a_{pb} in the FIR passband whose magnitude is

greater than unity and whose angle is most positive, the magnitude of the distance of the frequency mapped to the unit circle to a_{pb} is much smaller than the distances to the other zeros a_k. In addition, moving slightly on the unit circle changes the magnitude of the distance to a_{pb} while the magnitudes of the distances to other zeros a_k remain relatively unaffected.

Based on the above discussion, one method to increase the magnitude of the frequency response at the frequencies close to passband edge would be to increase the distance of the zero a_{pb} from the unit circle. This can be done by scaling the magnitude, but leaving the angle unchanged, of the zero a_{pb} outside of the unit circle by a factor $(1 + \delta)$. Of course, in order for the FIR filter to retain the property of generalized linear phase, the zero $1/a_{pb}$ on the inside of the unit circle must have its magnitude scaled by $1/(1 + \delta)$ in order to remain the inverse of the modified zero a_{pb}. In addition, the magnitude of the zero a_{pb}^* must be scaled by the factor $(1 + \delta)$ and its inverse zero scaled by $1/(1 + \delta)$. The frequency response of the resultant FIR filter is shown in Fig. 3-10. When placed in the D/A converter system, the overall frequency response is corrected to have a relatively flat passband, as shown in Fig. 3-11.

3.2.5   Digital Zero Order Hold Interpolation

The remainder of the interpolation done after the final upsampling after the interpolation filtering chain is performed by a digital zero-order hold register. As shown in Fig. 3-12, the digital zero-order hold simply interpolates between upsampled values by repeating the original sample P times. Like the zero-order hold mentioned in the discussion on the DT-CT interface, this digital zero-order hold introduces a slight frequency domain droop in the signal band; however, if the rate at which the signal is upsampled is on the order of 10, this droop is negligible and could at any rate be corrected by the same postfilter droop compensation technique discussed earlier. The sinc filter response of the zero-order hold also attenuates the spectral images intro-
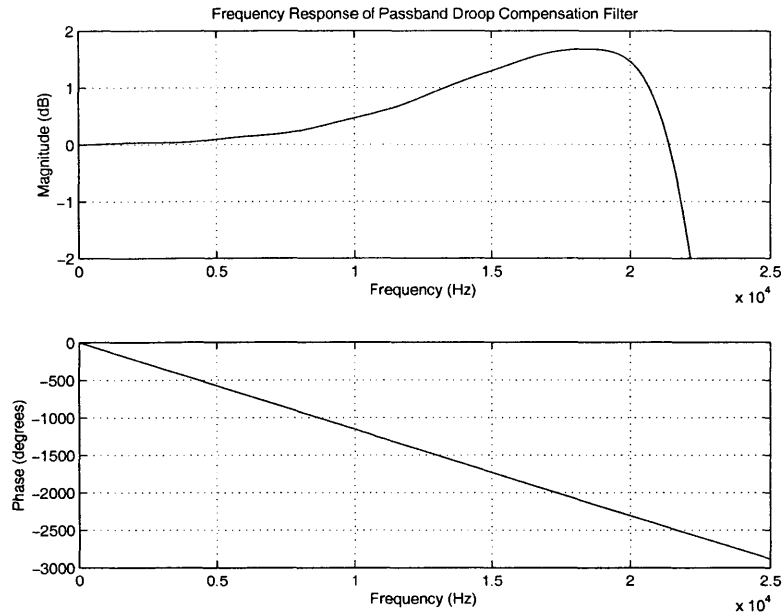
Figure 3-10: Signal Band Frequency Response of Compensating Filter

duced by the final upsampling to some extent, although these images are in general high enough in frequency to be sufficiently attenuated by a second-order postfilter.

3.3   Sigma-Delta Noise Shaping

The noise shaping operation in the oversampling D/A converter shown in Fig.2-3 is realized by a sigma-delta modulation operation. The key feature of the sigma-delta modulator is the placement of a feedback loop around a quantizer such that the modulator input and quantization error see different transfer functions to the output. It was found in Chapter 2 that the placement of an integrator in the forward path of the sigma-delta modulator results in a unity-magnitude transfer function from the input to the output, but a high-pass transfer function from the additive quantization noise source to the output. Using this technique, it was shown to be possible to quantize a N bit input signal into a B bit output signal while maintaining close to N bits of
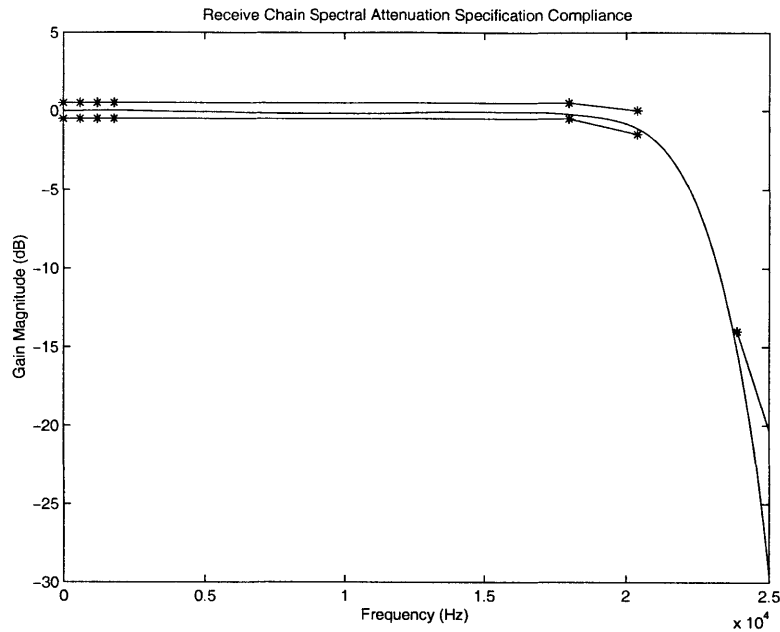
Figure 3-11: Frequency Response of D/A Converter Chain with Compensating Filter
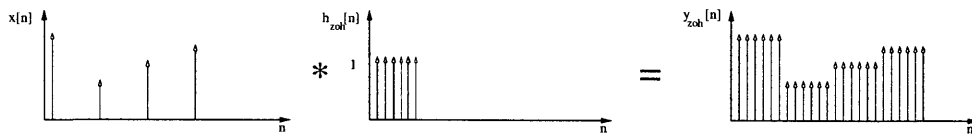
Figure 3-12: Discrete Time Operation of Digital Zero Order Hold

resolution in the signal baseband for a lower oversampling ratio than would be the case without a sigma-delta modulator.

In general, it is possible to increase the efficiency of the sigma delta modulation over that of the first order case described in Chapter 2 by increasing the order of modulator. As shown in Fig. 3-13, an arbitrarily high-order cascaded modulator can be implemented with the addition of more feedback loops to the circuit. However, the stability of cascaded modulators with order greater than two is not guaranteed, especially for the ubiquitous case in which a two-level quantizer is employed [13][15].

64

The discussion of the stability of higher-order quantizers is beyond the scope of this report, however, it will be shown shortly that for this project it is neither necessary nor desirable to implement a modulator of order greater than two.
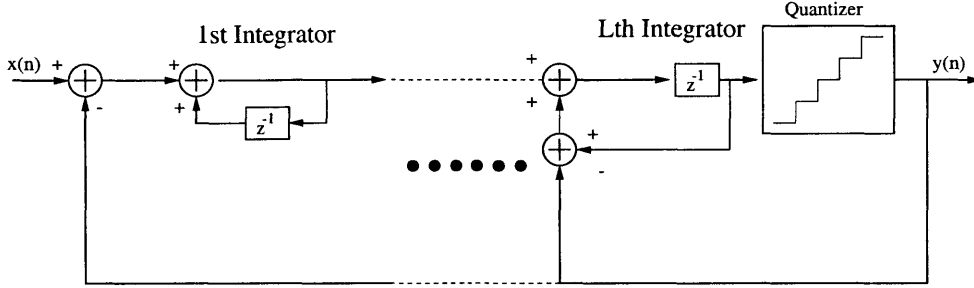
Figure 3-13: Block Diagram of Generic D/A Converter

3.3.1 Advantage of Multi-Order Sigma-Delta Modulation

If the error of the quantizer in Fig. 3-13 is again modeled as additive white noise, then the output of the L-th order cascaded modulator can be expressed as:

$$Y(z) = z^{-1}X(z) + (1 - z^{-1})^L E(z) \tag{3.44}$$

As in the single-order case, the output consists of a delayed version of the input signal and the high-pass shaped error signal. The transfer function from the additive quantization noise source to the output is given by:

$$H_e(z) = (1 - z^{-1})^L|_{z=e^{j2\pi f/f_s}} \tag{3.45}$$

$$H_e(f) = \left[\left(\frac{e^{j\pi f/f_s} - e^{-j\pi f/f_s}}{2j}\right) \cdot 2j \cdot e^{-j\pi f/f_s}\right]^L \tag{3.46}$$

$$H_e(f) = [\sin(\frac{\pi f}{f_s}) \cdot 2j \cdot e^{-j\pi f/f_s}]^L \tag{3.47}$$

65

Taking the magnitude of both sides, we obtain the high pass transfer function:

$$|H_e(f)| = (2\sin(\frac{\pi f}{f_s}))^L \tag{3.48}$$

Recalling that the power spectral density of the unshaped additive quantization noise in an oversampled system is expressed as:

$$S_e^2(f) = \frac{\Delta^2}{12} \cdot \frac{1}{f_s} \tag{3.49}$$

it is possible to obtain the power spectral density of the shaped noise by multiplying the power spectral density of the unshaped quantization noise with the square of the magnitude of the noise shaping function. The inband shaped noise power is then obtained by integrating the power spectral density across the two-sided signal band. This operation is expressed as:

$$P_e = \int_{-f_0}^{f_0} S_e^2(f)|H_e(f)|^2 = \int_{-f_0}^{f_0} \frac{\Delta^2}{12} \cdot \frac{1}{f_s} \cdot [2\sin(\frac{\pi f}{f_s})]^{2L} df \tag{3.50}$$

Assuming that $f_0 << f_s$, it is possible to approximate that $\sin(\pi f/f_s) \approx \pi f/f_s$ over the signal band. Performing the integral with the approximation noted above yields:

$$P_e \approx \left(\frac{\Delta^2}{12}\right)\left(\frac{1}{OSR}\right)^{2L+1} \cdot \frac{\pi^{2L}}{2L+1} \tag{3.51}$$

Assuming that the maximum SNR is obtained with a sinusoidal input, it is possible to develop an expression for the maximum SNR available to an Lth-order modulator for a given oversampling ratio.

$$SNR_{max} = 10\log(P_s/P_e) = 10\log_{10}(\frac{3}{2}2^{2N}) + 10\log_{10}\left[\frac{2L+1}{\pi^{2L}}(OSR)^{2L+1}\right] \tag{3.52}$$

$$SNR_{max} = 6.02N + 1.76 + 10\log_{10}(2L+1) - 9.94L + 10(2L+1)\log_{10}(OSR) \tag{3.53}$$

Where N is the number of bits in the sigma-delta modulator quantizer.
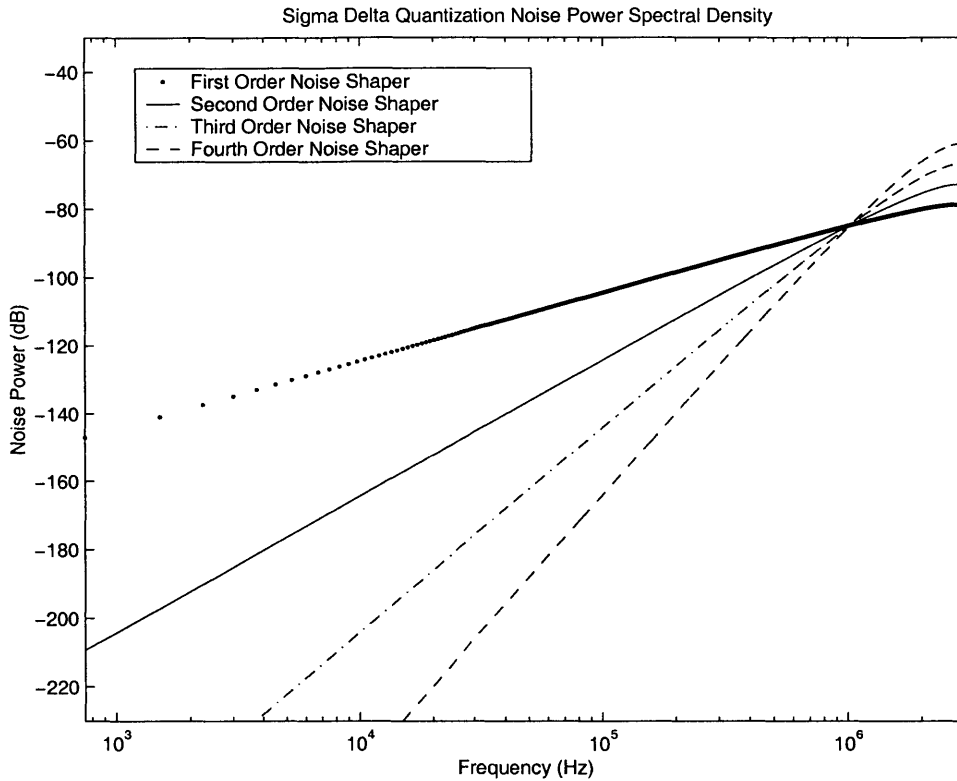
Figure 3-14: Theoretical Power Spectral Density Functions for Lth Order Modulators with 1-bit Quantization

It can be readily seen that even for a modulator for which $N = 1$ and $L = 2$, the equation given above predicts that an OSR of only 201 is required to produce a baseband resolution of 18 bits. While this figure turns out to be a bit liberal due to the explicit violation of Bennett's conditions in the 2-level quantizer, it shows that, as an oversampling ratio of 201 is easily achievable in modern process technology, the implementation of a two-level quantizer is certainly viable given the use of a second-order noise shaper.

Since the in-band quantization noise of the monolithic oversampled D/A is domi-

nated by the initial quantization of the input signal to N bits, we only require that the signal band resolution of the sigma-delta modulator be on the order of $N + 2 - N + 3$ such that the noise it introduces is negligible. In industry audio applications, a typical value for N is 16, meaning that a second order modulator operating at an OSR on the order of 100 will satisfy the above condition. As will be discussed in Section 4.4, it is also required to operate at a high oversampling ratio to reduce the effects of *clock jitter* at the DT-CT interface. Clock jitter contributes noise to the signal and increases as the OSR decreases. Its effects also turn out to constrain the OSR to be greater than 100. In addition, as the order of sigma-delta modulation is increased, the amount of out-of-band noise also increases as a result of the noise shaping operation. This requires a higher order analog postfilter to attenuate. Since it is desirable to minimize the order of the analog postfilter, it is hence also desirable to keep the order of the sigma-delta modulator as small as possible while still meeting the design objectives. As is evident, a sigma-delta modulator of order 2 represents a reasonable compromise between the aforementioned objectives.

3.3.2   Single Bit vs. Multibit Modulation

Single-bit, or two-level, quantizers are a popular choice in contemporary D/A converter design because of their inherent linearity. A misplacement of one level as a result of device mismatch only changes the quantization range and DC offset, neither of which are critical in a differential postfiltering application [13]. However, because only having two levels of quantization with a step size Δ equal to its output range seriously violates the conditions set forth to make the additive white quantization noise approximation, the single-bit modulator has serious drawbacks.

First, consider the application of a DC input to a first-order modulator with a two-level quantizer. We know that the gain of the digital integrator in the modulator at DC is infinite and thus the average value of the output that is fed back to this in-

tegrator must equal the DC value of the input. In general, the sigma-delta modulator will output a periodic sequence of 1s and -1s whose time-averaged value equals the value of the DC input. Since the sequence is periodic, it has a small amount of power concentrated at the frequency corresponding to the period of the sequence used to represent the DC input. This concentration of frequency is referred to as *tonal behavior* in the modulator and is extremely undesirable, as the human ear is very sensitive to such tones. [3]. One way to reduce the effect of these tones is to deliberately add a pseudorandom digital noise source in the sigma-delta modulator. This technique, known as *dithering*, can add enough randomness to the quantizer input to break up the periodic behavior of the quantizer output signal.

This additive pseudorandom digital noise source is normally placed immediately before the quantizer such that the pseudorandom dither noise is shaped along with the quantization noise. Although this technique can usually reduce the presence of tones to acceptable levels, it increases the quantization noise floor of the modulator, thus requiring a higher oversampling ratio to achieve a desired signal band resolution.

For a given order of sigma-delta modulation and a given oversampling ratio, multibit topologies provide about 6dB more in-band SNR per bit over a 1 bit implementation. Because of their superior noise performance, multibit topologies have become more popular in D/A architectures in recent years. Since they produce less in-band noise than their single-bit, use of a multibit modulator permits the reduction of the oversampling ratio while still maintaining the same SNR. As is described later in the discussion on switched-capacitor filtering, reducing the oversampling ratio is critical in achieving low analog die area consumption.

In addition, multibit D/A topologies more closely meet the Bennett quantization noise approximation conditions. Because of this, multibit D/As realize a dramatic

reduction of in-band idle tones without the use of dither and achieve greater loop stability for higher-order modulators. [13][17] However, multibit sigma-delta modulators rely on multibit D/A architectures that consist of an array of passive elements. As the matching of these elements corresponds to a resolution of 10-12 bits, some form of dynamic element matching or element calibration is necessary to improve the linearity of the D/A converter element array. In general, both techniques require digital overhead circuitry that increases in complexity proportional to 2^B. Since this circuitry must be implemented in dedicated hardware on the analog die, it is desirable to keep B small to minimize digital power and area consumption.

In the context of power and area optimizing the oversampling D/A converter it is important to consider the maximum amplitude signal that can pass through the sigma-delta modulator without overloading the quantizer. The attentive reader will recall from Chapter 2 that if the gain of the noise shaper must decrease in order to accommodate the signal, any noise introduced after the sigma-delta modulator will have a more adverse effect on the SNR than it would if the signal magnitude at the output of the sigma-delta were greater. In a sigma-delta modulator, the oscillation of the signal within the modulator uses up some of the dynamic range of the circuit, causing the quantizer to overload if the input amplitude is not limited. [13] Simulation results from MATLAB shown in Fig. 3-15 give the maximum available input amplitude as a function of number of quantizer bits for a second order cascaded modulator. As intuition might suggest, as the number of bits B increases, the dynamic range asymptotically approaches unity.

3.3.3 Implementation of a Sigma-Delta Modulator

The sigma-delta modulator implemented in this project was first designed as a behavioral model, then implemented as an equivalent digital block in combinational logic. The second-order modulator behavioral model was implemented as shown in
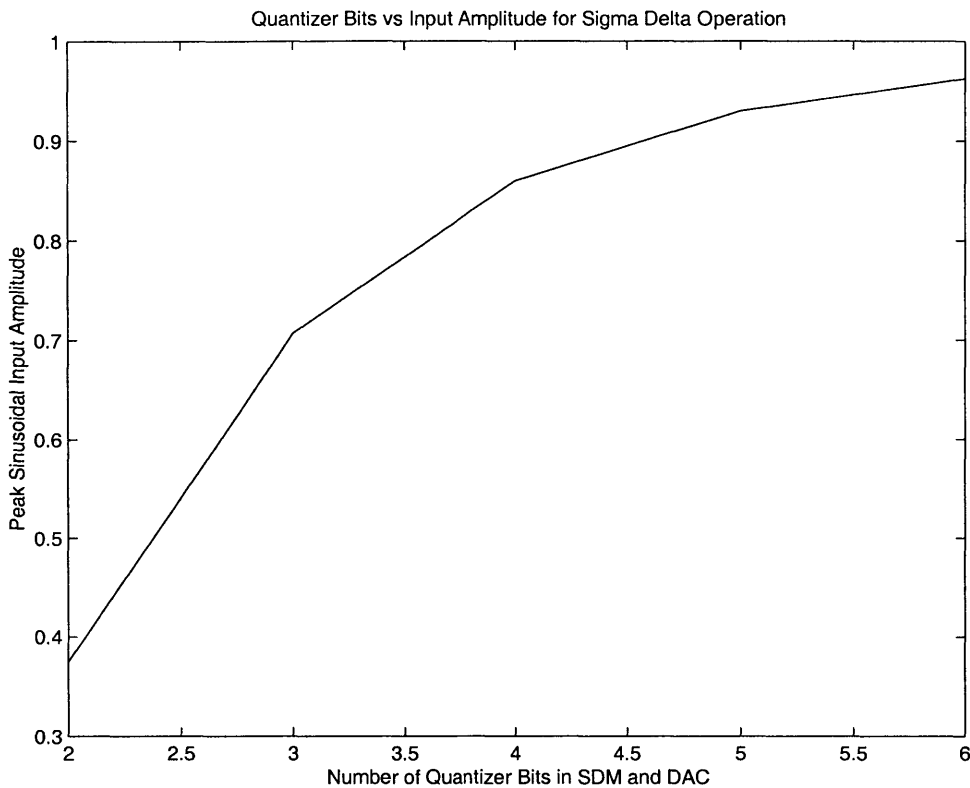
Figure 3-15: Maximum Amplitude of Input Sinusoid, as Fraction of Digital Full Scale

Fig. 3-16 below, with the coefficients **a1=1** and **a2=2**.

The oversampling ratio and number of quantizer bits B were chosen in conjunction with the following goals in mind:

1. Negligible sigma-delta quantization noise in the signal band.

2. Negligible additive noise due to clock jitter.

3. Good D/A converter signal swing to shift gain farther back in the D/A converter chain, hence reducing total output referred noise.

4. Low D/A converter area.
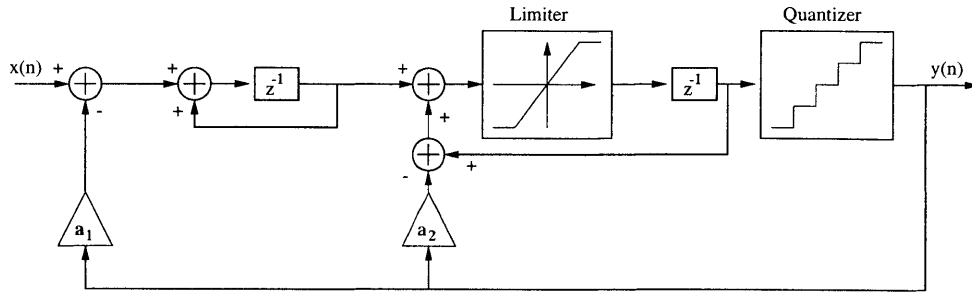
Figure 3-16: Behavioral Model of Second Order Sigma-Delta Modulator

OSR ·· Quantizer Bits	3	4	5
64	94.20dB	96.06dB	97.13dB
128	97.82dB	98.36dB	98.50dB
256	98.52dB	98.53dB	98.56dB

Table 3.2: Peak SQNR for Various OSR/Bit Combinations

To determine what combination of oversampling ratio and quantization bits would satisfy the first of these criteria, the peak D/A digital chain output-referred SQNR was simulated for the set of combinations shown in Table 3.2. These data were obtained from a full simulation modeling D/A components mismatched to 1.5% (to account for 6σ process variation) and the dynamic element matching circuitry used to linearize this D/A converter. The dynamic element matching circuitry is described in the following chapter.

It was found that for an oversampling ratio of 64, the SQNR was severely degraded due to a combination of in-band sigma-delta quantization noise and to a reduced effectiveness of the dynamic element matching linearization scheme. In addition, as noted in the following chapter, noise due to clock jitter is no longer negligible at an oversampling ratio of 64 for a worst-case yield scenario. From Fig. 3-15 it is also apparent that a 3-bit converter begins to significantly reduce the available signal

swing at the output of the sigma-delta modulator. (at the time of the sigma-delta modulator design, it was thought that this signal swing would even be too small to meet the overall signal swing requirements for a postfilter gain of unity). For a large OSR and number of quantization bits, the vast majority of the noise introduced by the sigma-delta modulator exists outside of the signal band, while the noise still in the signal band is negligible compared to the quantization noise introduced by the initial 16-bit and digital interpolation filtering quantizations.

Thus, a sigma-delta modulator with **OSR=128** and **B=4** was chosen to obtain a close to optimal in-band SQNR and good signal swing, with the minimal OSR and number of D/A converter components necessary to achieve this performance. Note that the numbers given in Table 3.2 are greater than that given in Fig. 3-8 because postfilter droop compensation in the interpolation filter chain magnifies the noise in the 10kHz-20kHz range, however, this noise is then attenuated by and equal amount by the postfilter droop.

The behavioral model of the resultant sigma-delta modulator design, in addition to the implemented version, accepts as its input the 16-bit output of the digital zero order hold multiplied by 1.625. The area and power consumed by this multiplication is minimal in that it consists of adding the 16-bit signal to itself, downshifted by 1 bit, and to itself again, this time downshifted by 3 bits. Since the sigma-delta modulator has an input bit width of 17 bits, this corresponds to an effective attenuation of the signal by 0.8125, but without introducing truncation noise. This is attenuation is necessary so as to allow a full scale signal from the interpolation chain to pass through the 4-bit sigma-delta modulator without causing the modulator to go into overload.

The performance of the digital interpolation chain terminated by the sigma-delta modulator and analog postfilter is shown in Fig. 3-17, where the magnitude of the

input sinusoid has been swept to obtain the output SQNR. Note that since this simulation was performed with the element mismatch and dynamic element matching behavioral code in place, the data on the graph represent worst-case results over several trials. This simulation was also performed with the analog postfilter in place and thus also takes into account the postfilter droop at higher frequencies, although this attenuation of noise is offset by the increase in passband noise due to the interpolation filter droop compensation. The peak SNR occurs for an input sinusoid at 0dB (by design) and falls off thereafter due to signal saturation in the 16-bit data bus.
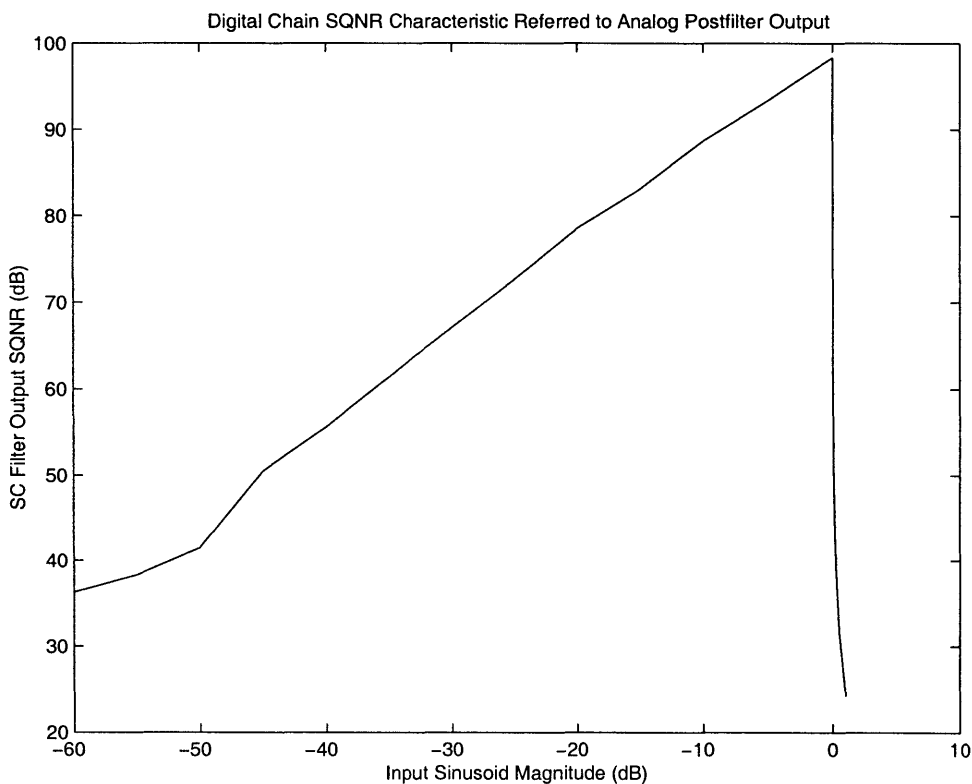
Figure 3-17: Simulated Postfilter Output-Referred In-band SQNR

The quantization noise spectrum at the output of the D/A converter, shown in Fig. 3-18 shows that in the signal band from 20Hz to 20,000Hz, sigma-delta quan-

tization noise is negligible compared to the initial 16-bit quantization noise. The waveform at the output of the D/A converter is also shown in Fig. 3-19.
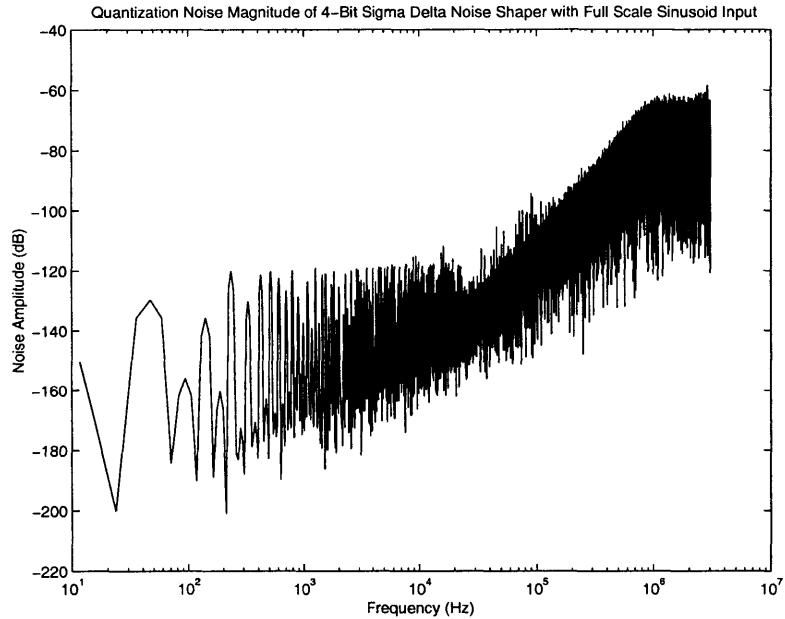
Figure 3-18: Quantization Noise Spectrum at Output of D/A Converter

The quantization noise spectrum at the output of the postfilter, shown in Fig. 3-20, shows that the sigma-delta quantization noise has been suppressed such that its power per unit frequency is approximately equal to that of the initial 16-bit quantization noise floor. As will be described in the next section, it is important to minimize sigma-delta quantization noise before the DT-CT interface to reduce the effects of sampling clock jitter.

The actual gate level implementation of this sigma-delta modulator is shown in Fig. 3-21. Note that the internal bit widths in the modulator are determined by the behavioral MATLAB implementation of the modulator, which keeps track of the largest digital number to appear at each integrator. Also, note that the adders in the

75
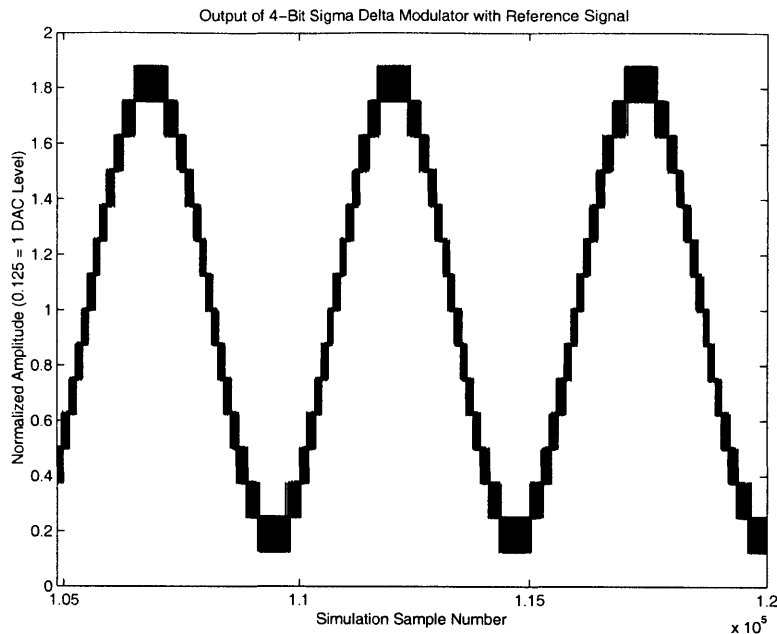
Figure 3-19: Waveform at Output of D/A Converter

circuit are implemented as ripple-carry adders, as the combinational logic available in the 0.25μm CMOS process was fast enough to allow such a slow adder implementation. The functionality of this circuitry was verified by running the transistor level simulation in the Spectre simulation environment alongside the behavioral simulation, where the MATLAB and C code of the latter had been ported to AHDL so as to run in the Spectre simulation environment. It was assumed that the critical path delay of the sigma-delta modulator was dominated by the adder performance and thus the critical path of the sigma delta modulator was found to be 6.5ns (0.226ns per adder block). Since the sampling period is 162.76ns, this speed of operation is more than sufficient.

In a 0.25μm process, the implementation shown in Fig. 3-21 consumes **0.257mW** of power for $B = 4$, $OSR = 128$, and for a full scale input sine wave. The sigma-delta modulator digital circuitry occupies approximately **0.0278mm²** of silicon die

area. In addition, one 15-bit adder and one 17-bit adder are required to perform the multiplication by 1.625. These adders consume approximately **0.0085mm²** of silicon die area and consume approximately **0.1mW** of power. One can expect the power consumption of this circuitry to increase linearly with *OSR*.

3.3.4 Alternative Architectures

Before concluding this discussion, it is appropriate to note that the cascaded sigma-delta modulator described above is not the only structure capable of realizing a noise shaping operation. In Fig. 3-22 below, an error feedback structure is depicted [16]. Using the same linear $\mathcal{Z}$-domain analysis used for the cascaded modulator, it can be seen that the transfer function from the input $x[n]$ to the output $y[n]$ is unity, while the transfer function from the quantizer to the output is equal to $G(z)$ Thus, choosing $G(z)$ to be $(1 - z^{-1})^L$ by choosing the appropriate combination of delay blocks and scaling coefficients for $G(z) - 1$ results in a transfer function identical to that of the cascaded structure.
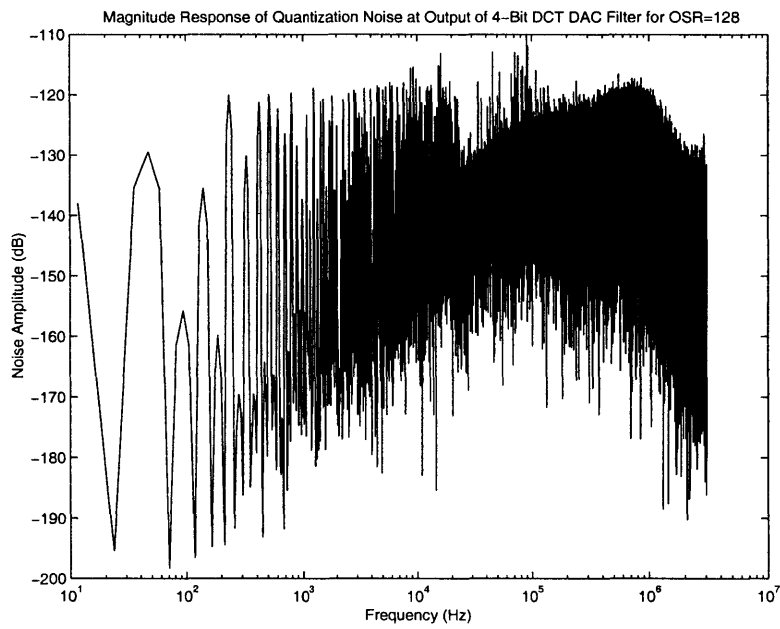
Figure 3-20: Quantization Noise Spectrum at Output of Postfilter
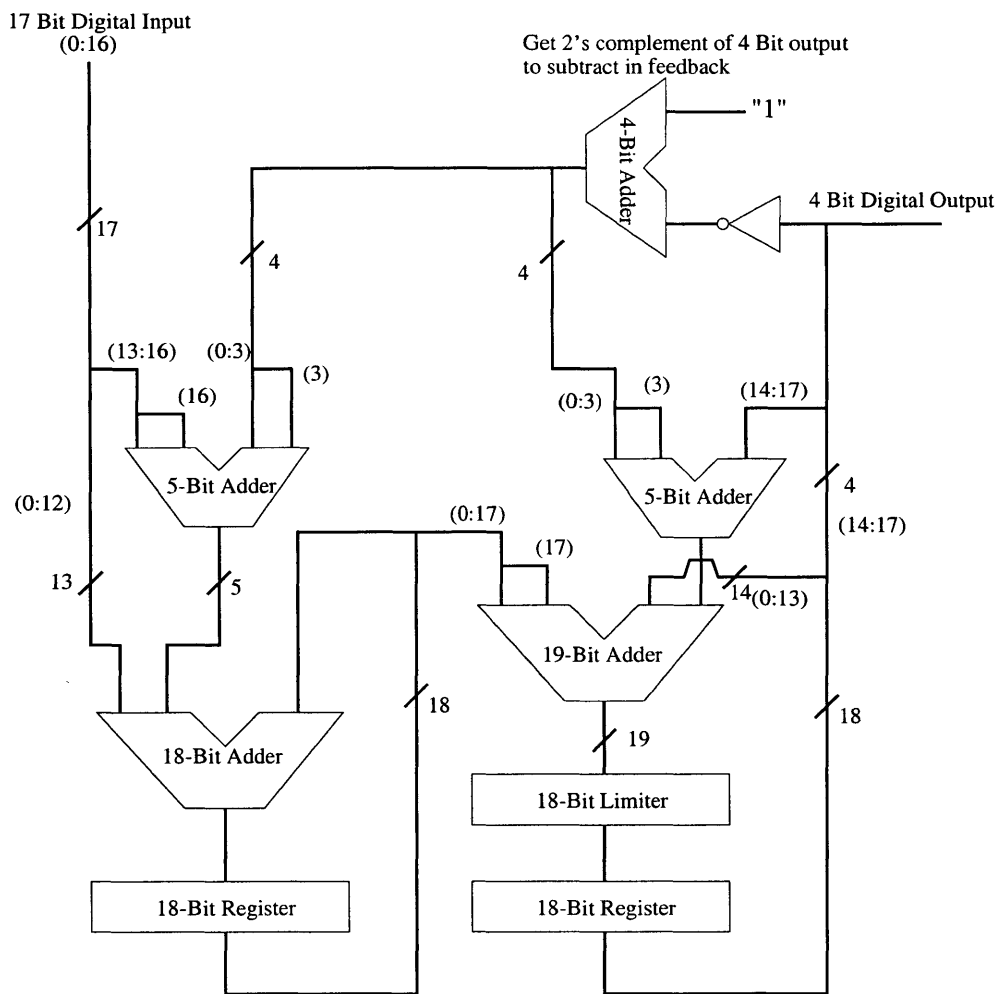
Figure 3-21: Gate Level Implementation of Second Order Sigma-Delta Modulator
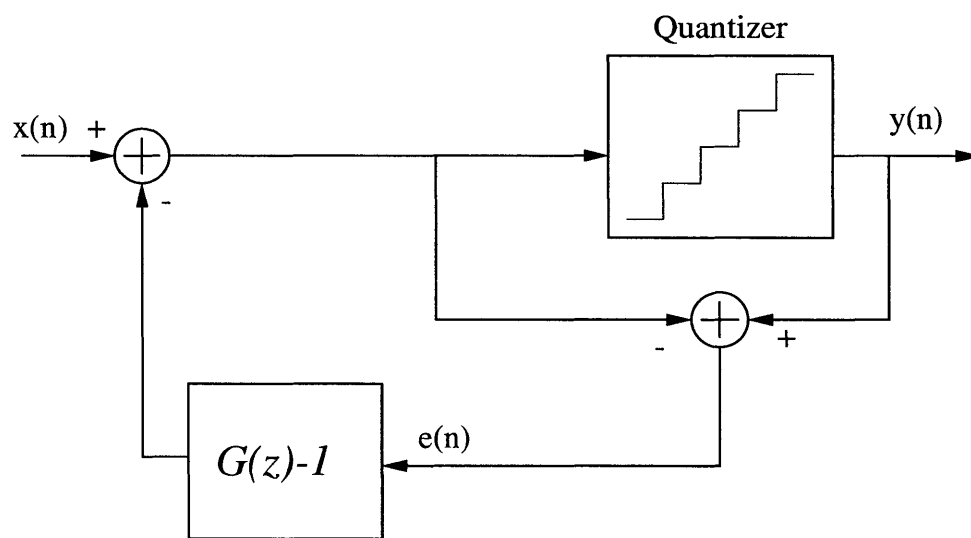
Figure 3-22: Error Feedback Modulator Structure

Chapter 4

Oversampled D/A Converter Topologies

Various literatures in the past have reported on the suitability of particular D/A architectures for low power applications[5][21]. The optimal architecture, however, may depend on a number of subtle requirements of the specific application. For example, the D/A converter described in this document is constrained by a number of unique factors.

The first of these is the requirement that the frequency response of the D/A converter and its analog postfilter scale in bandwidth automatically with the frequency of the incoming clock waveform. In order to optimize power usage, the D/A converter and its postfilter should operate only at the bandwidth required to produce the desired audio quality. Therefore, when the phone outputs voice quality audio, the bandwidth should be 4kHz, while music quality audio should have a bandwidth of 24kHz (although all noise measurements are specified over the 20Hz-20kHz band). The second requirement is that the output of the D/A converter chain postfilter be a voltage signal, implying that the output of any current-mode D/A converter be passed through an current-to-voltage converter. Finally, all of the DAC and post-

filter components must be implemented on-chip. As off-chip filtering introduces the possibility of external noise coupling and adds cost in the form of additional discrete components, it is undesirable in applications that demand good noise performance and low board space consumption.

4.1 Current-Mode Topologies

Current-mode D/A topologies generate an analog output waveform by using the digital sigma-delta modulator output to switch an array of current sources to either the D/A summing junction or to ground (or to the inverted summing junction in a differential implementation as shown in Fig. 4-1). Current mode architectures have become popular in many applications because the alternative, a switched-capacitor D/A followed by an integrated switched-capacitor postfilter has a severe tradeoff between the noise power, capacitor area, and power dissipation. [12] The rationale is that to achieve low kT/C noise in the postfilter, large capacitors are needed, consuming area. In addition, opamps with high output stage current, and hence higher power dissipation, are required to drive these larger capacitances [12]. It also has been reported that for D/A converters requiring bandwidths in the MHz range, current-mode converters provide superior dynamic performance over switched-capacitor topologies [5].

Current-mode converters also retain their share of disadvantages. For example, their current-mode output is susceptible to intersymbol interference [3], the condition in which the rise and fall times of the output waveform are not equal. When this is the case, the integral of the output waveform over a given output symbol's time period will be dependent on the value of the previous symbol. Often, this drawback requires particular attention in the design of the output elements [12] in order to avoid serious distortion in the output waveform. In addition, attention must be paid

**Current - to-Voltage
Conversion**
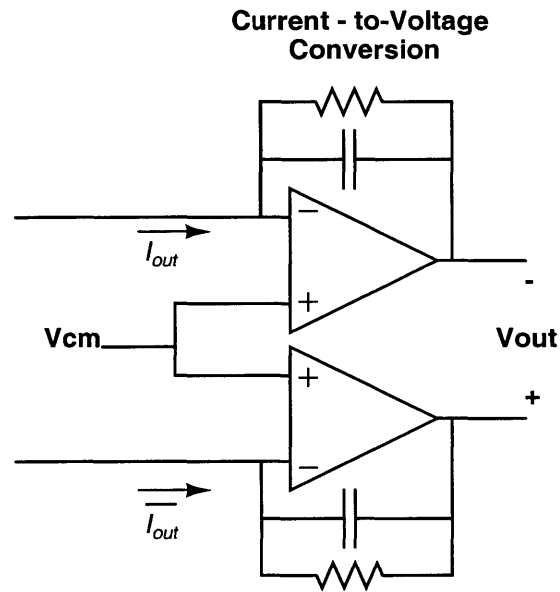
Figure 4-1: Fully Differential Current to Voltage Conversion with Filtering

to the current routing such that the output of the current source always has a path to the output or ground. If the switching of the current source output is done such that both switches might be off at the same time, charge will build up at the drain of the current source cascode, resulting in a transient when the current source outlet is opened again [5].

4.1.1 Calibrated Current-Mode Topologies

As stated in the previous chapter, multibit D/A topologies are desirable in that they follow from the use of a multibit sigma-delta modulator, which has improved quantization noise, distortion, jitter, and stability properties over its single-bit counterpart. The only drawback is that the mismatch of the elements of the D/A array, which left untreated would result in a converter resolution of 8-10 bits, must somehow be made negligible or irrelevant.

For applications in which Dynamic Element Matching, the alternative linearization method to be discussed later in this chapter, is not feasible, such as those which cannot support the high oversampling ratio required for DEM to be effective, calibration techniques present an attractive alternative. A calibrated current-mode topology consists of an array of $2^B + 1$ switched current sources, whose routing switches accept as their inputs the thermometer-encoded output bits of the B sigma-delta modulator outputs. Each array element appears as shown in the simplified schematic below in Fig. 4-2 and consists of both a fine current source and a coarse current source. The coarse source will be biased such that its output is some fraction $1 - k$ of a reference current I_{ref} where k is typically less than 0.2. Of course, each of these coarse current sources will be mismatched to the effect of 8-10 bits.

The fine current source is dynamically biased to conduct the difference of the coarse current source and I_{ref}. Thus, on average, a fine current source will conduct kI_{ref} immediately after dynamic biasing, or *calibration*. For each of the $2^B + 1$ cycles of operation, one of the array elements is taken out of the array of 2^B functioning elements to be calibrated. Taking its place will be the element that has just been calibrated. During calibration, switch S2 will close and a reference current I_{ref} will be forced into the parallel combination of the coarse and fine current sources. $(1 - k - \text{mismatch})I_{ref}$ will flow into the coarse current source, while the remainder flows into the fine current source, which is diode-connected in this configuration. Based on the current flowing through it, a voltage develops on the gate-source capacitance of the fine current source such that when the array element is taken out of the calibration configuration, the voltage remains on the gate of the fine current source. Since this voltage remains roughly the same over the cycle of operation in which the element is part of the D/A array, the overall element will conduct an amount of current very close to I_{ref}.
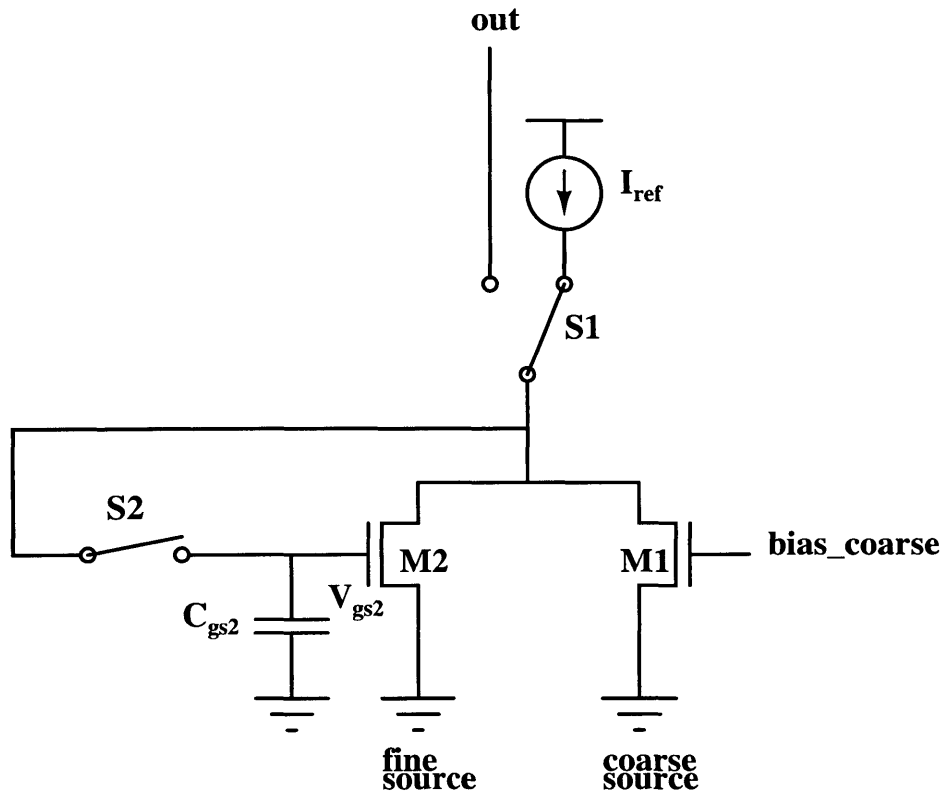
Figure 4-2: Calibrated Current-Mode DAC Element

One benefit of the current mode calibration scheme is that since the current source elements are recalibrated at a relatively fast rate, low frequency component noise is eliminated by the calibration process. This means that current source $1/f$ noise is eliminated to a first order approximation.

One limiting factor on this topology is how well the gate capacitance of the fine current source can hold its charge between calibration cycles. The switches which place the fine current source into a diode configuration in the calibration phase contain parasitic diodes from their drains to bulk which bleeds leakage current from the gate capacitance when turned off. Thus, it is desirable to keep these switches as small as possible to minimize the diode area. According to Wouter, et al., a typical value for

this leakage current would be on the order of [21]:

$$I_{leak} = 0.01 W_{switch} L_{diff} A \qquad (4.1)$$

Assuming that the calibration of a current source is done at time t=0, the gate voltage equals:

$$V_{gs,leak} = V_{gs,0} - \frac{I_{leak}}{C_{gs}} t \qquad (4.2)$$

at any given time t until the next calibration cycle.

Another source of nonideality between array elements is charge injection from the switches used to diode-configure the fine current sources. Although charge-cancelling techniques can be used to lessen the effect of charge injection, in general about 1/10th of the channel charge will still end up on the gate of the fine current source MOSFET. In addition, it is reasonable to assume that for such a switch, the charge injected from the switch will be mismatched on the order of 10%. This switch should be a CMOS transistor to avoid threshold voltage effects, and the PMOS and NMOS transistors should be sized the same so that their channel charges cancel to a large extent upon switch turn-off.

Thus,

$$\Delta q_{ch} = 0.1 \cdot \frac{C_{ox} W_{switch} L_{switch} V_{eff,switch}}{10} \qquad (4.3)$$

$$\Delta V_{gs,q} = \frac{\Delta q_{ch}}{C_{gs}} \qquad (4.4)$$

The changes in the gate voltage of the MOSFET are transformed into changes in the fine current source drain current by its transconductance. Thus, we would like to

design the transconductance of this device to be very low.

$$I_{ds,q} = I_{ref} - g_m \frac{\Delta q_{ch}}{C_{gs}} \tag{4.5}$$

$$I_{ds,leak} = I_{ref} - g_m \frac{I_{leak}}{C_{gs}} \Delta t \tag{4.6}$$

Noting that for the bottom transistor in the fine current source:

$$C_{gs} = \frac{2}{3} W L C_{ox} \tag{4.7}$$

and that

$$g_m = \sqrt{2\mu_p C_{ox} \frac{W}{L} k I_{ref}} \tag{4.8}$$

It is possible to substitute and obtain

$$I_{ds,q} = I_{ref} - \frac{3}{2}\sqrt{\frac{2\mu_p}{C_{ox}}} \frac{\Delta q_{ch}}{L} \sqrt{\frac{k I_{ref}}{WL}} \tag{4.9}$$

$$I_{ds,leak} = I_{ref} - \frac{3}{2}\sqrt{\frac{2\mu_p}{C_{ox}}} \frac{1}{L} \sqrt{\frac{k I_{ref}}{WL}} I_{leak} \Delta t \tag{4.10}$$

If we want to retain close to N bit baseband resolution in the output signal while maintaining most of the noise budget for component noise in the postfilter, it would be desirable to have $N + 2$ bit matching guaranteed between each of the array elements. That is, the maximum deviation of the current source element will be kept to $\frac{I_{ref}}{2^{N+2}}$.

Dividing both sides by I_{ref} yields:

$$\frac{\Delta I_{ref}}{I_{ref}} = \left(\frac{3}{2}\sqrt{\frac{2\mu_p}{C_{ox}}} \sqrt{\frac{k}{I_{ref}WL}} \right) \left(\frac{\Delta q_{ch}}{L} + \frac{1}{L} I_{leak} \Delta t \right) \tag{4.11}$$

With the aid of the above equations in spreadsheet form, a current source array

with 16 elements ($B=4$), W=15μm, L=150μm, C_{ox}=0.006384$\frac{F}{m^2}$, μ_p=0.0064223$\frac{A}{V^2}$, k=0.2, 2^B=16, and with a minimum sized calibration switch of W=0.5μm, L=0.25μm, and V_{eff}=0.5V was designed. Note that for these parameters, the time constant of the fine current source transistor is given by:

$$\tau = R_{switch}\frac{2}{3}WLC_{ox} \qquad (4.12)$$

The resistance of this switch can be calculated as [32]:

$$R_{switch} \approx \frac{2V_{dd}}{k_n(V_{dd} - V_{th,n})^2 + k_p(V_{dd} - |V_{th,p}|)^2} = 26.6k\Omega \qquad (4.13)$$

Since 18 bits of component accuracy are desired over the operation of the converter, the gate voltage of the fine current source should settle to about 20 bit accuracy, meaning that the calibration period for each element must be 14τ=3.6μs and that the time in between calibration periods Δt is 57.6μs. Thus, the total current $16I_{ref}$ required to guarantee the aforementioned matching criterion would be 0.36μA, resulting in a power dissipation of 0.89μW and a transistor area consumption of 0.041 mm^2 even prior to any postfiltering.

It turns out, however, that thermal noise considerations prevent the implementation of a current source array with such a small total output current value. The thermal noise voltage power referred to the output of the I-V converter following the current source array is given by:

$$\overline{V_{n,T}}^2 \approx 4kT\frac{2}{3}g_{m,total}R_{out}^2 \qquad (4.14)$$

$$R_{out} = \frac{1.6V}{I_{out,total}}\Omega \qquad (4.15)$$

$$\overline{V_{n,T}}^2 \approx \frac{4kT\frac{2}{3}2.56\sqrt{2\frac{W}{L}_{total}\mu_pC_{ox}}20000}{I_{out,total}^{3/2}} \qquad (4.16)$$

where items denoted as *total* represent the composite value of the referenced quantity for the entire current source array. Since the majority of the current flows through the coarse current sources, the W/L and g_m quantities in Equations 4.14 and 4.16 will be assumed to belong to them. Further assuming that the lengths of the transistors are limited by layout considerations to be on the order of 250μm, the minimum achievable composite W/L ratio for $B=4$ is 0.032. For a reasonable thermal noise voltage power of $2 \cdot 10^{10}V^2$, the total output current is required to be 2.76μA.

In terms of postfiltering for the calibrated current mode topology, there are two options. The first option is to integrate the I-V conversion into an active-RC postfilter as shown in Fig. 4-1. This option presents a problem in that the single ended swing required is 1.6V. Since the current is already given as 2.76μA, this calls for a resistor of size 0.58MΩ. Since the -3 dB frequency of the postfilter must be scalable down to 4000Hz, two 68.2pF capacitors are required. Such large resistors generate a thermal noise voltage power of $2 \cdot 4kTRf_0 = 3.8 \cdot 10^{-10}V^2$. When combined with the thermal noise of the current source array, a composite noise approaching the limit of the analog component noise budget is produced.

In addition to these noise sources, the 1/f and thermal noise contributed by the I-V opamps and the components comprising the second order of postfiltering have yet to be considered. In order to reduce the opamp 1/f noise, the transistors of the input stage must be made large, which results in the addition of large load capacitances (seen through the I-V feedback network) to the opamp, requiring a large power dissipation at the output to drive. Finally, the I-V resistors consume a 0.05mm^2 of die area while the capacitors consume 0.14mm^2, which is a considerably large area consumption considering that another order of postfiltering must be implemented on-chip. Increasing the output current reduces the amount of thermal noise generated by the D/A current source array and the I-V resistors, however, the requirement that the

system produce a pole at 4000Hz constrains either R or C to be rather large. Most reported works solve this problem by implementing any active-RC filtering off-chip.

The second postfiltering option is to perform differential I-V conversion followed by either a switched capacitor second order postfilter or some efficient second-order Sallen-Key filter. The first of these techniques offers the advantage that the post-filter bandwidth will scale automatically with clock frequency and requires no clock frequency detection scheme to know when to alter its bandwidth. However, either case requires a large number of opamps or capacitors and is hence not optimal from a low-power, low area perspective.

4.1.2 Current Mode with Dynamic Element Matching

An alternative to calibration as a linearization scheme is the use of Dynamic Element Matching. Many reported schemes for achieving dynamic element matching have been reported [22][23][24] and some of these techniques will be discussed in detail later in this chapter. For now, it is sufficient to argue the functionality of DEM by claiming that if the output elements used in a given output symbol are chosen at random, the total mismatch of the elements used at that time will also be random and can be modeled as a pseudorandom white noise process. We will also assume for the time being that this "noise" is negligible compared to the in-band noise introduced by the initial PCM quantization provided that a certain level of mismatch is achieved through proper sizing and biasing of the current sources.

In general, a current mode topology utilizing dynamic element matching uses an array of nominally identical current sources that accepts the thermometer encoded and randomly scrambled output of the sigma-delta modulator as inputs to its routing switches. Like the current-calibrated topology, an I-V conversion is required in

addition to postfiltering. Below, we will analyze the feasibility of implementing this topology on-chip.

Suppose that a B-bit sigma-delta modulator is used. Then the output array requires 2^B current sources. The relative mismatch error of a current source is given by [25]:

$$\frac{\sigma I_{out}}{I_{out}} = \sqrt{\frac{4\sigma_{vt}^2}{(V_{gs} - V_{th})^2} + \left(\frac{\sigma\beta}{\beta}\right)^2} \qquad (4.17)$$

Where σ_{vt} is the threshold voltage variation and $\sigma\beta$ is the variation in the quantity $\beta = \frac{W}{L}\mu_p C_{ox}$. These quantities are dependent on the process, and for the purposes of this project can be given as:

$$\sigma_{vt} = \left(\frac{5 \cdot 10^{-6}}{\sqrt{WL}} + 0.1316\right) \cdot 0.001 \qquad (4.18)$$

$$\frac{\sigma\beta}{\beta} = \left(\frac{0.71 \cdot 10^{-6}}{\sqrt{WL}} + 0.0231\right) \cdot 0.01 \qquad (4.19)$$

Note that for the threshold voltage expression, which is the dominant term in the relative mismatch equation, the current source transistor width terms cancel out, leaving the relative mismatch inversely proportional to the square root of the individual transistor output current and inversely proportional to the transistor length.

MATLAB simulations show that for 6σ process mismatch variation and for a sampling rate of f_s=6144000Hz, the relative mismatch must be less than or equal to $4.16 \cdot 10^{-3}$. It turns out that if the lengths of the transistors are made large enough, this number can be easily met even for very low output currents. Of course, we want to take the overdrive voltage V_{eff} of the transistor to be as large as possible while keeping all devices in the current source array in saturation.

Although meeting mismatch specifications is easy in this case, there is no inherent mechanism that cancels the 1/f noise generated by the transistor connected to small signal ground in the cascode current source. The gate-referred 1/f voltage noise power of a PMOS transistor integrated over the audio bandwidth is given by the expression:

$$\overline{V_{n,1/f}}^2 = \int_{20}^{20000} \frac{K_p}{WLC_{ox}f^{1.2828}} \tag{4.20}$$

$$\overline{V_{n,1/f}}^2 = \frac{1.3K_p}{WLC_{ox}} \tag{4.21}$$

Since the current noise is of interest here, we must multiply the voltage noise by the square of the total transconductance of the current source array:

$$g_m^2 = 2\mu_p C_{ox} \frac{W}{L} I_{out,element} 2^B \tag{4.22}$$

Finally, the output current noise must pass through a differential I-V converter. Since all of the output current sources are either passing through the positive or negative branch, we can sum all of their output noise current powers and multiply them by the square of the I-V converter output resistance, which is $\frac{1.6V}{I_{out,total}}\Omega$, where:

$$I_{out,total} = 2^B I_{out,element} \tag{4.23}$$

When combined with the expression for thermal noise in Equation 4.16, the output-referred noise voltage power of the current sources is given by:

$$\overline{V_{n,cs}}^2 = \frac{2 \cdot 1.3 \cdot 2.56 K_p \mu_p}{I_{out,total} L^2} + \frac{4kT\frac{2}{3}2.56\sqrt{2\frac{W}{L}_{total}\mu_p C_{ox}}20000}{I_{out,total}^{3/2}} \tag{4.24}$$

Given that: $K_p = 1.183 \cdot 10^{-23} V^2 F$, W=0.5$\mu$m, $L = 250\mu$m, $I_{out,total} = 2.79\mu$A, the output rms noise voltage power is: $2 \cdot 10^{-10} V^2$, which is an acceptable figure

for component noise outside of the postfilter, although the 1/f noise from the I-V converter opamps is likely to be much more substantial unless the input devices are made to be very large, which increases the feedback loads, and hence the power dissipation of the opamps. In addition, like the current source calibration technique, this topology must utilize either an area and noise intensive active-RC filter to implement one order of postfiltering or a switched-capacitor filter. Thus, the same disadvantages seen by the previous topology with respect to noise and area consumption apply and this topology can likewise be judged noncompetitive for the goals set forth in this project.

4.1.3 Current Mode Semidigital Filter

Instead of explicitly separating the digital and analog sections of a D/A converter, the current-mode semidigital filter architecture seeks to lift some of the burden from the analog postfiltering circuitry by shifting some of the filtering operation prior to the D/A conversion but after the sigma-delta modulator, as shown in Fig. 4-3.
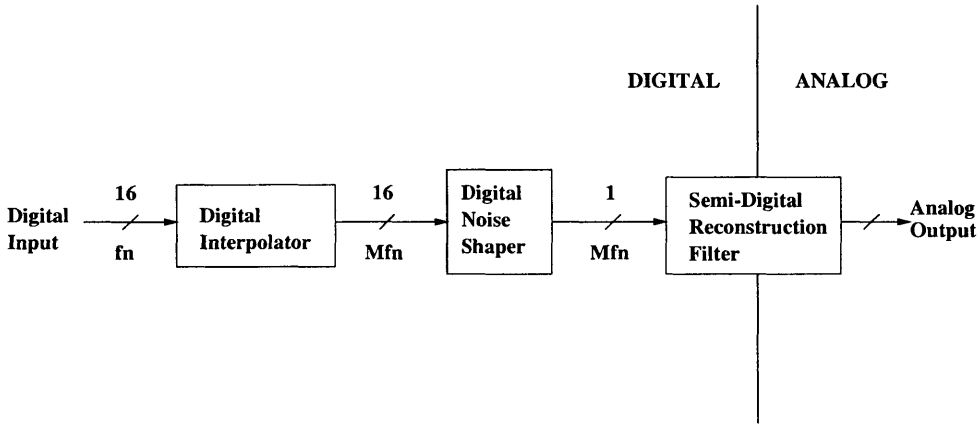
Figure 4-3: Current Mode Semidigital Filter Block Diagram

This filtering operation is performed with the use of a single-bit sigma-delta mod-

ulator, whose output is fed to a shift register. As shown in Fig. 4-4, the outputs of the shift register control the routing switches for an array of weighted current sources. The weights a_n of the current sources comprise a first-order lowpass FIR filter and correspond to the relative W/L ratios of the current source transistors. These weights can be easily generated in MATLAB using either the Remez algorithm [26] or the frequency sampling method [27]. The current-mode output is then passed through a current-to-voltage converter and another order of low-pass filtering. Since an FIR filter is inherently linear, the D/A conversion process suffers no degradation in integral or differential nonlinearity as a result of current source coefficient error. However, errors in the filter taps will result in a degradation in phase linearity and maximum stopband attenuation.

One advantage that this topology offers over the two previous implementations is that the DT-CT interface is separated from the D/A interface. This allows discrete-time postfiltering to be applied prior to the DT-CT interface, reducing jitter noise due to clock waveform nonidealities.

Despite only requiring one order of purely analog postfiltering, this topology also suffers from similar noise-area tradeoffs as the previous two current-mode topologies described. Because approximately 100 filter taps are required to achieve a filter rolloff comparable to a first-order continuous-time filter, the lengths of the current sources are constrained to be on the order of 20μm so that an array of them can fit neatly onto the chip. Keep in mind that associated with each current source is a shift register delay element, which can take up a considerable amount of area in addition to the area of the current source transistor. Given this constraint on device length, we calculate the noise introduced by the current sources using Equation 4.24 and the process parameters given earlier in this section. Assuming that the minimum sized width available were used to minimize thermal noise, the total W/L ratio for the
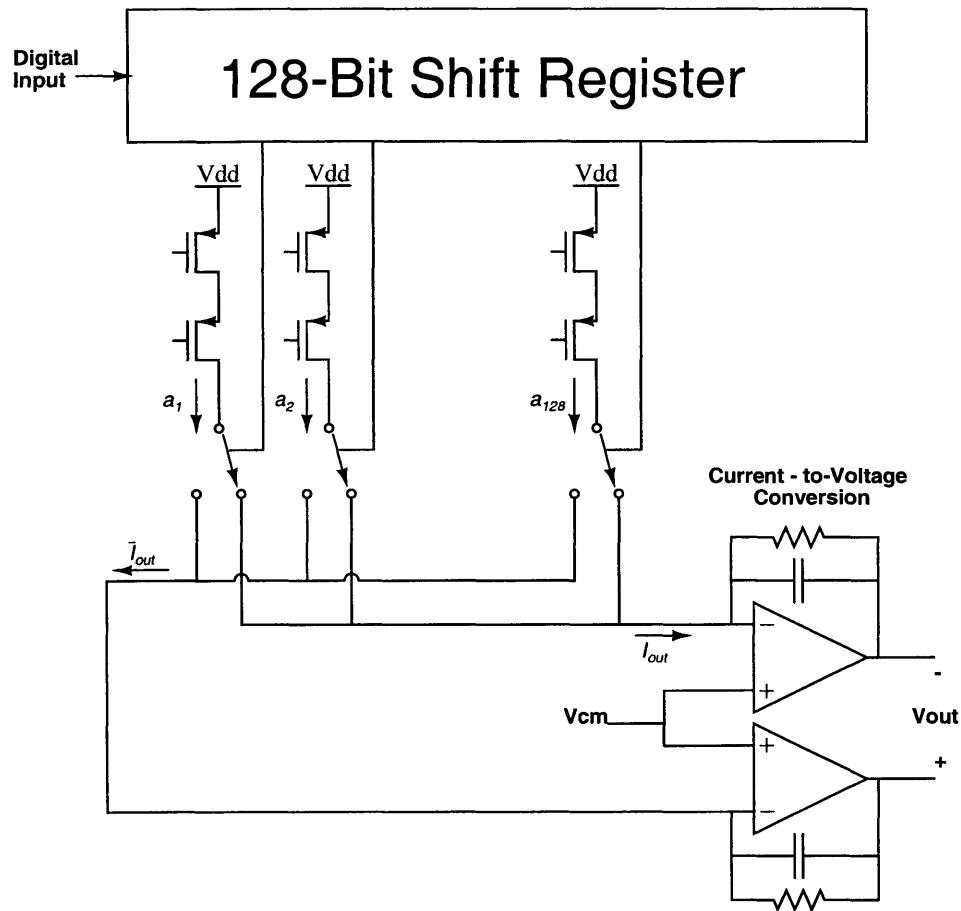
Figure 4-4: Current Mode Semidigital Filter

current source array would be 120.3.

Using Equation 4.24 reveals that a total output current of about 40μA yields a noise voltage power of $2.2 \cdot 10^{-10}$V^2. This number is more significant than those noise power quantities found earlier in this section considering that the component noise budget is now smaller due to the fact that a 1-bit sigma-delta modulator must be used with this topology. Of course, this level of full scale current necessitates a 40kΩ resistor in the I-V converter and hence a very large 1nF capacitor if a composite filter/I-V converter is used. The alternative is to use a first-order switched-capacitor

filter as a postfilter, but this will also consume a good amount of power and area in addition to the area already consumed by the layout of the current source array.

4.2 Switched-Capacitor D/A and Postfilter Topologies

Switched-capacitor D/A converters function on the principle of charge distribution. In general, a switched-capacitor D/A converter consists of a bank of weighted or unit-sized capacitors that sample one of two reference voltages then integrate the resultant net charge onto an opamp feedback capacitor. One advantage of switched-capacitor D/As is that switched-capacitor network theory is well-developed and many of its concepts are directly applicable to switched-capacitor D/A converters. Another key selling point is that a switched-capacitor D/A converter can be integrated easily into a switched-capacitor postfilter by breaking up the input capacitor into a bank of weighted or unit-sized capacitors. Thus, no special conversion is required to interface the DAC to the postfilter, as proved to be a constraint in the current-mode topologies. If this is the case, then postfiltering can be performed before the DT-CT interface, removing the out-of-band quantization noise that can increase the effect of clock jitter.

Although switched-capacitor topologies face a tradeoff between noise, power, and area due to the kT/C noise relation [12], it can be shown that this tradeoff is not as severe as those described for monolithic current-mode converters. In addition, switched-capacitor techniques exist to reduce or nullify other sources of component noise. For example, the correlated double sampling technique[28] can eliminate the input-referred 1/f opamp noise in a switched-capacitor setup.

Interestingly, it can be noted that, in general, switched capacitor noise is proportional to $\frac{4kTf_0}{Cf_s}$ [29] Also, if the power dissipated in the opamps in the switched-

capacitor network is determined by the load capacitance and phase margin consid-erations, $\frac{g_{m,outputstage}}{C_{load}} \propto f_s \to I_{out} \propto \frac{V_{eff}}{2} C_{load} f_s$. Given these two relations, it can be seen that if the sampling rate is increased, the kT/C noise remains constant if the load capacitances are decreased proportionally. If this is done, then power consumption in the opamp output stages remains roughly constant. Thus, there is no major tradeoff between the oversampling ratio of the switched capacitor topology and its power dissipation. However, as we will see in the following chapter, area consumption increases with the oversampling ratio.

4.2.1 Calibrated Switched-Capacitor Topology

The calibrated switched-capacitor D/A converter topology [30] in Fig. 4-5 achieves analog correction of sampling capacitor mismatch using the calibration technique de-scribed below.
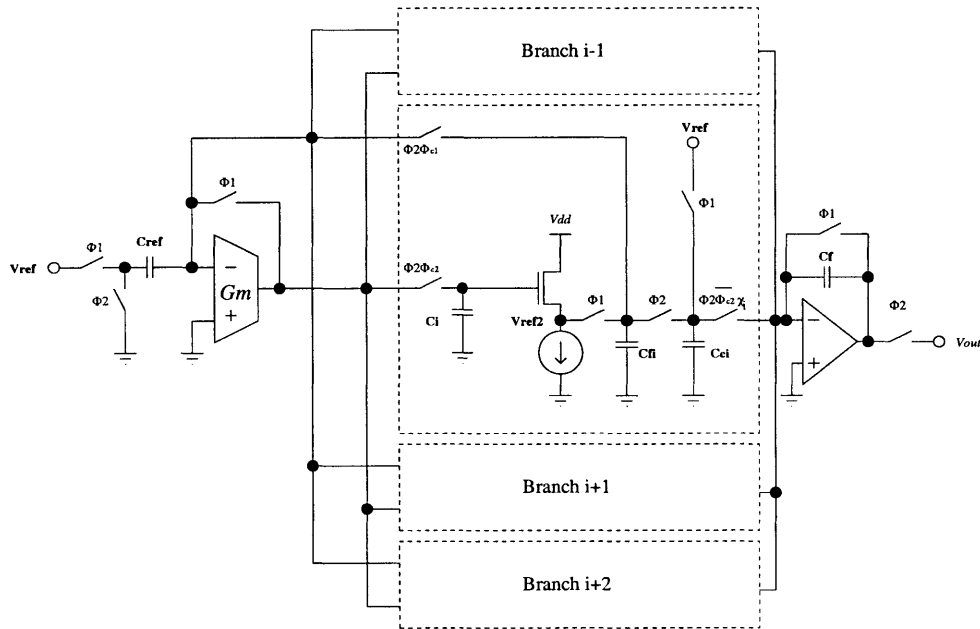
Figure 4-5: Switched-Capacitor Calibration Technique

Each branch i of the D/A converter contains a coarse input capacitor C_{ci}, which can deliver a charge $C_{ci}V_{ref}$ into the feedback capacitor, and a fine input capacitor C_{fi}, which can deliver a charge $C_{fi}V_{refi}$, where V_{refi} is an adjustable DC voltage. During the reset phase Φ_1, all input capacitors are charged to their reference voltages: C_{ci} to V_{ref} and C_{fi} to V_{refi}. Next, during the conversion phase Φ_2, both capacitors C_{ci} and C_{fi} are discharged into C_f if $x_i=1$, signaling that the cell is selected for output by the thermometer-encoded DAC output.

To correct for the mismatch between the input capacitors, the calibration stage shown above in Fig. 4-5 is connected to each of the unit elements one at a time, readjusting each reference voltage V_{refi} once per calibration cycle such that the combined charges stored in C_{ci} and C_{fi} iterate ever closer to $C_{ref}V_{ref}$. To replace the branch being calibrated at any given time while maintaining full input range, an additional output unit above the number needed to converter the output of the thermometer-encoder also needs to be added to the DAC array.

While the calibration routine of this topology avoids the need for large amounts of digital dynamic element matching circuitry, it adds another static-power consuming amplifier (in this case, a transconductor) to the overall topology in addition to requiring one current source per cell, potentially dissipating a significant amount of power for a 4 or 5-bit sigma-delta modulator. Also, this topology is subject to mismatched charge injection error from the switches used in the calibration process. It can be shown, however, [30] that errors due to switch mismatch will be at least 90dB below the input signal level for reasonable process parameters.

Further modifications to this topology may also be implemented, including adding correlated double-sampling techniques to correct 1/f noise, offset, and finite opamp gain nonidealities. Switched-capacitor filtering circuitry may also be added to the

integrating opamp to realize out-of-band noise attenuation with fewer opamps.

One possible limitation in this technique lies in the switched-capacitor noise from the coarse and fine sampling capacitors. Unlike most other charge-redistribution DAC topologies, not all of the sampling capacitors are connected to the opamp summing node on the integration phase of the clock cycle. This is due to the nature of the switched-capacitor calibration topology, in which the calibration routine seeks to calibrate the effective charge released by each DAC sampling element rather than the effective capacitance. Because of this, the sampling capacitors do not necessarily all join with the other sampling capacitors on the integration phase of operation.

Therefore, it is necessary to consider sizing the sampling unit capacitors based on the scenario that only one capacitor, and hence the minimum capacitance, is connected to the opamp summing node. However, the gain from the sampling capacitor to the integrating capacitor must be $\frac{1}{2^B}$, where B is the number of output bits in the sigma-delta modulator. To see why, assume that all 2^B sampling units were connected to the summing node. In this case, the opamp must send a charge of $2^B C_{ref} V_{ref}$ through the integrating capacitor. In order for the opamp to have a maximum output of V_{ref}, the integrating capacitor must have a value of $2^B C_{ref}$. In addition, when multiple sampling capacitors are connected to the summing junction, there exists a capacitive division equal to the number of sampling capacitors. Thus, at any given time, the kT/C noise voltage power at the output is equal to:

$$\overline{V_{n,kT/C}}^2 = \frac{2 \cdot 4kTf_0}{2^{2B} f_s C_{unit}} \qquad (4.25)$$

For $B = 4$, $f_s = 6144000$, $f_0 = 20kHz$, and $C_{unit} = 75fF$, the output referred noise is $2.4\mu V_{rms}$, which is a very manageable quantity. This is the case only because the gain from each unit capacitor to the output is so low. If it were the case that this calibration apparatus were integrated onto a switched-capacitor filter, the gain

seen to the output would be one or greater, necessitating a greater unit capacitor size.

Although kT/C noise seems to impose little constraint on the sampling capacitor size, fixed charge error from the switches in the calibration routine will. For example, the holding capacitor C_i must hold an amount of charge equal to $C_i(V_{refi} + V_{thresh})$ in order for unit element i to be perfectly calibrated, where V_{refi} is assumed to be the voltage required to be placed on C_{fi} in order to offset the charge error $C_{ref}V_{ref} - C_{ci}V_{ref}$.

As in the current-calibrated case, the charge held on this capacitor is subject to nonidealities [21]. First, leakage current present at the parasitic diode at the drain of the switch connecting to the capacitor causes the voltage V_{refi} to drop. In addition, mismatch in the clock feedthrough of the switch alters V_{refi} and degrades the linearity of the converter. The magnitude of these errors can be reduced by making C_i (the calibration charge holding capacitor) larger and by decreasing the ratio of C_{fi}/C_{ci}.

In order to maintain the SNDR of the D/A converter to an effective resolution of N bits, it is desirable to retain $N + 2$ bits of linearity in each unit element to leave a considerable budget for the component noise that will be introduced in any analog postfiltering that is done. This means that for $N = 16$, all output charges must be accurate to $(3.8 \cdot 10^{-6})C_{ref}V_{ref}$.

Choosing D/A converter capacitances as: $C_{fi} = 75fF$, which is the minimum sized capacitor, $C_{ref} = 250fF$ $C_{ci} = 0.95 \cdot, C_{ref}$, and $C_i = 0.35pF$.

Also, the switch to C_i is chosen to be minimum sized, that is, $W = 0.5\mu m, L = 0.25\mu m$, with a process-dependent diffusion length of $L_{diff} = 1\mu m$, and assuming the maximum overdrive voltage on the switch is about 0.5V, we can write:

$$I_{leak} \approx 0.01 W_{switch} L_{diff} \qquad (4.26)$$

$$\Delta q_{ch} \approx \frac{C_{ox} W_{switch} L_{switch} V_{eff,switch}}{10} \cdot \text{charge mismatch} \qquad (4.27)$$

where charge mismatch between switches is on the order of 10%.

$$\Delta V_{ref,q} = \frac{\Delta q_{ch}}{C_i} \qquad (4.28)$$

$$\Delta V_{ref,leak} = \frac{I_{leak}}{C_i} \Delta t \qquad (4.29)$$

where Δt is the time in between calibration refreshes for each unit element. For $B = 4$ and a calibration time per element of $0.2\mu s$, $\Delta t = 3.2\mu s$, and the relative maximum charge error is therefore:

$$\frac{C_f(\Delta V_{ref,q} + \Delta V_{ref,leak})}{C_{ref} V_{ref}} = 3.43 \cdot 10^{-6} \qquad (4.30)$$

for $V_{ref} = 1V$.

Although the unit fine sampling capacitors can be minimum sized, the fact that they have to be a certain fraction of the coarse sampling capacitors means that the integrating opamp has to drive a peak total capacitance of 5.2pF in addition to the load of the switched-capacitor biquad filter. In addition, the total capacitance required by a differential implementation is 26.8pF, a substantial number given that the mismatch calculations above were generous. This total capacitance was calculated assuming that the size of the integrating capacitor is sized such that the integrating voltage gain is 2 to achieve the required voltage swing. Considering that this D/A converter block already consumes a large amount of static power to drive the 5.2pF capacitance and 26.8pF of capacitance die area before even performing any postfiltering suggests that this topology will not be power and area competitive with topologies

to be described.

4.2.2 Pseudo-Passive Serial D/A Converter

Unlike most oversampling multibit D/A converters, this topology accepts a serial input of bits in binary representation [31]. The two-capacitor DAC, shown in Fig. 4-6, functions by first discharging its two capacitors, followed by a sequence of B cycles (where B is the number of bits from the output of the sigma-delta modulator) in which C_{11} is first charged to either V_{ref} or 0 according to the kth bit of the current word $x(n)$, and is then connected in parallel with C_{12} to facilitate charge sharing.
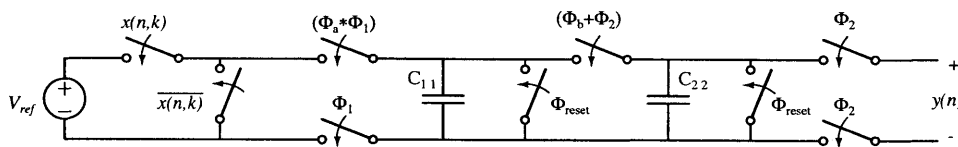
Figure 4-6: Pseudo-Passive Serial D/A Converter

An important feature of the two-capacitor DAC is that its symmetry makes it insensitive to clock feedthrough and charge injection errors. In addition, its symmetry provides motivation for techniques that can move the static mismatch between the two capacitors to higher frequencies. Since the roles of C_{11} and C_{12} can be changed any time that they are connected in parallel, they can be swapped in such a way that an arbitrary-order differentiation is performed on the mismatch error between the two capacitors, effectively noise-shaping much of this error out of the signal band. For example, a first-order mismatch differentiation is performed by preceding the D/A converter with a digital zero-order hold that multiplies the clock rate by a multiple of two such that the input sequence to the D/A converter is a sequence of pairs.

$$x(n) = ..., x_2(q), x_2(q), x_2(q+1), x_2(q+1), x_2(q+2), x_2(q+2), ... \qquad (4.31)$$

102

It follows that since C_{11} and C_{12} are interchanged in the two conversions of each value $x_2(n_2)$, the error signal will be of the form:

$$e(n) = ..., e_q, -e_q, e_{q+1}, -e_{q+1}, e_{q+2}, -e_{q+2}, ... \qquad (4.32)$$

which can be interpreted as the first-order difference of:

$$e^*(n) = ..., e_q, 0, e_{q+1}, 0, e_{q+2}, 0, ... \qquad (4.33)$$

Since a first-order difference has a high-pass characteristic, we can argue that the mismatch error has been shaped to high-frequency noise by this operation.

An interesting side note is that because the individual DACs can be made to occupy little area, they can be used as elements in an analog FIR filter of moderate length (2-10 taps) to avoid the hardware penalty of a brute-force switched-capacitor filter when suppressing out-of-band noise as shown in Fig. 4-7. Note that since all of the weighted filter capacitors $a_1 C_1 - a_n C_1$ are in parallel on the integrating phase of operation, it is the total filter capacitance that should be taken into account when determining the filter kT/C noise.

The reconstruction filter described above never sees the filter capacitors $a_1 C_1 - a_n C_1$ as a load in the feedback position. Therefore, the filter opamp does not have to drive the FIR sampling capacitance, relaxing the opamp drive requirements. The overall discrete-time transfer function of this reconstruction filter is:

$$H(z) = \frac{(a_1 + a_2 z^{-1} + ...)}{1 + \frac{C_f}{C_{DAC}} - \frac{C_f}{C_{DAC}} z^{-1}} \qquad (4.34)$$

$$C_{DAC} = (a_1 C_1 + a_2 C_1 + ... a_n C_1) \qquad (4.35)$$

103
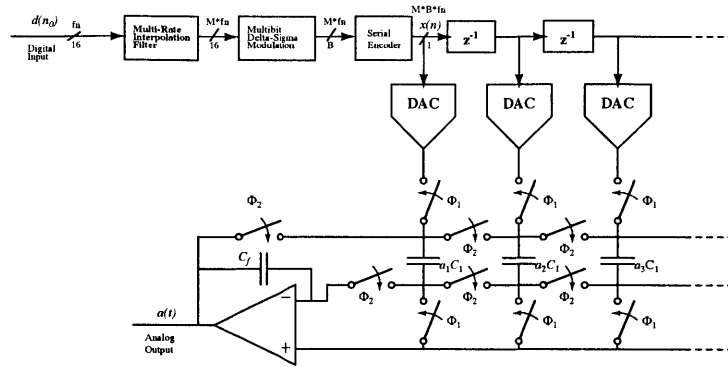
Figure 4-7: Serial DAC FIR Reconstruction Filter

which is an IIR filter whose cutoff frequency can be lowered as the size of the feedback capacitor is increased.

It turns out, however, that the FIR is of little additional benefit unless one is merely concerned with attenuating jitter effects due to out-of-band quantization noise at very high frequencies. MATLAB analysis shows, as in the current-mode semidigital filter case, that about 100-200 taps are required to obtain the effect of a first-order analog filter. Significant die area is required to lay out a weighted capacitor array of this size.

Although the die area consumed by the pseudo-passive D/A is not a direct function of the number of quantizer bits B that are output from the sigma-delta modulator, the clocks running the switches in the individual D/As must run at B times the oversampling frequency. While no high-speed opamps are required to operate at this frequency, this has the effect of requiring large switches that necessarily contain large parasitic capacitances. Also, additional clock buffering will be necessary to drive the switches at the accelerated rate.

The lowest achievable OSR in this topology is determined by the fact that the sampling clock has a worst-case jitter performance of $\sigma_j = 1$ns. In order to guarantee that jitter noise at the DT-CT interface is below 96dB, the oversampling ratio must be kept no less than 64, as predicted by the jitter equation given in the following section. Since the second-order mismatch shaping described in [31] requires an oversampling ratio that is a multiple of three, an oversampling ratio of 72 will be used.

According to Steensgaard, et al. [31], for an OSR of 72 and for a capacitor mismatch error of $\delta = 0.1\%$, first order mismatch shaping achieves an SNDR of -85dB, much too high to obtain the required 16 bit resolution. Second order mismatch shaping achieves an SNDR of -130dB for this same level of mismatch. Assuming that, for an increase in δ by a factor K, the SNDR of the mismatch-shaping scheme degrades by $20\log_{10}(K)$dB, a capacitor mismatch of 1% will result in an SNDR of -110dB. This resolution is sufficient to guarantee that the shaped mismatch error is negligible compared to the component noise.

For commercial design purposes, the factor δ is equal to the value 6σ to account for process variation across a large batch. The value of σ is therefore 0.16%, which corresponds to a capacitance of 0.204pF in the process available for this project.

It turns out that noise requirements set the final capacitor size. Assuming that, since a large FIR is infeasible, only one switched-capacitor DAC will be used prior to the IIR lowpass filter. Since both capacitors of the two-capacitor D/A converter are seen in parallel at the output during their sampling into the analog IIR filter, the kT/C noise is dependent on the sum of their values. Thus, the output referred kT/C noise is given by:

$$\overline{V_{n,kT/C}}^2 = \frac{4kTf_0}{Cf_s} = \frac{4k \cdot 300 \cdot 20000}{C \cdot 3456000} = (10\mu V_{rms})^2 \rightarrow C_{total} = 1pF \qquad (4.36)$$

Where $10\mu V_{rms}$ of total component noise has been budgeted to the D/A converter capacitance, leading to a capacitance of 0.5pF for each of the twin capacitors.

As the switches to these capacitors are responsible for carrying and holding the signal voltages, the design is constrained to use CMOS switches to avoid threshold voltage errors in the signal path. For an oversampling ratio of 72, a $B=5$ bit sigma-delta modulator is required to remove all sigma delta quantization noise from the signal band. For this setup, the internal switches inside the pseudopassive D/A converter must operate at $f_a = (N+1)f_s = 20.736MHz$ in order to handle the incoming serial bitstream.

Good design practice calls for switches to be sized such that their time constants, in conjunction with their load capacitances have sufficient linear settling accuracy. For settling accuracy to 0.01%, the RC time constant formed by the switches should be about 1/7th of the sampling period, that is, $\frac{1}{2\pi RC} = 7f_s$. Thus, to drive the combined load capacitance, as the switches need to do in the worst-case scenario, the resistance required is 548Ω. Noting that two switches are in series, and noting that the resistance of a CMOS switch can be approximated as [32]:

$$R_{switch} \approx \frac{2V_{dd}}{k_n(V_{dd} - V_{th,n})^2 + k_p(V_{dd} - |V_{th,p}|)^2} \qquad (4.37)$$

Resulting in the values:

$$W_n = 1.5\mu m, W_p = 7.12\mu m$$

106

assuming that, for the switches, $k_p = k_n$, $W_p = \frac{\mu_n C_{ox}}{\mu_p C_{ox}} W_n$.

The problem with switches such as these is that they have nonlinear parasitic capacitances that are significant in size compared to the charge storage capacitors. Since the drain- and source-to-bulk capacitances of the switches appear in parallel with the capacitors of the two-capacitor D/A converter, they can effectively create a sampling capacitor which is nonlinear with the applied voltage. To quantify the effects of these nonlinear capacitors, it is necessary to first calculate their values.

From the process handbook,

$$C_{jn} = 1.8366 \cdot 10^{-3} \frac{F}{m^2}, C_{jp} = 1.8339 \cdot 10^{-3} \frac{F}{m^2}$$

$$C_{jswn} = 4.235 \cdot 10^{-10} \frac{F}{m}, C_{jswp} = 3.473 \cdot 10^{-10} \frac{F}{m}$$

$$L_{diff} = 1\mu m, \quad m_j = 0.5, \quad \Phi_B = 0.9V, \quad V_{bulk,n} = 0V, \quad V_{bulk,p} = 2.5V$$

Noting that:

$$C_{dbn} = C_{sbn} = \frac{(C_{jn} \cdot W_n \cdot L_{diff}) + (C_{jswn} \cdot (W_n + 2L_{diff}))}{(1 - \frac{V_{bd}}{\phi_B})^{mj}} \tag{4.38}$$

$$C_{dbn} = C_{sbn} = \frac{0.00344pF}{(1 + \frac{V_d}{0.9})^{0.5}} \tag{4.39}$$

$$C_{dbp} = C_{sbp} = \frac{0.0154pF}{(3.78 - \frac{V_d}{0.9})^{0.5}} \tag{4.40}$$

From the two-capacitor D/A converter schematic, one can readily see that each capacitor sees at least two CMOS switches at any given time, in addition to one other

107

NMOS switch which will be neglected for the purposes of this discussion.

It is also important to note that $V_{d,max} = V_{ref} = 2V$ and that $V_{d,min} = 0V$

Inserting these numbers into the above equations reveals that

For $V_{d,max}$, the total parasitic capacitance seen by each capacitor equals: 0.02852pF.

For $V_{d,min}$, the total parasitic capacitance seen by each capacitor equals: 0.02272pF.

For a nominal worst-case capacitor value of 0.5pF (when the two capacitors are not in parallel), the parasitic capacitance variation described above results in a total capacitance variation of 1.02% over the specified voltage range. Although mismatch shaping can correct mismatches between capacitors, it is shown that mismatches between a single capacitor at different voltages can invalidate the first-order noise shaping process described by Steensgaard, et al.

We know from the Steensgaard paper that the error signal for a particular conversion is of the form:

$$e(n) = \delta \cdot V_{ref} \cdot F[x(n, k)] \qquad (4.41)$$

where $x(n, k)$ is the incoming serial sequence of bits, n is the current signal symbol, k is the current symbol bit, and F is a function that relates the bits of the current signal symbol the the error resulting from the two-capacitor D/A switching operation. The error shaping techniques described in Steensgaard, et al. rely on the fact that each input symbol n produces a distinct $e(n)$ and that $-e(n)$ can be generated merely by switching C_{11} and C_{22}.

Introducing the mismatch term

$$\delta = \frac{C_{11} - C_{12}}{C_{11} + C_{12}} \tag{4.42}$$

Swapping C_{12} and C_{11} yields

$$\delta_{new} = \frac{C_{12} - C_{11}}{C_{11} + C_{12}} = -\delta_{old} \tag{4.43}$$

Therefore,

$$e(n)_{new} = \delta_{new} \cdot V_{ref} \cdot F[x(n,k)] \tag{4.44}$$

$$= -\delta_{old} \cdot V_{ref} \cdot F[x(n,k)] \tag{4.45}$$

$$= -e(n)_{old} \tag{4.46}$$

However, if

$$C_{11} = C_{11,nominal} + C_{11,parasitic}(V_{in}) \tag{4.47}$$

$$C_{12} = C_{12,nominal} + C_{12,parasitic}(V_{hold}) \tag{4.48}$$

where V_{in} represents a voltage in the sequence $V_{ref} \cdot x(n,k)$, depending on the input bit, and where V_{hold} is the voltage seen by the signal holding capacitor, which can be denoted as $v(n, k-1)$.

With parasitics, the error is still a function of the particular input word, but the capacitor mismatch factor δ becomes:

$$\delta = \frac{C_{11}(V_{in}) - C_{12}(V_{hold})}{C_{11}(V_{in}) + C_{12}(V_{hold})} \tag{4.49}$$

and δ is thus a function of $x(n,k)$.

Note that because of the newly significant voltage dependency of the two capacitors, switching their positions in the circuit no longer has the effect of maintaining the magnitude of δ constant. After switching positions, C_{12} will see the voltages $V_{in,(n,k)}$ and C_{11} will see the voltages $V_{hold,(n,k)}$. Mathematically, if $\delta_{new} = -\delta_{old}$, then

$$\delta_{new} = \frac{C_{12}(V_{hold}) - C_{11}(V_{in})}{C_{11}(V_{in}) + C_{12}(V_{hold})} \qquad (4.50)$$

However, since C_{12} now sees V_{in} and C_{11} sees V_{out},

$$\delta_{new} = \frac{C_{12}(V_{in}) - C_{11}(V_{hold})}{C_{11}(V_{in}) + C_{12}(V_{hold})} \qquad (4.51)$$

which is only equal to $-\delta_{old}$ if $V_{in} = V_{hold}$ for the entire conversion operation of symbol n. To numerically examine the potential magnitude of such an error, consider the following example. If for the input symbol $x(n, k)$, the first $k - 1$ bits are equal to zero while the final bit k is equal to 1, the voltage V_{hold} will be zero until the final cycle of the serial DAC operation. Until this time, the effect of any mismatch between the two capacitors is zero, since they have been sharing zero charge on every cycle. On the final stage, however, $V_{in} = V_{ref} = 2V$ and $V_{hold} = 0V$ prior to conversion.

In this case,

$$C_{11,nominal} = 0.5025pF \text{(hereafter abbreviated } C_{11,n} \text{and } C_{12,n})$$

$$C_{12,nominal} = 0.4975pF \text{(so that } \delta_{nominal} = 1\%)$$

$$C_{11,parasitic}(V_{ref}) = C_{12,parasitic}(V_{ref}) = 0.02852pF$$

$$C_{11,parasitic}(V_{hold}) = C_{12,parasitic}(V_{hold}) = 0.02272pF$$

$$\delta = \frac{C_{11}(V_{in}) - C_{12}(V_{hold})}{C_{11}(V_{in}) + C_{12}(V_{hold})} \tag{4.52}$$

$$\delta = \frac{C_{11n} - C_{12n} + C_{11p}(V_{in}) - C_{12p}(V_{hold})}{C_{11n} + C_{12n} + C_{11p}(V_{in}) + C_{12p}(V_{hold})} \cdot \frac{C_{11n} + C_{12n}}{C_{11n} - C_{12n}} \cdot \delta_{nominal} \tag{4.53}$$

$$\delta = \delta_{nominal} \left(\frac{1 + \frac{C_{11p}(V_{in}) - C_{12p}(V_{hold})}{C_{11n} - C_{12n}}}{1 + \frac{C_{11p}(V_{in}) + C_{12p}(V_{hold})}{C_{11n} + C_{12n}}} \right) \tag{4.54}$$

Since the second term in the denominator is very small, it can be neglected

$$\delta = \delta_{nominal} \left(1 + \frac{C_{11p}(V_{in}) - C_{12p}(V_{hold})}{C_{11n} - C_{12n}} \right) \tag{4.55}$$

Plugging in values yields:

$$\delta = \delta_{nominal} \cdot 2.156$$

Switching the positions of the two capacitors yields

$$\delta = \delta_{nominal} \left(1 + \frac{C_{12p}(V_{in}) - C_{11p}(V_{hold})}{C_{12n} - C_{11n}} \right) \tag{4.56}$$

$$\delta = \delta_{nominal} \cdot (-0.156)$$

The two values δ do not cancel out when the two capacitors switch positions, thus invalidating any mismatch correction that could make this D/A topology feasible. Note that this problem is roughly independent on the size of the nominal capacitor used and worsens with increasing sampling frequency, in which case larger switches relative to the size of the capacitors are required.

4.2.3 Switched-Capacitor with Dynamic Element Matching and Direct Charge Transfer

As stated before, one disadvantage of switched-capacitor D/A topologies is the undesirable tradeoff between kT/C noise, capacitor area, and power dissipation. One circuit method that decouples the power dissipation factor from this tradeoff is known by several names, but for the purposes of this discussion will be referred to as Direct Charge Transfer [17]. Shown in Fig. 4-8, the Direct Charge Transfer (hereafter referred to as DCT) technique realizes a first-order filter transfer function while never connecting its sampling capacitance in a configuration in which the opamp sees the capacitance as a load through the feedback network. That is, unlike traditional RC-equivalent switched-capacitor networks in which the opamp supplies the charging current for the integrating capacitor, the sampling capacitance C_{DAC} connects in parallel with the integrating capacitance C_{hold}, passively sharing the input charge. The opamp is now only required to drive the bottom-plate capacitance of the feedback capacitor, which is negligible in many modern wafer processes that offer metal-insulator-metal capacitors. Since this input capacitance often forms the dominant load capacitance of traditional switched-capacitor implementations, this technique can save a substantial amount of power.

Although originally conceived as a method to introduce crosstalk between signal branches [34] and later used as a buffer [35] and finally a high-frequency quantization noise reject filter [33], DCT has the potential to fill the role of the primary analog postfilter in a monolithic D/A converter. It can be shown that the transfer function of the system shown in Fig. 4-9, in which a switched-capacitor D/A converter employing Dynamic Element Matching is integrated onto a second-order postfilter employing two DCT blocks, is given as:
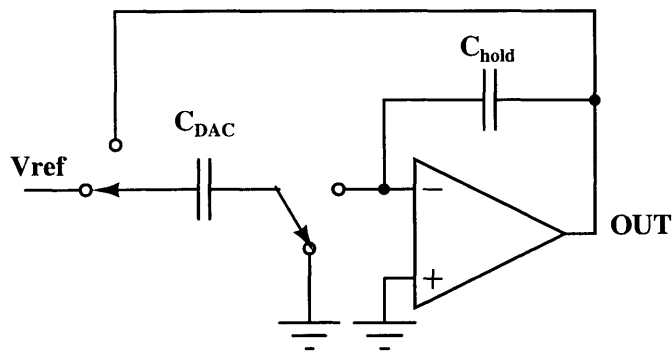
Figure 4-8: Direct-Charge Transfer Concept

$$H(z) = \frac{z^{-2}}{(1 + \frac{C_{FB}}{C_{DAC}} - \frac{C_{FB}}{C_{DAC}} \cdot z^{-1})^2} \tag{4.57}$$

As will be shown in Chapter 5, the required ratio of C_{FB} to C_{DAC} for an over-sampling ratio of 128 is 25.

It has already been stated that a four-bit dynamic element matching scheme can remove almost all quantization noise from the signal band. Thus, for a minimum capacitor size of 75fF, the input capacitor array will consume 1.2pF of capacitance. This results in an output-referred component noise power contribution of $9 \cdot 10^{-11} V^2$. It turns out that there is enough room in the quantization noise budget to make the input capacitors to the second stage 0.3pF each, contributing a component noise power of $3.6 \cdot 10^{-10} V^2$. For a differential implementation, the total approximate capacitance of this topology is 78pF while only 0.3pF of capacitance needs to be driven, along with the lumped capacitance seen at the output of the switched capacitor filter. These numbers, which will be explained in greater detail later, show that the topology described above will trump all others for the low-power, low-area monolithic solution.

113
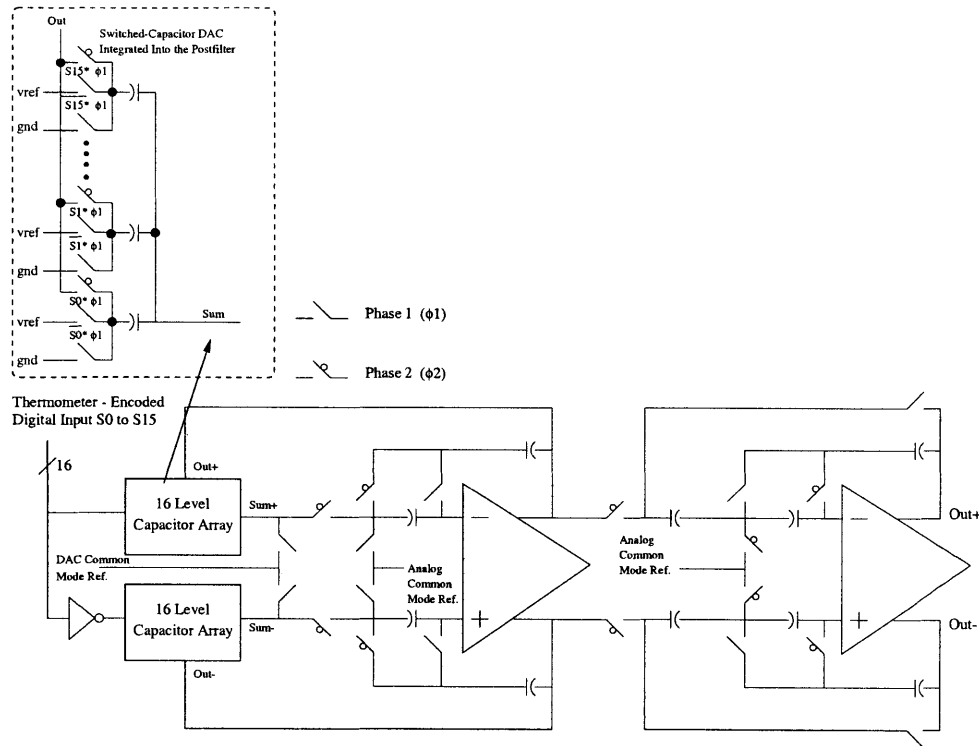
Figure 4-9: Four-bit SC D/A Converter with DCT Postfilter

4.3 Dynamic Element Matching Techniques

Although a D/A converter may have static errors resulting from mismatch between its unit elements, it is possible to select these elements in such a way as to convert these DC errors into a pseudo-random wideband noise signal [13] that can be partially removed by the analog reconstruction filter. The general class of such strategies known as dynamic element matching accomplishes this by choosing different elements to represent a digital input code at different times. This technique especially suits oversampling converters because, as with quantization noise, this mismatch noise power is spread over the signal bandwidth, and less noise falls in the signal band as the oversampling ratio is increased [13]. One caveat to these techniques is that the element selection process is governed by digital control circuitry which must be im-

plemented on the analog die. In general, the power dissipation and area consumed by this digital circuitry increases exponentially with the number of elements in the D/A converter, preventing the practical realization of multibit modulators with $B > 6$ [12].

In a thermometer-encoded D/A converter with mismatched elements, each element is assigned a weight w_i where ideally $w_i = 1$ but due to mismatch, will equal a value that is slightly different than unity. Although the average of the sum of these weights $w_{mean} = \frac{1}{N} \sum_{i=0}^{N-1} w_1$ may not equal unity, this deviation represents only a gain error and is of little consequence in most applications. Thus, mismatch errors for each unit element are equal to $w_i - w_{mean}$ and not $w_i - 1$. The concept of DEM can be graphically illustrated in the case of a 2-element, 3 level DAC, as shown in Fig. 4-10.

In conjunction with the discussion above, one of the DAC elements has a normalized error of: $\frac{w_i - w_{mean}}{w_{mean}} = 1\%$ while the other has a normalized error of: $\frac{w_i - w_{mean}}{w_{mean}} = -1\%$ While the output levels represented by having neither or both elements on at the same time necessarily have zero error, the output level represented by one element on necessarily contains a linearity error at any given time. However, if the two unit elements are swapped as shown in the bottom half of the figure, the time-averaged error drops to zero rather quickly and the distortion due to component mismatch has been moved to high frequencies, where it can be filtered out by the analog postfilter. Note that this is only feasible if the DAC reconstruction sample rate is much faster than the signal bandwidth of interest.

4.3.1   Random Element Selection

Perhaps the most intuitive method to implement DEM is by selecting the elements required to convert a digital word of size B via a Butterfly decoder controlled by a pseudo-random number generator. [13][36]. The idea is that if the mapping between

1% High
Output

Ideal
Output

DAC Output

10 10 10 10 10 10 10 10 10 10

Input Code
as Function of
Time

DAC Output

10 10 10 10 10 10 10 10 10 10

Input Code
as Function of
Time
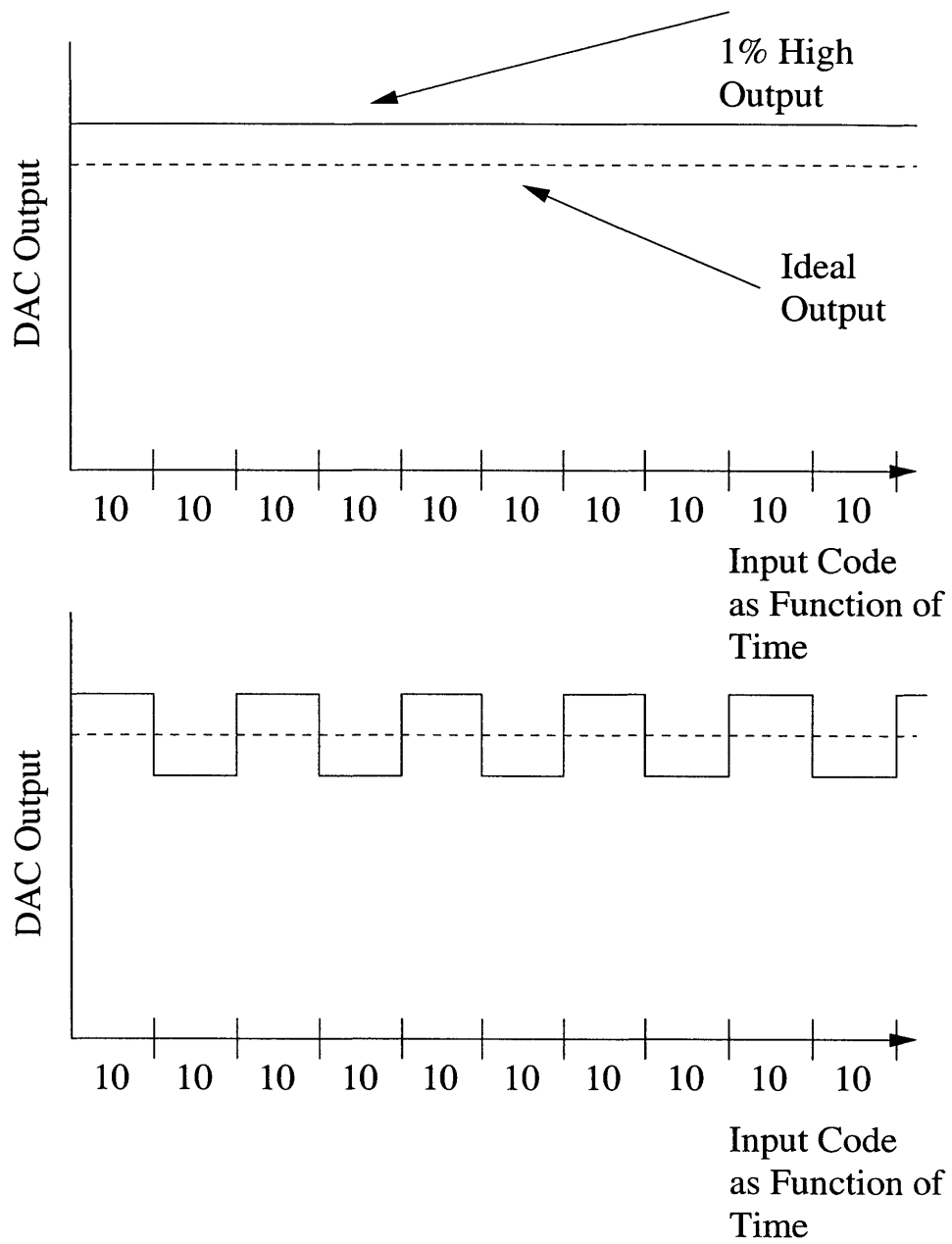
Figure 4-10: Dynamic Element Matching Concept

116

the thermometer encoded sigma-delta modulator output bits and the D/A converter elements are determined at random for every sample time, there will be no correlation between the total mismatch error between sample times, resulting in the mismatch error having white noise signal statistics.

Assuming that the sigma-delta modulator is oversampled with OSR=M, the pseudorandom mismatch noise will be spread uniformly across all frequencies, and only $1/M$ of the total mismatch noise power will fall in the signal band. Given that there are N levels in the thermometer encoded sigma-delta modulator output, the output signal swing has a maximum excursion from 0 to N. Given these parameters, it can be shown [36] that the maximum SNR attainable by this scheme is equivalent to:

$$SNR = \frac{\sqrt{\frac{NM}{3}}}{\sigma_w} \tag{4.58}$$

Where σ_w is the standard deviation of the mismatch between unit elements. Good design practice calls for the 6σ mismatch deviation given in the process handbook to be used for this value in order to guarantee acceptable process yield. As seen from the formula above, each doubling of the oversampling ratio yields an additional 3dB of signal to noise ratio.

4.3.2 Data Weighted Averaging

While this sort of linearity improvement is certainly better than leaving static errors in the D/A converter, it is generally not sufficient to realize a high performance implementation. The Data Weighted Averaging algorithm (DWA) potentially achieves a resolution benefit of 9dB per decade of oversampling without the addition of complicated digital control circuitry [22].

The DWA algorithm is performed by sequentially selecting elements for use from

117

the D/A array, beginning with the next available element, as shown in Fig. 4-11.

Active Multibit DAC Elements

Figure showing a grid with columns labeled 0-15 (Active Multibit DAC Elements) and rows labeled by Input Data values 2, 9, 10, 5, 6, 8, with Time axis pointing downward.
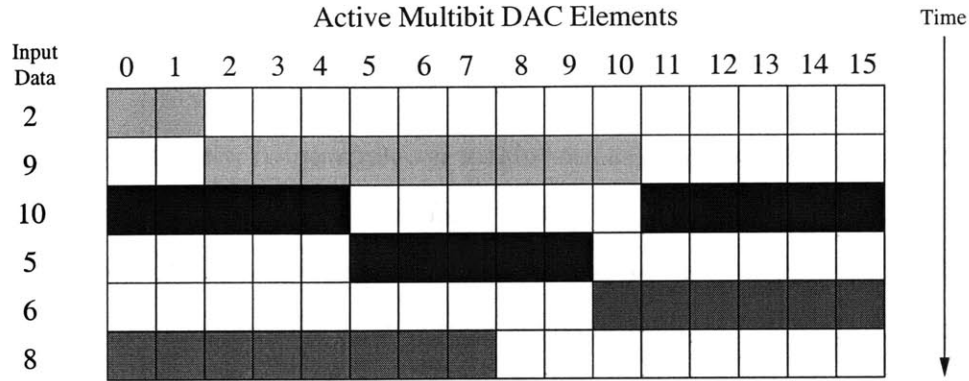
Figure 4-11: Conceptual Operation of DWA Algorithm

As can be seen in Fig.4-11, the DWA algorithm guarantees that each DAC element is used the same number of times and that all of the DAC elements are utilized at the maximum possible rate. [22]. Since it only takes a few cycles of operation before all of the DAC elements are used, their individual errors $w_i - w_{mean}$ quickly sum to zero. This implies that mismatch-induced distortion is moved to very high frequencies [22].

It can be demonstrated through hand analysis that the DWA algorithm in fact shapes the resulting mismatch error much as a first-order noise shaper [36] and that for a random input signal, the achievable resolution is approximately equal to:

$$\text{resolution} = \log_2 \left(\frac{\sqrt{3NM^3}}{\pi \sigma_w (1 - \frac{1}{N})} \right) (bits) \qquad (4.59)$$

where $M = OSR$, $N = 2^B$, and σ_w equals the 6σ process variation of the DAC unit elements [36]. In addition, MATLAB simulation shows that the DFT of the mismatch error noise from the DWA algorithm rises approximately as first-order shaped noise, as shown in Fig. 4-12.

118
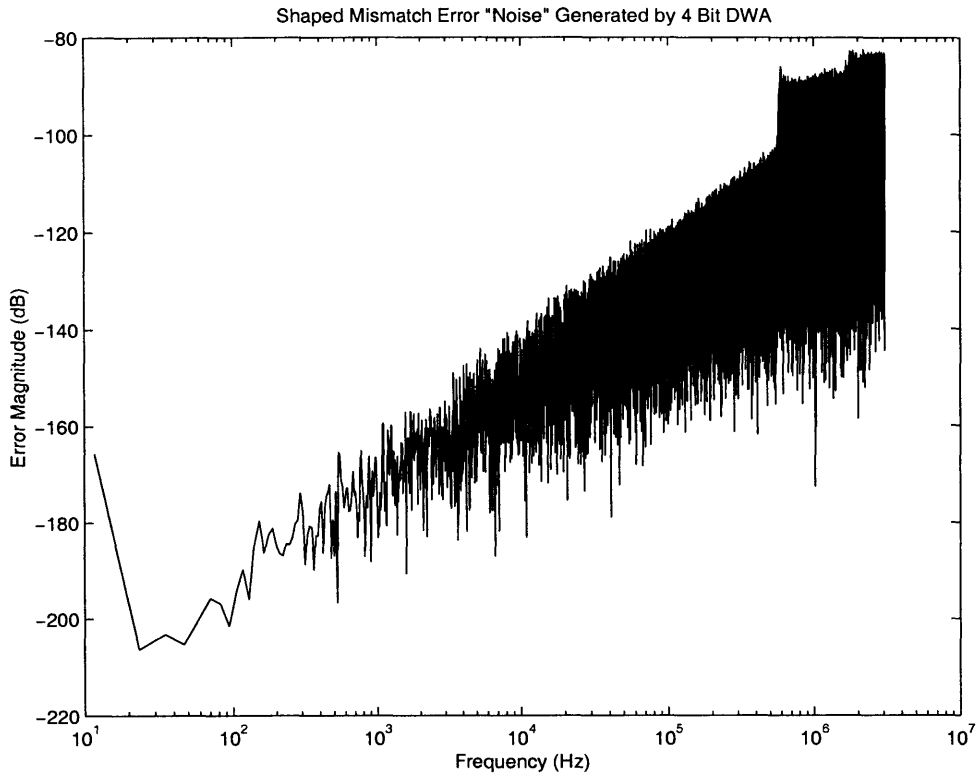
Figure 4-12: DFT of DWA Mismatch Error Noise

As predicted by the equation above, and as found by measurement [22], the improvement in SNR per sigma-delta modulator bit B decreases as the total number of bits increases, partly because of the fact that there are 2^{B-1} more elements to cycle through before the accumulated DAC errors sum to zero. However, as shown in Fig. 4-13, a 4-bit DWA implementation running at an oversampling ratio of 128 contributes negligible in band noise and is able to pass a signal large enough such that the overall system gain specifications can be met, confirming the appropriateness of this choice of B and OSR.

The data reported in Fig. 4-13 were generated in MATLAB using a behavioral representation of the DWA algorithm. The block diagram of this behavioral repre-
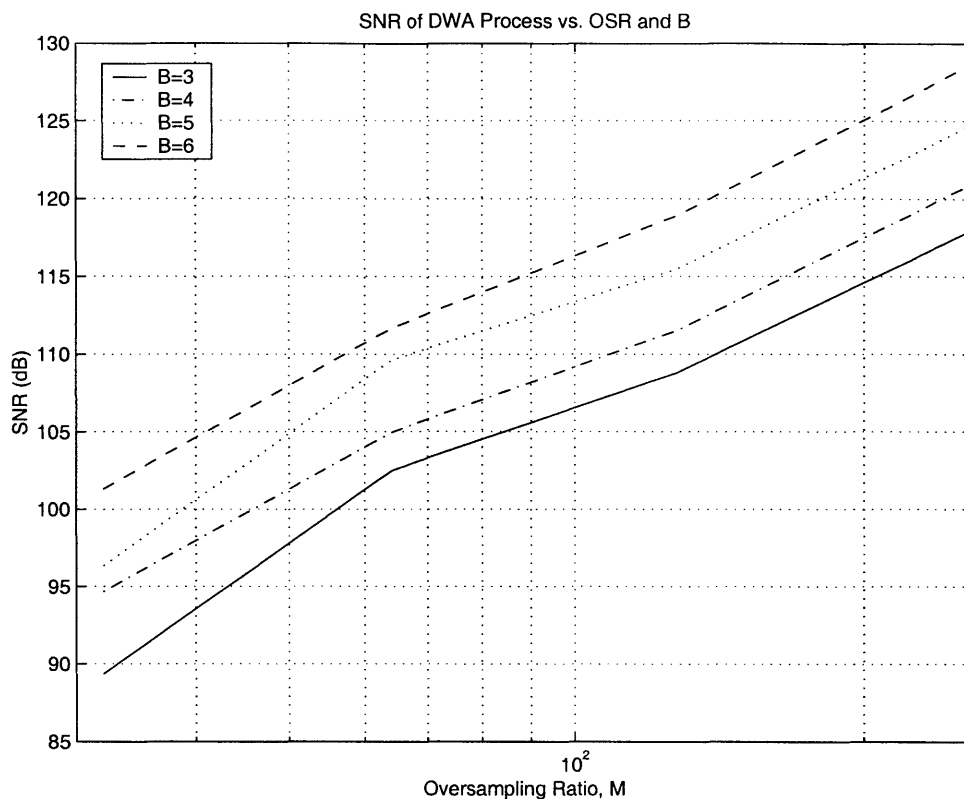
Figure 4-13: SNR Measurements for DWA from MATLAB Behavioral Simulation

sentation is shown in Fig.4-14. The DWA rotation is accomplished by passing the thermometer-encoded incoming digital signal through a cyclic selection array, where the first element to be used on a given cycle is indexed by the state variable $PTR(k)$. This state variable is the B LSBs of the running sum of the incoming data symbols with bit width B, where the MSBs have been allowed to wrap around. Allowing the LSBs to cycle in this manner is what provides the selection array with cyclic indexing.

4.3.3 Implementation of DWA Circuitry

This algorithm is straightforward to implement in digital circuitry, and is shown in Fig. 4-15 for a DWA implementation in which 2^B output levels are used for a digital
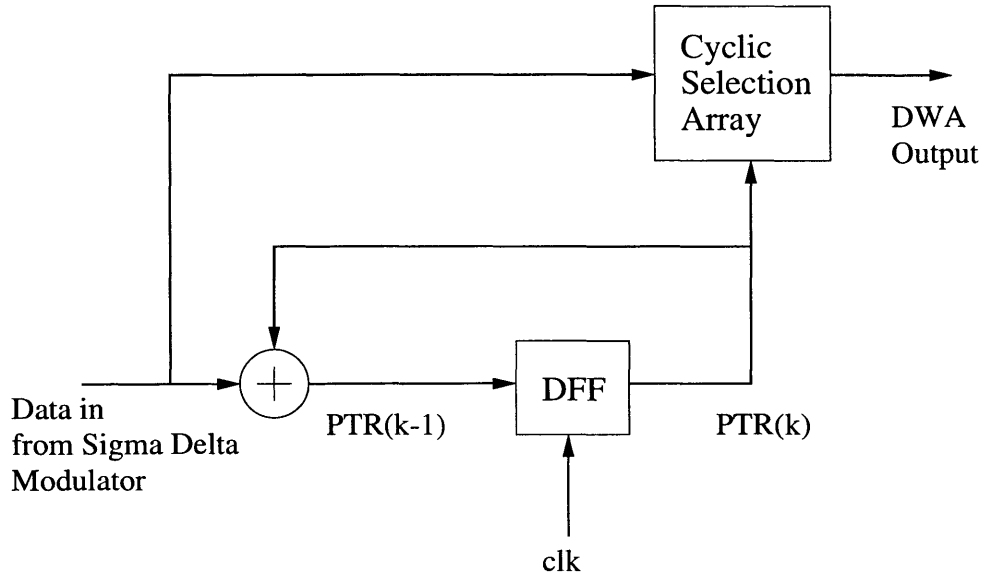
Figure 4-14: Behavioral Description of DWA Algorithm

output of B bits from the sigma delta modulator. The input signal is first converted from 2's complement representation to a single-signed positive number representation for ease of computation and indexing purposes. The resulting signal is then added to the state variable $PTR(k)$ to produce $PTR(k-1)$. In order to obtain the correct cyclical operation, $PTR(k-1)$ must "roll over" at the correct location for the 2^B level logarithmic barrel shifter. This is accomplished by checking to see if the sum of the incoming signal and $PTR(k)$ is greater than or equal to 2^B. If so, the $B+1$ bit output of the B bit adder should be added to "2^B" to force the lowest B bits to roll over to the correct location.

The incoming signal is thermometer encoded via combinational logic and produces minor glitching that can be remedied with the addition of a register following the logarithmic barrel shifter. The logarithmic barrel shifter is a B by 2^B array of two-element multiplexors that accepts a binary input and cyclically shifts the incoming thermometer-encoded signal.
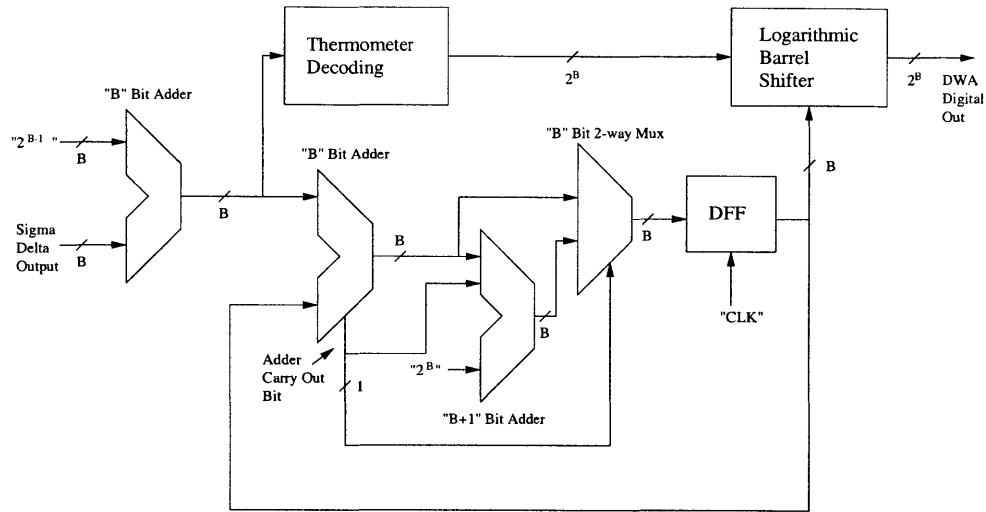
Figure 4-15: Digital Circuitry Implementation of DWA Algorithm

In a 0.25μm process, the implementation shown above occupies approximately **0.0257mm²** of silicon die area and consumes **0.14mW** of power for $B = 4$ and $M = OSR = 128$. One can expect power consumption to increase linearly with M and exponentially with B. Area consumption also increases exponentially with B. Assuming the use of combinational logic, the propagation delay of the critical feedback path of the DWA circuitry is 3ns, meaning that it will function correctly for the desired operating speed of 6.144MHz.

4.4 Clock Jitter at the DT-CT Interface

Clock jitter at the discrete time-continuous time interface is a source of nonlinearity because varying the sampling instance with time changes the amount of signal energy that appears at the output at a given instant. As shown in Fig. 4-16, a misplacement of the sampling instance results in an error that is defined as the difference between the actual output waveform and the ideal output waveform. As is evident from Fig.

4-16, the magnitude of the nonlinearity due to jitter increases with the output step size. For example, if a two-level DAC interfaced directly with the continuous-time domain, the resultant jitter distortion would be large. However, if a multibit DAC were utilized and a discrete-time postfilter appended to reduce the output step size further at the DT-CT interface, the clock jitter noise will be very small.
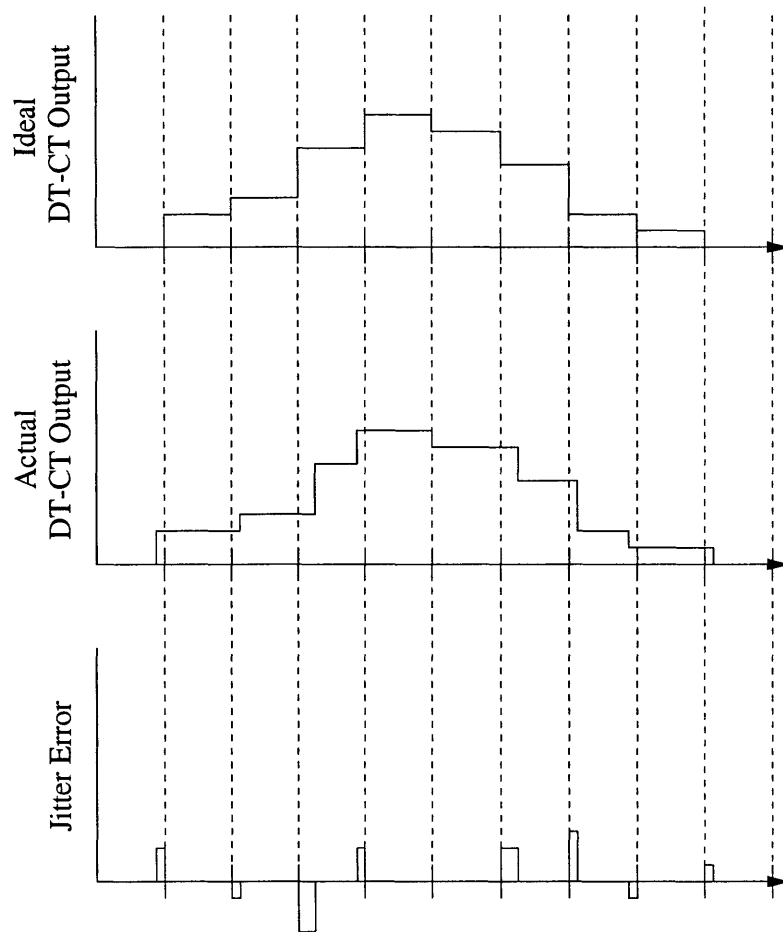
Figure 4-16: Effect of Clock Jitter on a Multi-Level DT-CT Zero Order Hold

In general, the deviation of the placement of the sampling clock edge can be assumed to be Gaussian randomly distributed [6], resulting in a jitter distortion that can be described as a noise process. It can be shown that for an oversampling D/A

converter, the in-band jitter noise power at the output is given by [40]:

$$N_j < \frac{2(\pi \sigma_j A f_o)^2}{M} \left[1 + \left(\frac{P}{A} \frac{f_s}{2 f_o} \right)^2 \right] \tag{4.60}$$

where P^2/A^2 is the ratio of out-of-band quantization noise power to signal power. Since this result applies at the DT-CT interface, the value P is the amount of out of band quantization noise after any discrete-time analog postfiltering (such as a switched-capacitor postfilter or a semidigital current source filter).

It is known that the input clock supplied to this project has a worst case $\sigma_j = 1ns$ and that the signal to noise ratio $\frac{\frac{A^2}{2}}{N_j}$ should be on the order of 98dB to keep jitter noise negligible. Also noting that MATLAB computations of P confirm that $P << A$ for the case of a multibit D/A converter followed by a second order discrete-time postfilter, so

$$10 \log_{10} \frac{\frac{A^2}{2}}{N_j} > 10 \log_{10} \frac{M}{4(\pi \sigma_j f_o)^2} \tag{4.61}$$

We find that M=128 yields an approximate SNR of 99dB while M=64 yields an approximate SNR of 96dB.

Chapter 5

Switched-Capacitor Postfiltering

Most on-chip filters, in addition to other circuits such as integrators, gain stages, and comparators, are implemented using switched-capacitor techniques. Switched-capacitor circuits move charge around a capacitive network based on an input clock and hence are discrete-time blocks operating in the analog domain, resulting in an explicit separation of the DT-CT and D/A interfaces. Thus, switched-capacitor circuits, and notably switched-capacitor filters, are typically analyzed using $\mathcal{Z}$-domain frequency response expressions. Careful application of the bilinear transform is essential to relating capacitor ratios to pole frequencies in the continuous-time domain.

Although nominal values of integrated circuit components vary widely, in most switched-capacitor filters key parameters such as gain and frequency response are set by capacitor ratios, whose matching can be very accurate, with error on the order of 0.1%. [3] Switched capacitor filters, in general, have good linearity and dynamic range properties, and as has been discussed previously, reduce the effect of clock jitter at the DT-CT interface.

5.1 Switched-Capacitor Theory

5.1.1 Switched-Capacitor/Resistor Equivalence

Prior to the advent of switched-capacitor filters, a large body of work had been compiled on continuous time RC filtering. However, because the value of an integrated resistor may vary by up to 20% such resistors have poor linearity and temperature coefficient characteristics. Thus, RC filters are not desirable for applications where the accuracy of the frequency response is an issue. In addition, active-RC filters do not permit the postponement of the DT-CT interface until after postfiltering.

Fortunately, switched-capacitor circuitry offers an alternative to integrated resistors. As shown in Fig. 5-1, applying a voltage $\Delta V = V_1 - V_2$ across a switched-capacitor block results in a charge $Q = CV_1$ being sampled on the sampling phase Φ_1 and a charge $Q = CV_2$ being sampled on the sampling phase Φ_2 where Φ_1 and Φ_2 are two nonoverlapping phases of the same clock waveform.
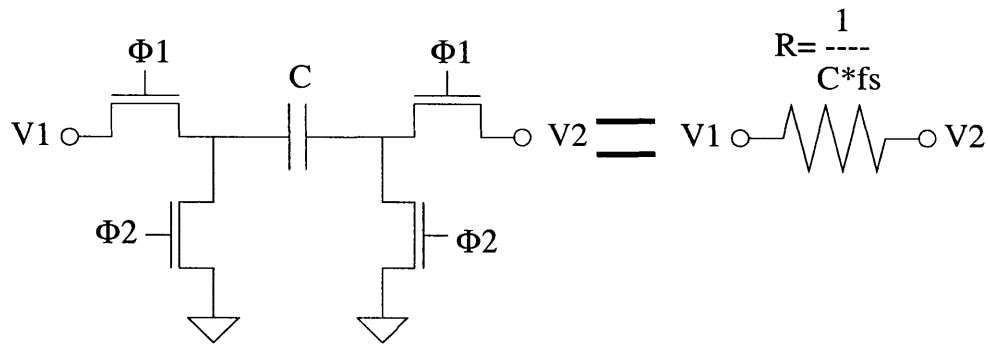
Figure 5-1: Switched-Capacitor Equivalence with Resistor

Thus, over a single period of the clock, an amount of charge $\Delta Q = C(V_1 - V_2)$ is transferred between the two terminals. Since this transfer of charge is performed over the time interval $\Delta t = \frac{1}{f_s} = T$, the charge transfer per time relationship is:

$$\frac{\Delta Q}{\Delta t} = C(V_1 - V_2)f_s \qquad (5.1)$$

Interestingly, this relation bears a striking resemblance to Ohm's law.

$$\frac{\delta Q}{\delta t} = I = \frac{V_1 - V_2}{R} \qquad (5.2)$$

If the assumption is made that the switched capacitor circuit is operating at a sampling rate much higher than the input frequency, then:

$$\frac{\Delta Q}{\Delta t} \approx \frac{\delta Q}{\delta t} \qquad (5.3)$$

and

$$R = \frac{1}{Cf_s} \qquad (5.4)$$

Note that the above relationship makes sense intuitively. If the capacitor is larger, more charge is transferred, and hence the effective resistance is smaller. Similarly, if the sampling rate is increased, more charge is transferred and the effective resistance is smaller again.

5.1.2 Equivalent Resistor-Capacitor/Switched-Capacitor Circuits

This concept of resistor-capacitor equivalence can be expanded to simple filtering circuits, such as the first-order filter shown below in Fig. 5-2, whose transfer function can be shown to equal:

$$\frac{V_{out}(s)}{V_{in}(s)} = -\frac{R_2}{R_1 + R_1 R_2 C s} \qquad (5.5)$$

In order to reliably integrate this filter, it is necessary to utilize a switched ca-
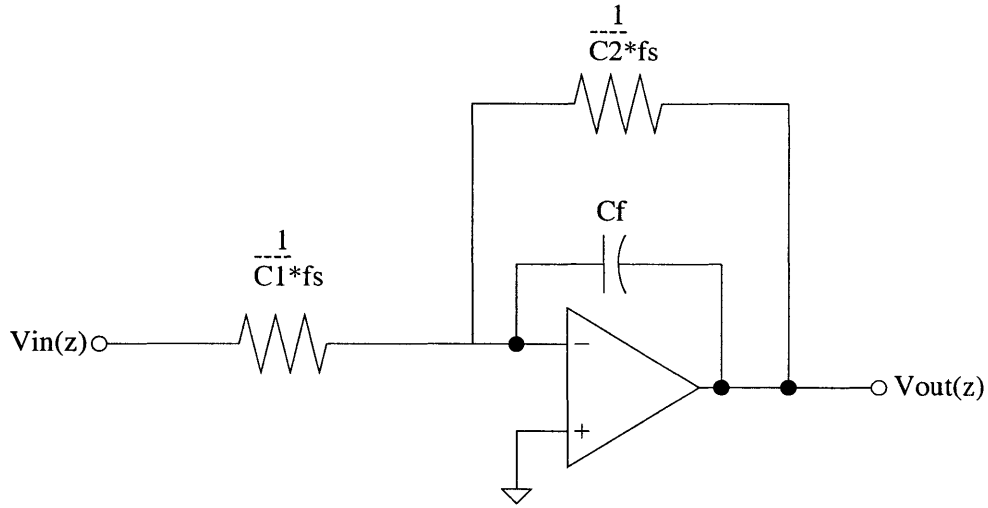
Figure 5-2: First Order Active-RC Lowpass Filter

pacitor implementation. This can be done as shown in Fig. 5-3 where the resistors have been replaced with equivalent switched-capacitor circuit blocks. Note that two switches are missing on the upper "resistor", however, careful inspection shows that these switches would be redundant and that the connections that they would have made are realized by the rightmost switches in the lower "resistor".

Discrete-time analysis of this filter can be shown to yield a transfer function of:

$$\frac{-\frac{C_1}{C_f}}{(1 + \frac{C_2}{C_f}) - z^{-1}} \tag{5.6}$$

Where the z-terms arise as a result of the delays inherent in each charge transfer.

A quick analysis confirms that the two topologies are functionally equivalent. At DC (s=0 and z=1), the gain of the RC filter is $\frac{R_2}{R_1}$ and that of the SC filter is $\frac{C_1}{C_2}$. Since $R_1 = \frac{1}{C_1 f_s}$ and $R_2 = \frac{1}{C_2 f_s}$, the two DC gains are hence the same. The $\mathcal{Z}$-domain pole of the SC-filter is $p_z = \frac{C_f}{C_2 + C_f}$. Using the bilinear relation that the continuous time pole is
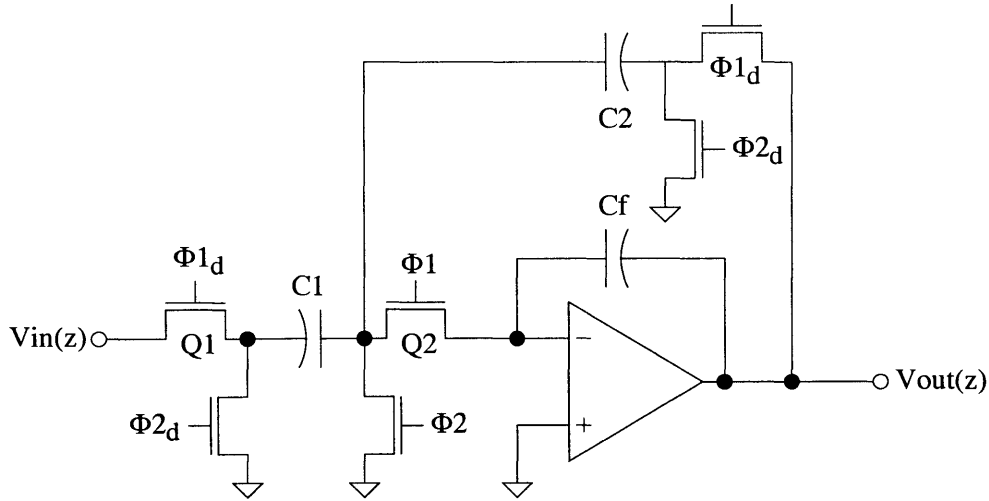
Figure 5-3: First Order Switched Capacitor Filter

$p_s = \frac{2}{T}\frac{p_z-1}{p_z+1}$ [3], the effective continuous time pole $p_s = \frac{2}{T}\frac{-C_2}{C_2+2C_f}$ is obtained. Typically in a SC filter, $C_f >> C_2, C_1$ and simplifying yields $p_s = -\frac{C_2}{C_f T} = -\frac{C_2 f_s}{C_f} = -\frac{1}{C_f R_2}$. Thus, the two filters have approximately an equivalent frequency response.

5.1.3 Switched-Capacitor Design Considerations

Noise

Although a capacitor itself is not noisy, the switches in the switched-capacitor circuit are composed of MOS transistors operating in the linear regime that have a parasitic series resistance. On each sampling phase, the effective resistor block is configured as shown in Fig. 5-4.

The series channel resistance of the MOS switches generates a spot noise voltage power of $\overline{V_n^2} = 4kTR\Delta f$ that is filtered by the series resistor-shunt capacitor combination, which has a -3 dB frequency of $\frac{1}{2\pi RC}$. To compute the total noise power in the circuit, a "brick-wall" approximation is employed which assumes that all of the thermal switch noise power exists in a frequency band ranging from DC to $\frac{\pi}{2}\frac{1}{2\pi RC}$.

129
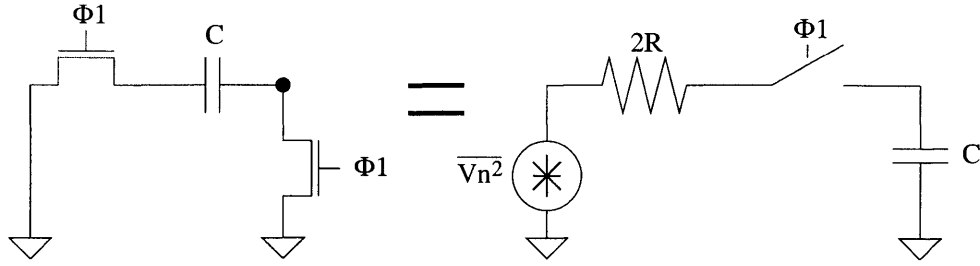
Figure 5-4: Switched Capacitor Noise Derivation

Given that the switch time constant must be smaller than the switched-capacitor circuit sampling period to ensure adequate settling, this noise bandwidth is larger than the sampling frequency. Thus, the sampling action of the switched-capacitor circuit undersamples the thermal noise, resulting in the out of band thermal noise being aliased back to the signal band $-\frac{f_s}{2} < f < \frac{f_s}{2}$. After aliasing, the thermal spot noise between $-\frac{f_s}{2}$ and $\frac{f_s}{2}$ is $\frac{BW_n}{\frac{f_s}{2}}$, where BW_n is the effective bandwidth of the noise. Multiplying terms out yields:

$$\frac{8kTR\pi\Delta f}{4\pi RC f_s} = \frac{2kT\Delta f}{C f_s} \tag{5.7}$$

Integrating over the signal bandwidth of interest f_0 yields:

$$\overline{V_{n,kT/C}}^2 = \frac{2kT f_0}{C f_s} \tag{5.8}$$

Since the sample and hold operation pins the actual noise voltage for half a sampling period, the expression derived above should technically include a sinc term which arises from the holding operation. However, since typically $f_o << f_s$, the sinc term can be well approximated as unity with the signal band.

During each period of the switched capacitor operation, this noise sampling and hold operation occurs once more, raising the total noise contributed by the switched capacitor to:

130

$$\overline{V_{n,kT/C}}^2 = \frac{4kTf_0}{Cf_s} \tag{5.9}$$

Note that this expression is again equivalent to that which would be generated by a resistor if $R = \frac{1}{Cf_s}$:

$$\overline{V_{n,kT/C}}^2 = 4kTRf_0 \tag{5.10}$$

Examining the expression derived above makes plain the aforementioned tradeoff between area and noise. In order to decrease noise, the capacitances composing the effective resistances must be large, and since it was mentioned earlier that typically the integrating feedback capacitors are much larger than the switched capacitances, the feedback capacitors must be very large. Interestingly, the output-referred thermal noise due to a switched capacitor is approximately equal to that of its equivalent resistor provided that the approximation $R = \frac{1}{Cf_s}$ still holds [29].

Once the noise associated with each capacitor is computed, its contribution to the total output-referred component noise can be calculated by multiplying the expression derived above with the effective gain seen by the capacitor to the filter output. This effective gain can be found using an AC analysis in a tool such as SWITCAP or SPICE.

Switch Design Tradeoffs

The MOS devices which are used to implement switches in the switched capacitor network come with a tradeoff of their own. As implied before, when sampling onto a capacitor through a switch, the channel resistance of the switch shunted with the sampling capacitance results in a lowpass filter with a time constant $\tau = RC$ where $R_{switch} \approx \frac{2V_{dd}}{k_n(V_{dd}-V_{th,n})^2+k_p(V_{dd}-|V_{th,p}|)^2}$ [32]. This time constant affects the settling ac-

curacy in that the voltage across the capacitor equals:

$$V_{cap}(t) = V_{in} + (V_{cap,initial} - V_{in})e^{-\frac{t}{RC}} \qquad (5.11)$$

Taking into account the worst case scenario that:

$$V_{cap,initial} = 0 \qquad (5.12)$$

The error voltage is thus:

$$V_e(t) = -e^{-\frac{t}{RC}} \qquad (5.13)$$

If it was desirable to limit linear settling errors in the circuit to -80dB, or 0.0001, then at the end of the sampling phase,

$$t \approx 9 \cdot RC \qquad (5.14)$$

And since each sampling phase occupies about half the sampling period,

$$T \approx 18 \cdot RC \qquad (5.15)$$

Since capacitance values are typically set to meet frequency response and noise specification, the RC time constant is set by increasing the widths of the switch transistors until R is low enough to meet the above constraint, or one like it.

Depending on the location of the switch inside the switched-capacitor network, even this sizing constraint may not be sufficient. For example, a switch seen as part of the load in the op-amp feedback network needs to be sized such that its RC settling time constant is five times larger than the nondominant pole of the opamp. When placed in the feedback network, the resistor introduces a LHP zero into the feedback transfer function, affecting the root locus in such a way as to significantly slow the

op amp settling time [42].

Although switches with very large widths have low channel resistances, increasing the size of the MOS devices also increases the clock feedthrough and charge injection of the switch. Charge injection was described earlier in the context of calibrated current sources and refers to the channel charge of the MOSFET exiting through both the drain and the source of the transistor when it is turned off and is proportional to WL. Clock feedthrough refers to the capacitive coupling between the gate and drain (source) of the MOSFET through the parasitic overlap capacitances. When the clock waveform abruptly changes the amount of charge on the overlap capacitance, some of it appears on the load capacitance through the capacitive divider that is formed between the overlap capacitance and the load capacitance. The voltage change on the load capacitance can be shown to be:

$$\Delta V = \frac{C_{ov}\Delta V_{gate}}{C_{load}} \tag{5.16}$$

where $C_{ov} \propto W$.

Although for a differential circuit, such errors are nominally common mode errors and are canceled out by the differential nature of the circuit, it is desirable to minimize these effects to the extent possible because of mismatch between the two differential paths, which requires the switch sizes to be as small as possible. Of considerable importance is the charge injected by the switch Q1 in Fig. 5-3. Since the channel charge in this switch is signal dependent, it can introduce distortion into the signal. On the other hand, since switch Q2 is always connected to virtual ground, its channel charge remains roughly constant and its introduction results only in a DC offset error which is eliminated by the differential nature of the circuit or is otherwise ignored.

The channel injection from switch Q1 can be mitigated using a switching scheme
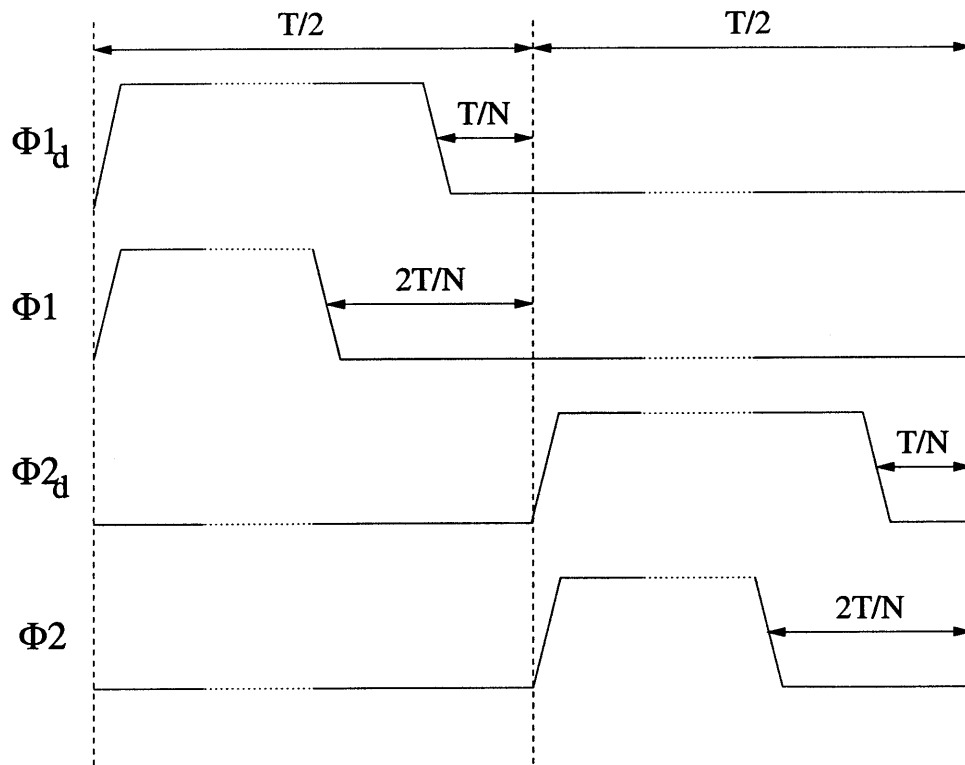
Figure 5-5: Clock Switching Scheme to Reduce Distortion

such as that shown in Fig. 5-5. It is seen that by turning the switches at the opamp
virtual ground off before the switches at the input of the filter, one terminal of the
capacitor is disconnected and is floating when the switches at the input of the filter
are turned off. Since one end of the capacitor is floating, the charge on that node
cannot be changed. Hence, charge cannot be injected onto the other node and the
voltage across the capacitor remains unchanged. This technique has been shown to
reduce the total amount of distortion in switched capacitor filters [48].

It should also be noted here that, as shown in Fig. 5-5, a nonoverlapping clock
waveform is used for the two clock phases Φ_1 and Φ_2 in all of the switched-capacitor
circuits described in this report. If the two phases were to overlap slightly, then direct
paths for the charge to feed forward through the circuit would arise, causing charge

134

to be lost and invalidating the intended discrete-time transfer function of the circuit. Also, the spacing between clock phases is significantly exaggerated. Normally the spacing is on the order of 1ns whereas the on-time of each phase is on the order of 100ns for a typical oversampling switched-capacitor system.

Opamp Nonidealities

Finite Opamp Gain Although finite opamp gain nonidealities do not have the same pernicious effects in D/A converter as they do in A/D converters, where they cause integrator leakage and mismatch between cascaded stages, their effects must still be taken into account in the switched-capacitor filter. In general, the finite gain of an opamp results in a finite DC gain error in the transfer function of the opamp. For audio filtering applications, this error causes only a slight linear gain compression at the opamp output. A high gain is necessary, however, for the proper functionality of the autozeroing and correlated double sampling techniques that are necessary to reduce the effect of DC offset and 1/f noise at the input of the opamp. A typical rule of thumb is to implement an opamp with a gain of about 80dB in order to obtain reasonable rejection of input-referred opamp noise with the correlated double sampling (CDS) technique. Such an opamp gain also limits linear settling errors to 0.01%.

Finite Opamp Bandwidth Finite opamp bandwidth prevents complete settling of the voltage signal at the opamp output, even assuming that opamp slewing is negligible or nonexistent. In order to minimize the opamp bandwidth required for a certain degree of settling, the phase margin of the opamp must be set such that the step response is optimally, or critically damped. Assuming that the opamp is a two-pole system, the opamp phase margin for optimum settling for a switched-capacitor integrator is given as: [42]

135

$$\phi_{MST} \simeq 90° - \tan^{-1}\left[\frac{1 + (\pi/0.693N)^2}{4}\right] \qquad (5.17)$$

where it is assumed that switch resistance is negligible and where N is the desired number of bits of resolution. For $N=18$, this results in an optimal phase margin of about 75°.

A rough approximation to the required settling time for a settling accuracy of N bits can be made by assuming that the opamp undergoes linear settling in response to a step and that the time constant of the step response is given by [3]

$$\tau = \frac{1}{\omega_{-3dB}} = \frac{1}{\beta\omega_{ug}} \qquad (5.18)$$

Where the opamp is assumed to be in a capacitive feedback configuration with feedback factor β. Note that in most switched-capacitor circuits, β is only slightly less than unity, however, in topologies where correlated double sampling techniques are employed, this may not be the case. Also note that for the remainder of this report, further instances of β denote the feedback factor seen by the opamp and not $\frac{W}{L}\mu C_{ox}$.

For a closed-loop circuit, the step response is known to be

$$V_{out}(t) = V_{step}(t)(1 - e^{-t/\tau}) \qquad (5.19)$$

And thus the settling error voltage at the end of the sampling interval, which can be approximated as $T_{sett} = \frac{0.5}{f_s}$, is given by:

$$V_{error} = \frac{1}{2^N} = e^{-T_{sett}/\tau}$$

Substituting and rearranging terms yields:

136

$$\frac{f_{ug}}{f_s} = \frac{0.693N}{0.5 \cdot 2\pi\beta} \tag{5.20}$$

which dictates that for N=18, the unity gain frequency in Hertz must be about 4 times greater than the switching frequency at the worst case process and temperature corner for a β of unity. Since β turns out to be about 0.7, the unity gain frequency needs to be about 5.7 times the switching frequency, where the unity gain frequency is measured directly at the opamp output during an AC sweep measurement.

A more involved analysis by Martin, et al. [43] develops expressions and guidelines for the design of a switched-capacitor biquad filter, and also reaches the conclusion that to make settling error negligible, the opamp must have a unity gain frequency 5 times greater than the circuit switching frequency.

Slew Rate   Since nonlinearities in the circuit are to be avoided wherever possible, it is desirable to guarantee that the switched-capacitor opamp never enter its slewing regime and hence contain nonlinear settling components. Note that just after a step input to the opamp, the slope of the output will be at its maximum [3] and is given by:

$$\frac{d}{dt}v_{out}(t)|_{t=0} = \frac{V_{step}}{\tau} \tag{5.21}$$

If the slew rate of the opamp is larger than this value, the opamp is guaranteed never to slew in a switched-capacitor implementation. For a classic, Miller compensated, two stage opamp, the internal slew rate is:

$$SR_{int} = \frac{2I_{in}}{C_c} = V_{eff1}\omega_{ug} \tag{5.22}$$

where I_{in} is the DC bias current through each input branch of the opamp and V_{eff1} is the overdrive voltage of the opamp input pair transistors. As will be discussed later,

137

this voltage is typically set to be the minimum overdrive voltage that keeps the MOS device in strong saturation. This results in the requirement that:

$$SR_{int} = V_{eff1}\omega_{ug} > V_{step}\omega_{ug} \tag{5.23}$$

For an oversampling multibit D/A converter, this requirement is typically inherently met. For example, the maximum (and minimum) output step on the first opamp in a DCT filter with a feedback to input capacitor ratio of 25 and with a 4 bit D/A converter is $V_{step} = 0.005V$.

5.1.4 Direct Charge Transfer

As stated in the previous chapter, the Direct Charge Transfer switched-capacitor technique saves power by never connecting its sampling capacitor, C_1 in Fig. 5-6 below, as a load seen through the opamp feedback capacitor C_f. In addition, for each order of postfiltering, there is only one capacitor that contributes to the switched-capacitor noise of the filter, a slight advantage over second order biquad filter structures, whose second-stage capacitors see a high-pass transfer function to the filter output.

As stated before, the filter block shown above has a transfer function of:

$$\frac{V_{out}(z)}{V_{in}(z)} = \frac{z^{-1}}{\left(1 + \frac{C_f}{C_1}\right) - \frac{C_f}{C_1}z^{-1}} \tag{5.24}$$

which is a first-order filtering operation in discrete time.

Robust Transfer Function

One advantage of the Direct Charge Transfer technique as a filtering option is its robust transfer function characteristics. As stated in the previous section, the 6σ absolute capacitor variation in the process used is approximately 1.5%. When matching capacitor ratios as is the case in filter design, the variation in the capacitance ratio is

138
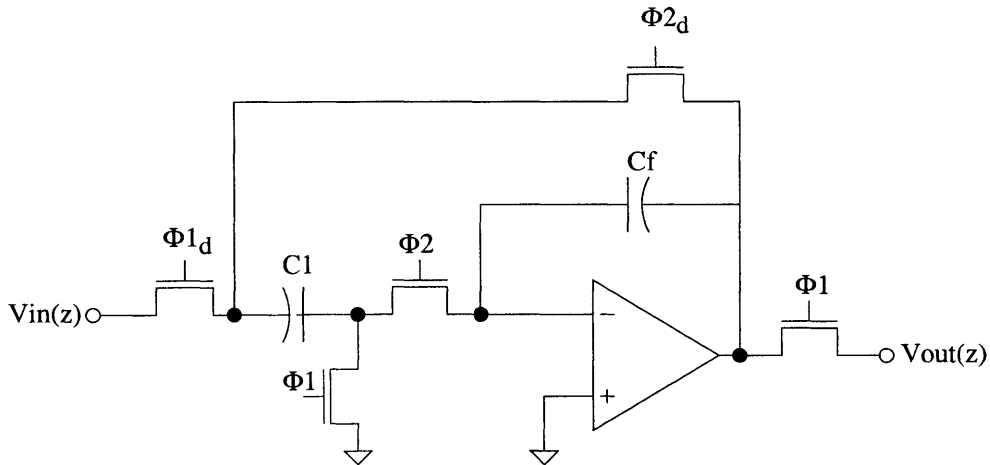
Figure 5-6: Direct Charge Transfer

typically about an order of magnitude lower. However, as shown in Fig. 5-7 below, even capacitor ratio matching inaccuracy of 1.5% barely changes the transfer function in the signal band (to 20kHz).

Fig. 5-7 was generated by cascading two first-order DCT blocks with a nominal capacitor ratio of 25. Note that the -3 dB point is set slightly outside the signal bandwidth so that the effect of capacitor variation is minimized within the signal band while still attenuating all of the out of band sigma-delta modulator noise to the level of the 16-bit quantization noise. Also note the in-band filter droop that requires the postfilter droop compensation that is discussed in Chapter 3. Since this droop compensation is done in the digital domain, it is similarly very robust.

Parasitic Insensitivity

Examination of the DCT technique suggests that its operation is parasitic insensitive. As shown in Fig. 5-8 below, all switches are connected to either ground (common mode voltage reference in a differential implementation), opamp virtual ground, modified virtual ground (in the case when correlated double sampling offset cancellation

139
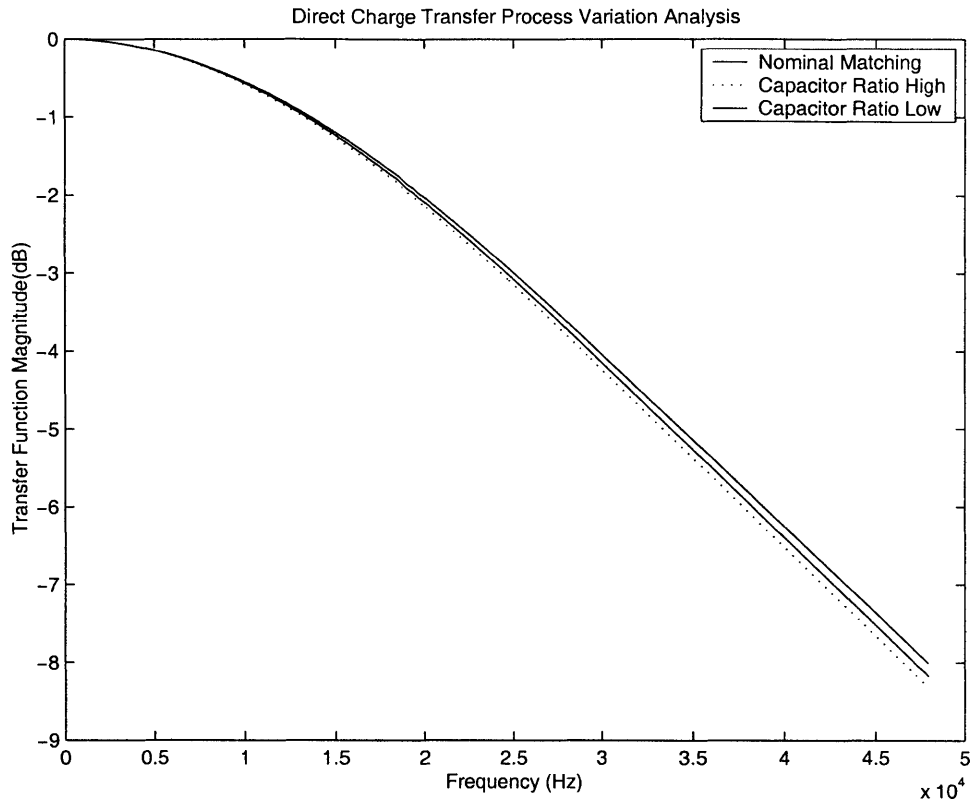
Figure 5-7: Direct Charge Transfer Over Process Variation

techniques are used), or the opamp output. Thus, the parasitic capacitances on these switches are either constantly charged to ground or are forced to a given voltage by an opamp output or voltage reference and do not contribute to the charge-sharing operation that defines the DCT transfer function. Typically, the primary parasitic capacitance of concern is the sampling capacitor C_1 bottom plate capacitance along with the switch nonlinear parasitic capacitance. This lumped capacitance is denoted as C_p.

On the sampling phase, C_p is connected to the input voltage (a DAC reference voltage for the first stage, an opamp output for following stages) and is hence charged to the input voltage. On the integration phase, C_p appears as a load to the output

140
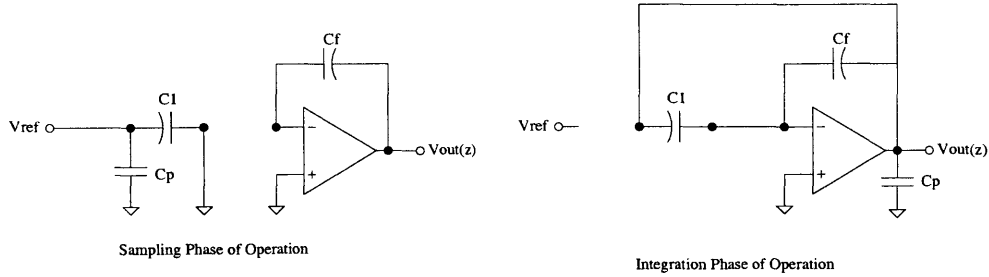
Figure 5-8: Direct Charge Transfer Parasitic Insensitivity

of the opamp and is hence charged to the output voltage dictated by the charges on the feedback and nominal sampling capacitances. Since this parasitic capacitance is small in a technology that supports metal-insulator-metal capacitors, C_p does not significantly alter the loading on the opamp. These assumptions were checked in SWITCAP by adding a large parasitic capacitance at the aforementioned location. No change in the filter transfer function occurred.

Switched-Capacitor Noise Analysis

Although the DCT operation is not analogous to that of a resistor, its noise performance can be analyzed in the same way as conventional switched-capacitor circuitry. To most easily see this, we ground the input of the DCT filter block and rearrange the position of the circuitry, as shown in Fig. 5-9 below.

This setup is immediately reminiscent of a switched feedback capacitor in a biquad, a capacitor that is commonly taken to have a thermal $\frac{kT}{C}$ noise power of $\frac{4kTf_0}{Cf_s}$ multiplied by an in-band gain of unity to the output. However, it is beneficial to review the assumptions made in the original switched-capacitor noise analysis.

On the input sampling phase of operation, the total series resistance R of the two sampling switches generate a wideband noise power of $4kTR\Delta f \frac{V^2}{Hz}$. However,

141
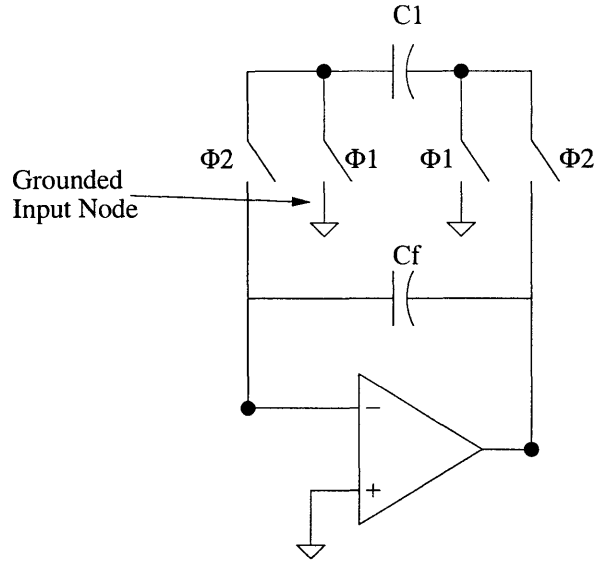
Figure 5-9: Direct Charge Transfer Noise Analysis

since the switches see a capacitive load to ground, this noise has an effective brick-wall bandwidth of $\frac{\pi}{2}\frac{1}{2\pi RC}$. When the switches are disconnected, the noise voltage is sampled and held. Since the sampling rate f_s is much lower than the thermal noise bandwidth derived above, the switch thermal noise is undersampled and thus aliases back into the sampling frequency band $-\frac{f_s}{2} \leq f \leq \frac{f_s}{2}$ such that the wideband noise power is $\frac{2kT\Delta f}{Cf_s}\frac{V^2}{Hz}$. The hold operation effectively multiplies this noise frequency response with a sinc function that is approximately unity over the signal band.

This sample and hold operation happens one more time during the integration phase, doubling the noise power on the capacitor integrated over the signal band to:

$$\overline{V_{n,kT/C}}^2 = \frac{4kTf_0}{Cf_s}V^2 \tag{5.25}$$

since the opamp retains the original noise voltage charge on the combined sampling/integration capacitor.

142

Two-phase Clock Waveform Considerations

It is important to note that the delayed two-phase clock waveform shown in Fig. 5-5 also applies to Direct Charge Transfer and in fact was developed with Direct Charge Transfer in mind [48].

RC-Equivalence

One disadvantage of DCT is that its operation does not have a clearly defined RC analogue. For conventional switched-capacitor circuits, this equivalence provides an advantage in some simulators such as Cadence where AC noise analyses are performed to obtain the input-referred noise contributions of opamps. Since an AC analysis cannot be performed on a real switched-capacitor circuit for lack of a DC path to the output on any given clock phase, the effective resistances are set in place of the switched capacitors to confirm the transfer functions and in-band power gain from various points in the circuit to the filter output.

5.1.5 Correlated Double Sampling

Correlated Double Sampling with Traditional Switched-Capacitor Structures

Correlated Double Sampling is one of a larger class of *autozeroing* techniques that are are used to eliminate opamp offset and finite opamp gain effects in switched-capacitor circuits [41]. As shown in the diagram of a canonical inverting switched-capacitor integrator in Fig. 5-10 below, the difference between error voltage and ground is sampled at the negative input of the opamp on C_{cds} on Φ_2. On the sampling/integrating phase Φ_1, the low frequency components of V_e will not have changed much, resulting in the terminal of C_{cds} opposite the opamp acting as a modified virtual ground at which the low frequency components of V_e have been cancelled out.
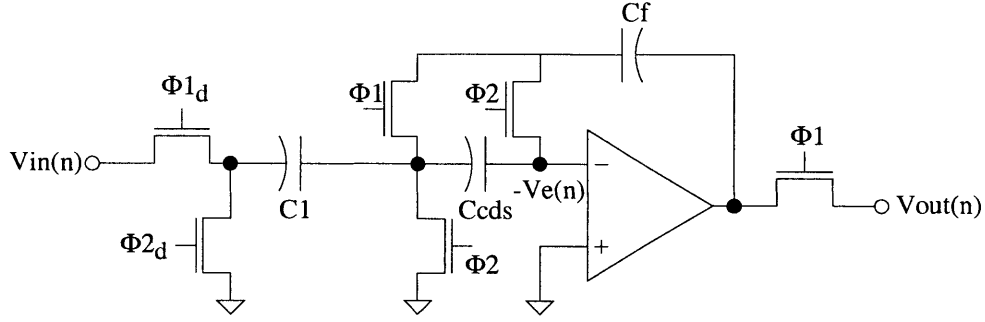
Figure 5-10: Correlated Double Sampling for a Switched-Capacitor Integrator

The transfer function of the error voltage V_e to the output can be derived as follows. Note that the cancellation is only valid on the integrating phase of the two-clock waveform (Φ_1 in this case).

Assuming that the opamp error voltage from a previous sample was zero, the charge on C_f at instance $n - \frac{1}{2}$ is:

$$Q = C_f(V_{out}(n-1)) \tag{5.26}$$

The charge on C_{cds} at instance $n - \frac{1}{2}$ is:

$$Q = C_{cds}(-V_e(n - \frac{1}{2})) \tag{5.27}$$

On the integrating/sampling instance of operation, n:

$$C_f(V_{out}(n)) = C_f\left(V_{out}(n-1) + V_e(n - \frac{1}{2}) - V_e(n)\right) + C_1\left(V_e(n - \frac{1}{2}) - V_e(n) - V_{in}(n)\right) \tag{5.28}$$

Rearranging terms, we obtain that:

144

$$V_{out}(n) - V_{out}(n-1) = \Delta V_{out} = (1 + \frac{C_1}{C_f}) \left(V_e(n - \frac{1}{2}) - V_e(n) \right) - \frac{C_1}{C_f} V_{in}(n) \quad (5.29)$$

Which is the result reported in Huang, et al. [44].

Taking the $\mathcal{Z}$-transform yields:

$$V_{out}(z) = \frac{-\frac{C_1}{C_f} V_{in}(z)}{1 - z^{-1}} - \frac{(1 + \frac{C_1}{C_f})(V_e(1 - z^{-1/2}))}{1 - z^{-1}} \quad (5.30)$$

Noting that:

$$V_e(n) = V_{os} + V_{noise}(n) + \frac{V_{out(n)}}{A} \quad (5.31)$$

where A is the low-frequency gain of the integrating opamp. Rearranging terms can yield an expression for the total output error voltage in the operation:

$$V_{outerror} = (1 + \frac{C_1}{C_f}) \left(V_{noise}(n) - V_{noise}(n - \frac{1}{2}) + \frac{V_{out}(n)}{A} - \frac{V_{out}(n - \frac{1}{2})}{A} \right) \quad (5.32)$$

Taking the $\mathcal{Z}$-transform yields:

$$V_{outerror} = (1 + \frac{C_1}{C_f}) \left(V_{noise}(1 - z^{-1/2}) + \frac{V_{out}}{A}(1 - z^{-1/2}) \right) \quad (5.33)$$

Thus, a first order differentiation is performed on the input-referred opamp noise voltage, and the finite-gain effects of the opamp also undergo a first-order differentiation, increasing the effective DC gain of the integrator. Typically, the exact magnitude of the effectiveness of this technique is determined by simulation.

One item to note is that on the integrating phase of operation, when the leftmost terminal of the feedback capacitor (as drawn on the schematics), the primary deter-

145

minant of the feedback factor β is the voltage divider between the CDS capacitor and the parasitic capacitance looking into one of the terminals of the opamp. Thus, care must be taken not to size the feedback capacitors so small that they unnecessarily degrade β and hence require a large opamp unity gain frequency to meet settling specifications.

5.1.6 Correlated Double Sampling and the DCT Technique

Although the benefits of the direct charge transfer technique are many, the technique is rendered useless if it cannot support a means to significantly reduce the input referred $1/\mathrm{f}$ opamp noise. In such a case, the $1/\mathrm{f}$ noise would occupy such a substantial part of the noise budget that the switched-capacitor filter capacitors would be required to be very large in order to reduce switched-capacitor noise to the point that the noise budget was met.

A direct charge transfer block enhanced with correlated double sampling circuitry is shown in Fig. 5-11.
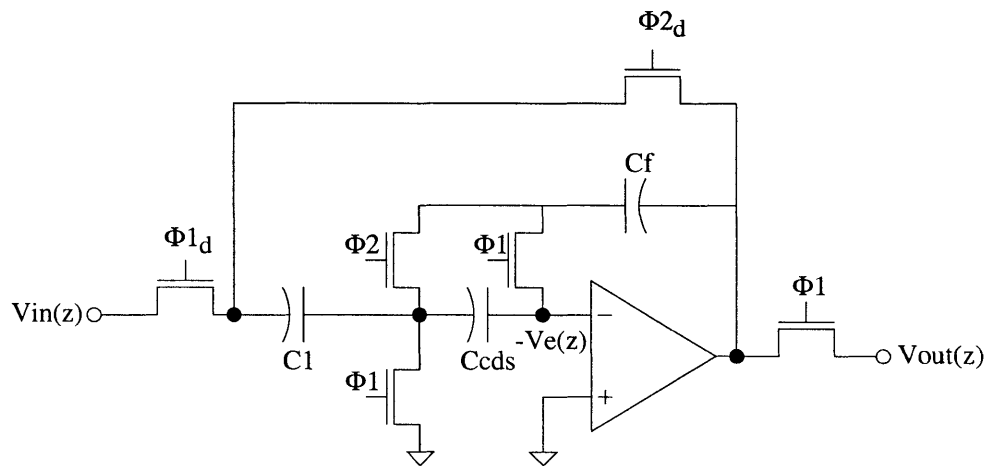
Figure 5-11: Correlated Double Sampling for Direct Charge Transfer

Assuming that at the beginning of the filter's operation, the input-referred opamp error voltage is zero, the charge on C_f at instance $n - \frac{1}{2}$ is:

$$Q = C_f(V_{out}(n - 1)) \qquad (5.34)$$

The charge on C_{cds} at instance n is:

$$Q = C_{cds}(V_e(n) - V_e(n - \frac{1}{2})) \qquad (5.35)$$

The charge on C_1 at instance $n - \frac{1}{2}$ is:

$$C_1(V_{in}(n - \frac{1}{2})) \qquad (5.36)$$

On the integrating phase of operation,

$$(C_f + C_1)\left(V_{out}(n) - V_e(n) + V_e(n - \frac{1}{2}) + V_e(n)\right) = C_f\left(V_{out}(n - 1)\right) + C_1\left(V_{in}(n - \frac{1}{2})\right) \qquad (5.37)$$

Rearranging and taking the $\mathcal{Z}$-transform, we obtain:

$$V_{out} = \frac{V_{in}z^{-1/2}}{(1 + \frac{C_f}{C_1}) - \frac{C_f}{C_1}z^{-1}} + \frac{(1 + \frac{C_f}{C_1})(V_e(1 - z^{-1/2}))}{(1 + \frac{C_f}{C_1}) - \frac{C_f}{C_1}z^{-1}} \qquad (5.38)$$

Note that although the discrete-time differentiated error term is multiplied by $(1 + \frac{C_f}{C_1})$, it has the same relative magnitude to V_{in} as in the case of the switched-capacitor integrator.

Another way to look at the problem is to note that the core charge sharing operation of DCT occurs independently of the input-referred error voltage of the opamp. Thus, on the integrating phase of operation, the output has the correct output voltage plus

$$V_{outputerror} = V_e(n) - V_e(n - \frac{1}{2})$$

And hence, the node opposite the opamp on C_{cds} also acts as a modified virtual ground.

The above hypothesis was initially tested with the aid of SWITCAP, which predicted a -43dB attenuation of low-frequency input-referred opamp noise with an opamp DC gain of 80dB when the DCT output was sampled on the integrating phase of operation. When the DCT output was taken as the continuous-time output, SWITCAP predicted a -6dB attenuation of input noise, taking into account the time-averaging nature of the buffer stage following the switched-capacitor filters. These results are shown in Fig. 5-12.

5.2   Switched-Capacitor Lowpass Filters

Despite its many advantages, the proposed Direct Charge Transfer filtering scheme does have its share of disadvantages compared to the traditional switched-capacitor biquad filter. For example, the output of the final opamp of the DCT filter must comprise the DT-CT interface. Because its output is seen on both clock phases and because the input of the opamp does not see a high-pass transfer function to the output, the CDS technique is not fully effective on this opamp. However, since the input of the second opamp of a biquad filter sees a high-pass transfer function to the output, its input-referred opamp 1/f noise is negligible when referred to the output of the entire filter.

This implies that the advantage offered by the DCT filter is not so clear cut, and hence a numerical comparison between the biquad and DCT filters is necessary to

148
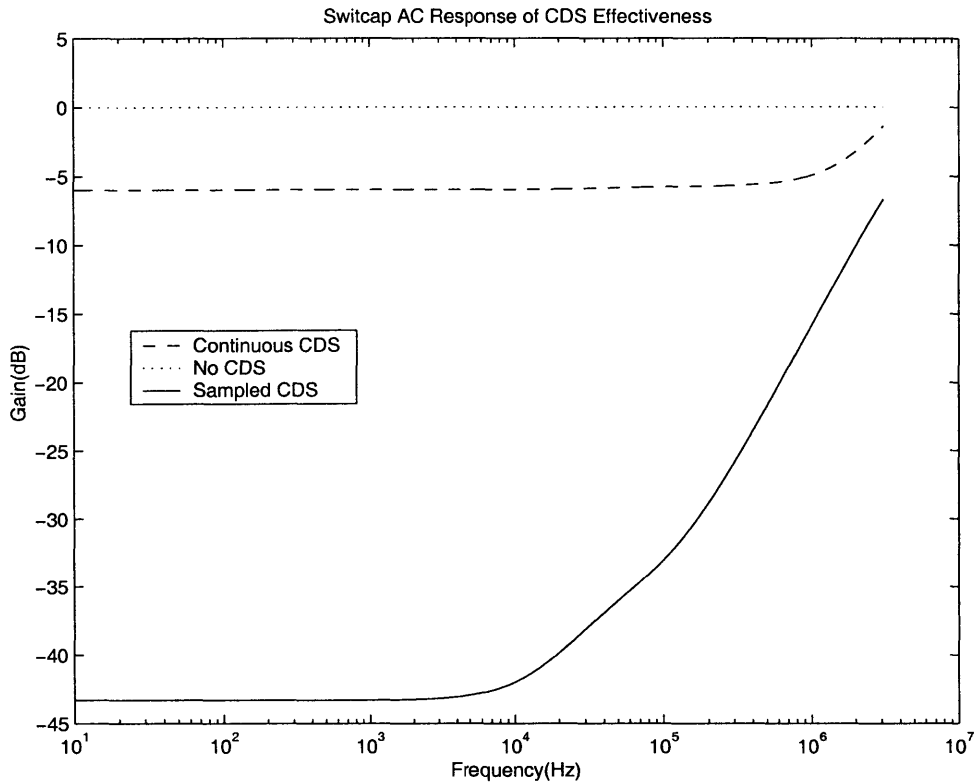
Figure 5-12: Correlated Double Sampling SWITCAP Simulation for DCT

determine which is superior from a low-power, low-area perspective.

5.2.1 Switched-Capacitor Biquad Filter Analysis

Biquad filters are a common choice for switched-capacitor implementation because they draw upon the vast body of work that has been performed on their continuous-time implementations. Perhaps more practically, biquad filters permit the use of complex poles in the filter transfer function, allowing the system designer to design a maximally flat frequency response over the signal band and hence do not require droop compensation.

149

Biquad filters are typically designed for either low or high filter Q such as to minimize the effect of component mismatch [3]. Lowpass biquad filters used in D/A applications are often designed with a Q slightly greater than that required to produce an optimally flat response (0.7) in order to steepen the rolloff immediately after the pole frequency. This section will, as an exercise, go through the design of a low Q filter with a Q of 0.8.

Derivation of Capacitor Ratios

It is known that for a stable biquad filter with the Q mentioned above, the two continuous time poles required to generate a "-3dB" point at 24kHz are, in units of rad/sec:

$$s_1 = -90368 + j113046, \quad s_2 = -90368 - j113046$$

A convenient approximation to the DT-CT bilinear transform that is valid for a reasonably large OSR is given by the relation [4]:

$$z_1 = e^{s_1 T_s} = e^{\frac{s_1}{f_s}} \tag{5.39}$$

For an oversampling ratio of 128 and hence $f_s = \frac{1}{T_s} = 6144000$Hz,

$$z_1 = 0.98523 + j0.01813, \quad z_2 = 0.98523 - j0.01813$$

We know that for a switched-capacitor biquad, we have a transfer function that can be used to determine the capacitor ratios. This transfer function is expressed as:

$$H_{bq} = \frac{-Az}{z^2 + Bz + C} \tag{5.40}$$

Since the poles have been determined, the coefficients A, B, and C are likewise

determined:

$$B = -(z_1 + z_2) = e^{\frac{s_1}{f_s}} + e^{\frac{s_2}{f_s}} \tag{5.41}$$

Since s_1 and s_2 form a conjugate pair with the same real part:

$$B = -2e^{\frac{Re\{s_1\}}{f_s}} \left(\cos \left(\frac{Im\{s_1\}}{f_s} \right) \right) \tag{5.42}$$

$$C = z_1 \cdot z_2 = e^{\frac{s_1 + s_2}{f_s}} \tag{5.43}$$

Since s_1 and s_2 form a conjugate pair with the same real part:

$$C = e^{\frac{2Re\{s_1\}}{f_s}} \tag{5.44}$$

Because a DC gain of unity is desired,

$$A = 1 + B + C \tag{5.45}$$

From these variables and from discrete-time flowchart analysis of the biquad, a set of constants can be derived that relate directly to the capacitor ratios in the biquad, shown in Fig. 5-13. Treating the capacitors C_g and C_a as design parameters, the following relations hold:

$$C_e = \frac{k_6}{k_5} C_a \tag{5.46}$$

$$C_d = \frac{1}{k_1} C_g \tag{5.47}$$

$$C_c = C_g \tag{5.48}$$

$$C_b = \frac{1}{k_5} C_a \tag{5.49}$$

Note that C_d and C_b are the dominant area consumers of this design. The con-

151

stants listed above relate to the biquad transfer function through the relation:

$$H_{bq}(z) = \frac{\frac{-k_1 k_5}{1+k_6} z}{z^2 + \frac{k_4 k_5 - k_6 - 2}{1+k_6} + \frac{1}{1+k_6}} \tag{5.50}$$

$$k_6 = \frac{1 - C}{C} = \frac{1}{C} - 1 \tag{5.51}$$

$$(1 + k_6) = \frac{1}{C} = e^{(-\frac{2Re\{s_1\}}{f_s})} \tag{5.52}$$
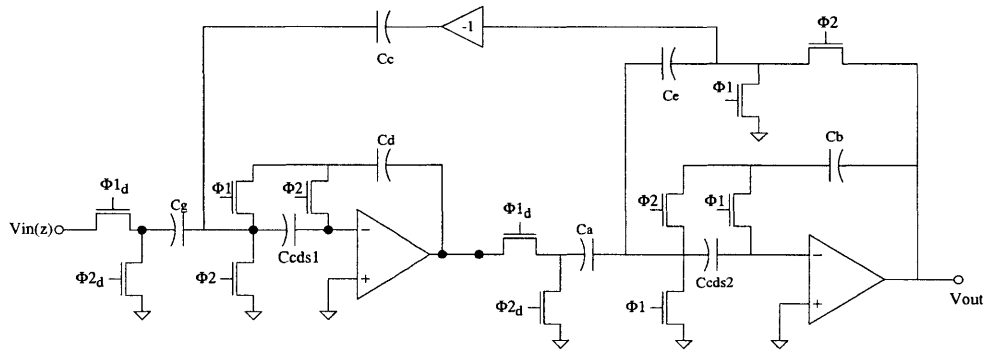
Figure 5-13: Switched-Capacitor Low Q Lowpass Biquad Filter

For a filter DC gain of unity, rearranging the expressions for A, B, and C will yield that $k_4 = k_1$. Then,

$$k_1 \cdot k_5 = B(1 + k_6) + k_6 + 2 \tag{5.53}$$

$$k_1 \cdot k_5 = A(1 + k_6) \tag{5.54}$$

An additional degree of freedom exists in the choice of k_1 and k_5 since the only constraint is on their product. For simplicity of calculation, k_1 will be chosen such that $k_1 = k_5$, although because k_1 and k_5 set the ratios between the sampling capacitors and the feedback capacitors, the prudent designer will realize that careful choice of these two coefficients can optimize the die area of the biquad. However, a brief in-

spection for the implementation described herein reveals that such optimization only results in an area savings of 20% over the choice of $k_1 = k_5$.

Proceeding, we have:

$$k_4 = k_5 = k_1 = \sqrt{A(1 + k_6)} \qquad (5.55)$$

For an oversampling ratio of 128, this yields:

$$k_6 = 0.02985$$

$$k_1 = k_4 = k_5 = 0.02373$$

For analysis purposes, we can rewrite Equation 5.55 as:

$$k_1 = \sqrt{\frac{1 + B + C}{C}} = \sqrt{\frac{1}{C} + \frac{B}{C} + 1}$$

$$= \sqrt{e^{-\frac{2Re\{s_1\}}{f_s}} - 2e^{-\frac{-Re\{s_1\}}{f_s}}\left(\cos^{-1}(\frac{Im\{s_1\}}{f_s})\right) + 1} \qquad (5.56)$$

To illustrate the tradeoff between OSR and area here, we will approximate:

$$\left(\cos^{-1}\left(\frac{Im\{s_1\}}{f_s}\right)\right) \approx 1 \qquad (5.57)$$

thus yielding:

$$k_1 = e^{-\frac{Re\{s_1\}}{f_s}} - 1 \qquad (5.58)$$

From the formulae given above, these coefficients are related to the key capacitor ratios by the relations:

$$C_d = \frac{C_g}{e^{-\frac{Re\{s_1\}}{f_s}} - 1} \tag{5.59}$$

$$C_b = \frac{C_a}{e^{-\frac{Re\{s_1\}}{f_s}} - 1} \tag{5.60}$$

These relations reveal a key tradeoff in the design of low-area D/A converters, that is, as the OSR, and hence f_s increase, the term $e^{-\frac{Re\{s_1\}}{f_s}}$ becomes closer to unity and hence the denominators of the above two relations becomes closer to zero, increasing exponentially the ratios of the sampling to feedback capacitors. Thus, it is vital to minimize the oversampling ratio of the D/A converter in order to save die area in the analog postfilter.

Transfer Function to Output and Switched-Capacitor Noise

Using SWITCAP, the transfer functions from various points in the circuit to the filter output were determined, allowing the calculation of the total output-referred noise of the filter.

Opamp Inputs   From the input of the first opamp, a DC power gain of 4=6dB was seen to the output.

From the input of the second opamp, a high pass transfer function approximately of the form: $20.3935 \cdot \log_{10}(f) - 81.0644$dB was seen to the output. Integrating over the signal band,

$$\text{Noise Power Gain} = \int_{20\text{Hz}}^{20000\text{Hz}} (10^{\frac{20.3935 \cdot \log_{10}(f) - 81.0644}{20}})^2 f \cdot df \tag{5.61}$$

$$\text{Noise Power Gain} = \int_{20\text{Hz}}^{20000\text{Hz}} f^{3.0395} \cdot 10^{-8.10644} \tag{5.62}$$

154

$$\text{Noise Power Gain} = \frac{10^{-8.10644}}{3.0395} \cdot f^{2.0395} \Bigg]_{20}^{20000} = 1.53022 \qquad (5.63)$$

Capacitors Both C_g and C_c see a unity gain transfer function to the output.

Capacitor C_a sees a high pass transfer function approximately of the form: $20.252 \cdot \log_{10}(f) - 87.968$dB to the output. Integrating over the signal band, this represents a total power gain of:

$$\text{Noise Power Gain} = \frac{10^{-8.7968}}{3.0252} \cdot f^{2.0252} \Bigg]_{20}^{20000} = 0.27 \qquad (5.64)$$

Capacitor C_e sees a high pass transfer function approximately of the form: $19.594 \cdot \log_{10}(f) - 83.13$dB to the output. Integrating over the signal band, this represents a total power gain of:

$$\text{Noise Power Gain} = \frac{10^{-8.313}}{2.9594} \cdot f^{1.9594} \Bigg]_{20}^{20000} = 0.44 \qquad (5.65)$$

5.2.2   Direct Charge Transfer Filter Analysis

The direct charge transfer filter consists of two identically ratioed filter blocks, although like the biquad capacitor the two sampling capacitors C_1 and C_2 can be independently set. Using a similar analysis as for the biquad filter, it is possible to set the capacitor ratio.

Derivation of Capacitor Ratios

From the transfer function of a first-order DCT filter, it can be seen that a discrete time pole exists at:

$$z = \frac{C_f}{C_f + C_1} \qquad (5.66)$$

And that the ratio between the sampling and feedback capacitors is given by:

155

$$\frac{C_f}{C_1} = \frac{1}{z^{-1} - 1} \qquad (5.67)$$

Unlike a biquad filter, the cascaded DCT filter can only implement two poles on the real axis. To obtain a "-3 dB" frequency of 24000Hz for the composite filter, the "-3 dB" pole frequencies of the first-order filter blocks can be determined analytically by the relation:

$$\left(\frac{1}{1 + (\frac{24000Hz}{k_1})^2}\right)^2 = \frac{1}{2} \qquad (5.68)$$

$$k_1 = -37290Hz \qquad (5.69)$$

The continuous time pole of interest thus lies on the real axis at $-37290 \cdot 2\pi \text{rad/s}$. Using the same approximation as for the biquad filter,

$$z = e^{\frac{s_1}{f_s}} \qquad (5.70)$$

$$\frac{C_f}{C_1} = \frac{1}{e^{-\frac{s_1}{f_s}} - 1} = \frac{1}{e^{-\frac{2\pi \cdot 37290}{6144000}} - 1} = 25.73 \qquad (5.71)$$

Again, we see the same tradeoff between oversampling ratio and die area as in the biquad filter. However, the ratio between the feedback and sampling capacitor for the DCT implementation, as predicted by the formula above, is 25, which results in a total capacitor area about 1.4 times less than the lowest achievable area for a biquad topology for the same noise budget. We round down to 25 because pushing the "-3 dB" frequency out slightly does not alter the system transfer function while reducing in-band droop and ensuring that the filter dropoff will not cut into the signal band over process variations.

Intuition and SWITCAP analysis show that the power gain from each node in the DCT structure to the filter output is unity.

5.3 Opamp Design for Switched-Capacitor Filters

Knowing the capacitor ratios along with the network structure of both topologies permits the calculation of output-referred kT/C noise, the dominant consumers of die area of the circuit, and a set of effective output loads for the two opamps. However, in order to design the filter holistically, it is important to first lay down the principles by which the opamps will be designed.

5.3.1 Topology Choice

Before designing the opamp itself, the opamp topology must be chosen. As stated earlier, the requirements of the two opamps are:

1. High Linearity
2. DC Gain $\geq$ 80dB
3. Unity Gain Frequency $\geq$ 4f$_s$ on slow process corner
4. Optimal settling on slow process corner (when f_{-3dB} is the lowest)
5. Low Noise

Class A opamps were chosen over class AB opamps for this project because of their superior linearity performance and because their power dissipation can be predicted and optimized in a straightforward manner [45]. Since each output of the opamp must swing 1.625V through a 2.5V supply voltage, the swing has only about 400mV headroom on either end. This headroom is insufficient to keep the resistance of a wide-swing cascode relatively constant over the maximum voltage swing and thus

we require that the output stage of the opamp consist of only one NMOS and one PMOS transistor. Of course, with such an output stage, a separate input stage is also required in order to achieve 80+ dB of DC gain. Since the bandwidth specification should be easy to meet, the opamp topology that comes to mind is the classic Miller-compensated two-stage opamp.

The schematic of such an opamp is shown in Fig. 5-14

5.3.2   Assigning Overdrive Voltages to Key Transistors

The first task to be performed while designing an opamp is to design the transistors of the input stage (M1-M4) to minimize voltage offset as a result of sizing and threshold voltage mismatches.

For the input pair of transistors (M1-M2), the gate offset voltage must be minimized. Given that the MOSFET saturation current relation is given by:

$$I_D = \frac{1}{2}\frac{W}{L}\mu_p C_{ox}(V_{GS} - V_T)^2 \tag{5.72}$$

The gate voltage mismatch can be approximated by [25]

$$\delta V_g = \delta V_T + (\frac{V_{GS} - V_T}{2})(\frac{\delta W}{W} + \frac{\delta L}{L}) \tag{5.73}$$

Thus, the gate overdrive voltage $V_{eff} = V_{GS} - V_T$ must be kept as low as possible while maintaining the device in strong inversion. This limit is typically around $V_{eff} = 0.18V$ for a 0.25μm process. Note that this arrangement for V_{eff} maximizes transconductance per current, which is important for transistors M1, M2, M7, and M9. Also note that $V_{eff}=V_{DS,sat}$ and thus this voltage needs to be minimized for M7 and M9 to maximize voltage swing and thus to reduce distortion at the output node.
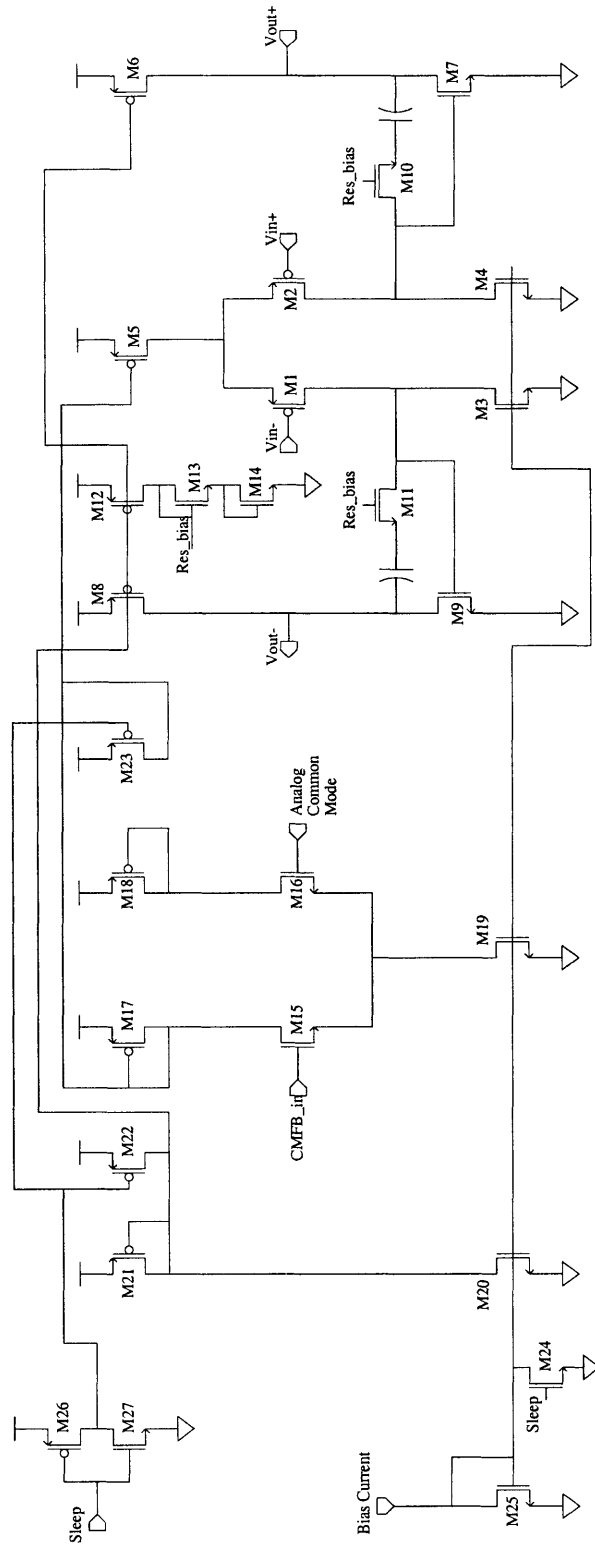
Figure 5-14: Schematic of Two-Stage Miller Compensated Opamp

For the current source active load in the input stage (M3-M4), current mismatch results in a gate voltage offset when referred back to the input pair (M1-M2). The objective here is thus to minimize current mismatch. If channel length and threshold voltage are independent, the drain current mismatch is [25]:

$$-\frac{I_D}{I_D} = \frac{\delta W}{W} + \frac{\delta L}{L} + \frac{2\delta V_T}{(V_{GS} - V_T)} \tag{5.74}$$

Thus, V_{eff} on M3 and M4 must be kept large. In practice, channel length and threshold voltage are not independent [49] and voltage swing requirements dictate that V_{eff} not be too large. Typical design values for V_{eff} on these transistors range from 0.3V to 0.4V.

5.3.3 Gain

The gain of a two-stage opamp is typically large, with the only parameter under the control of the designer being the lengths of the transistors. However, it is undesirable to increase the lengths of transistors M1 and M2 because they form a considerable portion of the load seen by the opamp and decrease β when increased. It is also undesirable to increase the lengths of M7 and M9 because their gate capacitances decrease the frequency of the non-dominant pole, reducing the opamp's phase margin.

As following analysis will show, however, it is desirable to increase the lengths of transistors M3 and M4 in order to reduce opamp input-referred thermal and 1/f noise. Gain is usually sufficient at this point to necessitate increasing the lengths of M6 and M8. Assuming that $L_{1-2,5-8} = 1\mu m$ and that $L_{3-4} = 8\mu m$, the total gain of the opamp is:

$$A = g_{m1}(r_{o1}//r_{o2})g_{m7}(r_{o6}//r_{o7}) \tag{5.75}$$

$$A \approx \frac{2I_1}{V_{eff1}\lambda_p I_1} \frac{2I_7}{V_{eff7}(\lambda_n + \lambda_p)I_7} \tag{5.76}$$

160

$$A \approx \frac{2}{V_{eff1}\lambda_p} \frac{2}{V_{eff7}(\lambda_n + \lambda_p)} \tag{5.77}$$

For approximation purposes, we take $V_{eff1} = V_{eff7} = 0.18V$, $\lambda_n = 0.1V^{-1}$, and $\lambda_p = 0.05V^{-1}$ to find that $A = 16500$, or 84dB.

5.3.4 Bandwidth

The bandwidth of the opamp is defined by its unity gain frequency ω_{ug}. For a two-stage opamp,

$$\omega_{ug} = \frac{g_{m1}}{C_c} = \frac{2I_1}{(V_{eff1})C_c} \tag{5.78}$$

As stated earlier, ω_{ug} must be greater than $\frac{4*OSR*48000Hz}{\beta}$ for the slow process corner. This occurs for a slow process and low temperature, when the PTAT current source supply current is at its minimum. Designing for the nominal case, a correction factor of 1.3 guarantees that the bandwidth specification is met over all corners. Thus, the input branch current of the opamp is set by treating the compensation capacitance as a design variable and is hence constrained to be:

$$I_1 = \frac{1}{2} \frac{5.2 \cdot OSR \cdot 48000Hz \cdot C_c}{\beta} \tag{5.79}$$

5.3.5 Phase Margin

A typical rule of thumb to designing optimally compensated opamps is to place the nondominant pole approximately three times away from the closed-loop crossover frequency ω_{-3dB}. This sets the phase margin ϕ_m to be:

$$\phi_m = 90° - \tan^{-1}(\omega_{-3dB}/\omega_{nd}) = 90° - \tan^{-1}(1/3) = 71.6° \tag{5.80}$$

We note that is slightly cumbersome to relate the opamp parameters to ω_{-3dB} if $\beta < 1$. However, if $\beta < 1$ and the frequency of the nondominant pole is set to $3\omega_{ug}$,

161

the actual phase margin will be slightly higher than 71.6° and will thus be closer to 75°. Thus, the hand design will be carried out assuming that $\omega_{nd} \approx 3\omega_{ug}$. In addition, the lead compensation of the two-stage opamp is the final determinant of the phase margin, and hence this relation is merely useful in setting the nondominant pole to a frequency at which such compensation is easily achieved.

In a two-stage opamp, the nondominant pole is approximately located at the frequency:

$$\omega_{nd} = \frac{\frac{g_{m7}\beta}{C_{Load,OL}}}{1 + \frac{C_{gs7}}{C_c}} \tag{5.81}$$

Where $C_{Load,OL}$ is the load capacitance seen at the output of the amplifier. This calculation is often performed by calculating an effective closed loop capacitance $C_{Load,CL} = \frac{C_{Load,OL}}{\beta}$ and writing:

$$\omega_{nd} = \frac{\frac{g_{m7}}{C_{Load,CL}}}{1 + \frac{C_{gs7}}{C_c}} \tag{5.82}$$

For design purposes, it is desirable to solve for g_{m7} as a function of C_{load} and C_c, as these two parameters will set the power through the output stage of the device.

Solving for g_{m7}

Realizing that:

$$g_{m7} = \frac{W}{L}\mu_n C_{ox} V_{eff7} \tag{5.83}$$

$$C_{gs7} = \frac{2}{3}\frac{W}{L}L^2 C_{ox} \tag{5.84}$$

Rearranging terms yields:

$$C_{gs7} = \frac{\frac{2}{3}g_{m7}L^2 C_{ox}}{\mu_n C_{ox} V_{eff7}} \tag{5.85}$$

162

$$\omega_{nd} = \dfrac{\dfrac{g_{m7}}{C_{Load}}}{1 + \dfrac{\frac{2}{3}g_{m7}L^2 C_{ox}}{\mu_n C_{ox} V_{eff7} C_c}} \qquad (5.86)$$

Noting that $\omega_{nd} = 3\omega_{ug}$ and solving for g_{m7} yields:

$$g_{m7} = \dfrac{3\omega_{ug}C_{Load}}{1 - \dfrac{3\omega_{ug}C_{Load}\frac{2}{3}L^2 C_{ox}}{C_c \mu_n C_{ox} V_{eff7}}} \qquad (5.87)$$

Also noting that the static current required to flow through the output stage is:

$$I_7 = \dfrac{1}{2}g_{m7}V_{eff7} \qquad (5.88)$$

$$I_7 = \dfrac{1}{2}\dfrac{3\omega_{ug}C_{Load}V_{eff7}}{1 - \dfrac{3\omega_{ug}C_{Load}\frac{2}{3}L^2 C_{ox}}{C_c \mu_n C_{ox} V_{eff7}}} \qquad (5.89)$$

Calculating Load Capacitance

The effective closed loop load capacitance seen by the opamp is equal to:

$$C_{Load,CL} = C_1 + C_p + \dfrac{C_2}{\beta} \qquad (5.90)$$

where C_1 is the sampling capacitance seen through the feedback network, C_p is the effective opamp parasitic input capacitance seen through the feedback networks, and C_2 is the effective capacitance seen at the output of the opamp. These capacitances C_1 and C_2 vary with the phase of operation, however, the worst-case scenario is not difficult to predict.

The worst-case loading scenario for the biquad filter opamp exists on the integrating phase of operation, when the opamp sees the sampling capacitance and when β is at its smallest due to the CDS capacitor. In this phase of operation, the CDS capacitor appears in series with the parasitic capacitance of the opamp, resulting in a capacitance smaller than the parasitic capacitance appearing in parallel with the sampling capacitance. Typically the CDS capacitor is sized to be the same as the dominant

load capacitance driven on this phase of operation, because the CDS capacitor forms the dominant load on the second phase of operation.

$$C_{Load,BQ} = C_1 + C_p + \frac{C_2}{\beta} \tag{5.91}$$

where C_p is the opamp input parasitic capacitance plus the CDS capacitor in series.

The worst case loading scenario for the DCT filter opamp also occurs on the integrating phase of operation when β is degraded through the CDS operation. Note that if the CDS capacitor equals the output capacitance driven by the opamp, the loading on the opamp is approximately equal to the value of the output capacitance C_2 over both phases of operation.

$$C_{Load,DCT} = \frac{C_2}{\beta} + C_p \tag{5.92}$$

5.3.6   Input-Referred Noise

An operational amplifier is an inherently noisy device, with most of its input-referred noise being generated by the transistors in its input stage. The channel resistance in the transistors generates a thermal noise current which can be referred back to the input voltage of the opamp. In addition, imperfections in the gate oxide of the transistors generates a low frequency 1/f noise voltage that can also be referred back to the opamp input.

Thermal Noise

The gate-referred thermal noise voltage of a MOS transistor is given by:

$$\overline{V_{n,T}}^2 = \frac{8}{3} \frac{kT\Delta f}{g_m} \tag{5.93}$$

164

Often, a more conservative estimate is used where:

$$\overline{V_{n,T}}^2 = \frac{4kT\Delta f}{g_m} \tag{5.94}$$

We are concerned about the noise contributions from both the input pair transistors (M1-M2) and from the input stage current source transistors (M3-M4). To obtain the contributions of the latter two transistors, the noise current is first obtained:

$$\overline{I_{n3,T}}^2 = 4kTg_{m3}\Delta f \tag{5.95}$$

Since this noise current appears in the input pair (M1-M2), it can be referred to the input terminals through multiplication by: $(\frac{1}{g_{m1}})^2$.

Thus, after appropriate substitution, term cancellation, and integration of the white noise over the signal band of 20kHz, the total input-referred thermal noise can be given by:

$$\overline{V_{n,T}}^2 = \frac{4kT \cdot (20000Hz)}{\sqrt{2\mu_p C_{ox}\frac{W_1}{L_1}I_1}} \left[1 + \sqrt{\frac{\mu_n\frac{W_3}{L_3}}{\mu_p\frac{W_1}{L_1}}}\right] \tag{5.96}$$

This thermal noise power has a bandwidth equal to the effective "brick-wall" bandwidth of the opamp, which is constrained by opamp settling requirements to be greater than the sampling frequency. If the signal from the input of the opamp is sampled before reaching the output of the filter, the noise is undersampled and aliases back into the baseband. Although this is the case for both topologies as implemented in this report, this would not be the case for a DCT filter that has not been enhanced with correlated double sampling, as the thermal noise at the input of the opamp will not fold due to undersampling [33]. We note that the second DCT filter has been enhanced with CDS because the reduction in 1/f noise is greater than the aliasing increase in thermal noise. Finally, the aliased thermal noise power must be multiplied by a factor of 2 to account for the differential nature of the circuit and

must be multiplied by the power gain from the opamp inputs to the output. Thus, for the biquad filter,

$$\overline{V_{n,T}}^2 = 2 \cdot \frac{2(\omega_{ug}\frac{\pi}{2})}{2\pi f_s} \cdot \left(4 \cdot \frac{4kT \cdot (20000Hz)}{\sqrt{2\mu_p C_{ox}\frac{W_{1,1}}{L_{1,1}}I_{1,1}}} \left[1 + \sqrt{\frac{\mu_n \frac{W_{3,1}}{L_{3,1}}}{\mu_p \frac{W_{1,1}}{L_{1,1}}}} \right] \cdots \right.$$

$$\left. 1.53 \cdot \frac{4kT \cdot (20000Hz)}{\sqrt{2\mu_p C_{ox}\frac{W_{1,2}}{L_{1,2}}I_{1,2}}} \left[1 + \sqrt{\frac{\mu_n \frac{W_{3,2}}{L_{3,2}}}{\mu_p \frac{W_{1,2}}{L_{1,2}}}} \right] \right) \tag{5.97}$$

For the DCT filter,

$$\overline{V_{n,T}}^2 = 2 \cdot \frac{2(\omega_{ug}\frac{\pi}{2})}{2\pi f_s} \cdot \left(\frac{4kT \cdot (20000Hz)}{\sqrt{2\mu_p C_{ox}\frac{W_{1,1}}{L_{1,1}}I_{1,1}}} \left[1 + \sqrt{\frac{\mu_n \frac{W_{3,1}}{L_{3,1}}}{\mu_p \frac{W_{1,1}}{L_{1,1}}}} \right] + \cdots \right.$$

$$\left. \frac{4kT \cdot (20000Hz)}{\sqrt{2\mu_p C_{ox}\frac{W_{1,2}}{L_{1,2}}I_{1,2}}} \left[1 + \sqrt{\frac{\mu_n \frac{W_{3,2}}{L_{3,2}}}{\mu_p \frac{W_{1,2}}{L_{1,2}}}} \right] \right) \tag{5.98}$$

1/f Noise

For the biquad filter, we assume that the 1/f noise is sufficiently attenuated by the high-pass transfer function of the CDS circuitry for the first opamp. Although the second opamp only achieves a benefit of 6dB attenuation of 1/f noise due to its CDS circuitry, the fact that its inputs see a high-pass transfer function to the output justifies the neglect of the 1/f noise component of this opamp as well.

For the DCT filter, we also assume that the 1/f noise is sufficiently attenuated by the high-pass transfer function of the CDS circuitry for the first opamp. The second opamp, however, achieves only a 6dB attenuation of 1/f noise across the signal band, as shown in Fig. 5-12. Its contribution to the total output-referred filter noise, accounting for the differential nature of the circuit and the CDS attenuation, is given by:

$$\overline{V_{n,1/f}}^2 = \frac{2k_p \int_{20}^{20000} \frac{1}{f^{1.2828}} \delta f}{4 \cdot W_1 L_1 C_{ox}} + \frac{2k_n \int_{20}^{20000} \frac{1}{f^{0.8824}} \delta f}{4 \cdot W_3 L_3 C_{ox}} \cdot \frac{g_{m3}^2}{g_{m1}^2} \qquad (5.99)$$

5.4 Hand Design for Noise Budget

In order to compare the biquad and DCT filter topologies, the equations derived above will be utilized to construct a preliminary hand design of the two filters for the same noise budget. This noise budget can be constructed using the sigma-delta SNR for an oversampling ratio of 128 found in Chapter 4 along with the output-referred swing and noise requirements.

At the output of this filter, the maximum output voltage swing must be 3.25Vpp and the total rms noise voltage power must be no greater than:

$$\text{Total Noise Power Budget} = \left[\frac{\frac{3.25}{2\sqrt{2}}}{10^{\frac{90dB}{20}}} \right]^2 = 13.2 \cdot 10^{-10} V^2 \qquad (5.100)$$

From Table 3.2, the simulated SNR of the digital portion of the D/A converter is 98.36dB. Thus, the output-referred voltage noise power from the digital portion of the D/A converter is given by:

$$\overline{V_{n,\Sigma\Delta}}^2 = \left[\frac{\frac{3.25}{2\sqrt{2}}}{10^{\frac{98.36dB}{20}}} \right]^2 = 1.93 \cdot 10^{-10} V^2 \qquad (5.101)$$

Finally, the average reference noise voltage power is given by:

$$\overline{V_{n,ref}}^2 = 0.73 \cdot 10^{-10} V^2 \qquad (5.102)$$

This leaves a component noise budget of:

$$\text{Component Noise Power Budget} = \text{Total N. P. B.} - \overline{V_{n,\Sigma\Delta}}^2 - \overline{V_{n,ref}}^2 = 10.54 \cdot 10^{-10} V^2$$

$$(5.103)$$

5.4.1 Switched-Capacitor Noise Contributions

The design of the filters began with the choice of the first input capacitor $C_1 = C_g = 1.2\text{pF}$. In Chapter 4, 75fF was presented as the minimum size capacitor, and for a 4 bit D/A converter, 16 such capacitors are required. The second input capacitor $C_2 = C_a$ was then chosen to make the switched-capacitor noise equal to about half the noise budget. The value of this capacitor for both topologies turned out to be $C_2 = C_a = 0.3\text{pF}$. Thus, for the biquad filter, the total integrated switched-capacitor noise power is given by:

$$\overline{V_{n,kT/C}}^2 = 2\left(\frac{4kT(20000)}{f_s(C_g)} + \frac{4kT(20000)}{f_s(C_c)} + 0.27\frac{4kT(20000)}{f_s(C_a)} + 0.44\frac{4kT(20000)}{f_s(C_e)}\right)$$

$$(5.104)$$

$$\overline{V_{n,kT/C}}^2 = 2\left(\frac{4kT(20000)}{f_s(C_g)} + \frac{4kT(20000)}{f_s(C_g)} + 0.27\frac{4kT(20000)}{f_s(C_a)} + 0.44\frac{4kT(20000)}{f_s(C_a\frac{k_6}{k_5})}\right)$$

$$(5.105)$$

$$\overline{V_{n,kT/C}}^2 = 2\left(\frac{4kT(20000)}{f_s(1.2pF)} + \frac{4kT(20000)}{f_s(1.2pF)} + \ldots\right.$$

$$\left. 0.27\frac{4kT(20000)}{f_s(0.3pF)} + 0.44\frac{4kT(20000)}{f_s(0.377pF)}\right) = 4.03 \cdot 10^{-10} V^2 \qquad (5.106)$$

For the DCT filter, the total integrated switched-capacitor noise power is given by:

$$\overline{V_{n,kT/C}}^2 = 2 \left(\frac{4kT(20000)}{f_s(1.2pF)} + \frac{4kT(20000)}{f_s(0.3pF)} \right) = 4.492 \cdot 10^{-10} V^2 \qquad (5.107)$$

5.4.2 Input Current and Opamp Noise Power

The next step is to set the input currents of the opamps such that the filter output-referred noise for both topologies are approximately the same. Since the V_{eff} voltages for M1-M4 are known, and since the input stage current is constrained by V_{eff1} and ω_{ug}, the only free design parameters are the compensation capacitors C_c of the opamps. Although β is dependent on the current flowing through the input stage and V_{eff1}, prior exploration of these calculations suggests that β will be close to 0.7.

Choosing a total noise budget of $6.2 \cdot 10^{-10} V^2$ to overdesign the noise performance of the circuit, the design parameters C_{c1} and C_{c2} were chosen using the following iteration algorithm: C_{c2} was set to a particular value while C_{c1} was swept until the total noise power equaled the total noise power budget. With these values selected, the total power of the circuit was computed using the loading relations described in the following section. The value of C_{c2} was then shifted by an increment of 0.1pF and the sweep of C_{c1} performed again until the noise power budget was met with the optimal static power dissipation. This procedure resulted in the following values of compensation capacitor and input branch current for the two opamps of the biquad filter:

$C_{c1} = 3.38pF$, $I_{1,1} = 76.33\mu A$
$C_{c2} = 1.35pF$, $I_{1,2} = 30.53\mu A$

For the DCT filter:

$C_{c1} = 0.78pF$, $I_{1,1} = 22.8\mu A$

$$C_{c2} = 1.80pF, \ I_{1,2} = 40.65\mu A$$

Using these values, we can calculate the total filter output-referred noise power. Note that subsequent iteration in Cadence has shown that a nominal case opamp bandwidth equals approximately 45MHz in order to meet settling time requirements over all process corners. Also note that as per the design guidelines given in subsection 5.3.2:

$$V_{eff1} = V_{eff7} = 0.18V, \ V_{eff3} = 0.34V$$

and $C_{ox} = 0.006384F/\mu m$, $\mu_n C_{ox} = 194A/V^2$, $\mu_n C_{ox} = 41A/V^2$

For the biquad filter, we fill in the values for Equation 5.97:

$$\overline{V_{nT}}^2 = 2 \cdot \frac{2 \cdot 45MHz \cdot 1.57}{6.144MHz} \cdot \left(4 \cdot \frac{4kT \cdot (20000Hz)}{\sqrt{2\mu_p C_{ox} \frac{115\mu m}{1\mu m} 76\mu A}} \left[1 + \sqrt{\frac{\mu_n \frac{54\mu m}{8\mu m}}{\mu_p \frac{115\mu m}{1\mu m}}} \right] \cdots \right.$$

$$\left. +1.53 \cdot \frac{4kT \cdot (20000Hz)}{\sqrt{2\mu_p C_{ox} \frac{46\mu m}{1\mu m} 30.5\mu A}} \left[1 + \sqrt{\frac{\mu_n \frac{21.6\mu m}{8\mu m}}{\mu_p \frac{46\mu m}{1\mu m}}} \right] \right) = 2.14 \cdot 10^{-10} V^2 \qquad (5.108)$$

For the DCT filter, including 1/f noise from the second opamp, Equations 5.98 and 5.99 are filled in. Note that $k_p=1.183 \cdot 10^{-23} V^2 F$ and that $k_n=3.454 \cdot 10^{-24} V^2 F$.

$$\overline{V_{n,T}}^2 = 2 \cdot \frac{2 \cdot 45MHz \cdot 1.57}{6.144MHz} \cdot \left(\frac{4kT \cdot (20000Hz)}{\sqrt{2\mu_p C_{ox} \frac{34\mu m}{1\mu m} (22.8\mu A)}} \left[1 + \sqrt{\frac{\mu_n \frac{16.25\mu m}{8\mu m}}{\mu_p \frac{34\mu m}{1\mu m}}} \right] \cdots \right.$$

$$\left. + \frac{4kT \cdot (20000Hz)}{\sqrt{2\mu_p C_{ox} \frac{61\mu m}{1\mu m} (40.65\mu A)}} \left[1 + \sqrt{\frac{\mu_n \frac{29\mu m}{8\mu m}}{\mu_p \frac{61\mu m}{1\mu m}}} \right] \right) = 1.44 \cdot 10^{-10} V^2 \qquad (5.109)$$

$$\overline{v_{n,1/f}}^2 = \frac{2k_p \int_{20}^{20000} \frac{1}{f^{1.2828}} \delta f}{4 \cdot (61\mu m)(1\mu m)C_{ox}} + \frac{2k_n \int_{20}^{20000} \frac{1}{f^{0.8824}} \delta f}{4 \cdot (29\mu m)(8\mu m)C_{ox}} \cdot \frac{g_{m3}^2}{g_{m1}^2} = 0.239 \cdot 10^{-10} V^{-2} \quad (5.110)$$

$$\overline{V_{n,Opamps}}^2 = 1.682 \cdot 10^{-10} V^2 \qquad (5.111)$$

5.4.3 Output Load and Output Stage Current

While the output stage power dissipation was optimized holistically with the filter design in a spreadsheet using the iteration procedure with C_{c1} and C_{c2} earlier, as an exercise, the calculation will be demonstrated below:

For the biquad:

$$C_{p1} = \frac{2}{3} W_{1,1} L_{1,1} C_{ox} = 0.49 pF$$

$$C_{p2} = \frac{2}{3} W_{1,2} L_{1,2} C_{ox} = 0.19 pF$$

Assuming that β is around 0.7, the opamp input parasitic capacitor and CDS capacitor are in series, reducing the value of C_p seen at the opamp output by about 2/3 from the actual value of the opamp input capacitance. Note that the output load of the filter is 0.5pF.

$$C_{Load,BQ} = C_{sampling} + (2/3)C_p + \frac{C_{output}}{\beta} \qquad (5.112)$$

$$C_{Load1,BQ} = 1.2pF + 0.32pF + \frac{0.3pF}{0.7} = 1.95pF \qquad (5.113)$$

$$C_{Load2,BQ} = 0.3pF + 0.12pF + \frac{0.5pF}{0.7} = 1.13pF \qquad (5.114)$$

171

Substituting in design values for Equation 5.89 yields:

$$I_{7,1} = \frac{1}{2} \frac{(848.2Mrad/s)(1.95pF)(0.18V)}{1 - \frac{(848.2Mrad/s)(1.95pF)\frac{2}{3}(1\mu m)^2 C_{ox}}{(3.38pF)\mu_n C_{ox}(0.18V)}} = 158\mu A \qquad (5.115)$$

$$I_{7,2} = \frac{1}{2} \frac{(848.2Mrad/s)(1.13pF)(0.18V)}{1 - \frac{(848.2Mrad/s)(1.13pF)\frac{2}{3}(1\mu m)^2 C_{ox}}{(1.35pF)\mu_n C_{ox}(0.18V)}} = 95\mu A \qquad (5.116)$$

For the DCT filter:

$$C_{p1} = \frac{2}{3}W_{1,1}L_{1,1}C_{ox} = 0.14pF$$

$$C_{p2} = \frac{2}{3}W_{1,2}L_{1,2}C_{ox} = 0.26pF$$

$$C_{Load,DCT} = \frac{C_2}{\beta} + (2/3)C_p \qquad (5.117)$$

$$C_{Load1,DCT} = \frac{0.3pF}{0.7} + 0.09pF = 0.52pF \qquad (5.118)$$

$$C_{Load2,DCT} = \frac{0.5pF}{0.7} + 0.17pF = 0.88pF \qquad (5.119)$$

Again, substituting design values into Equation 5.89 yields:

$$I_{7,1} = \frac{1}{2} \frac{(848.2Mrad/s)(0.52pF)(0.18V)}{1 - \frac{(848.2Mrad/s)(0.52pF)\frac{2}{3}(1\mu m)^2 C_{ox}}{(0.78pF)\mu_n C_{ox}(0.18V)}} = 42.6\mu A$$

$$I_{7,2} = \frac{1}{2} \frac{(848.2Mrad/s)(0.88pF)(0.18V)}{1 - \frac{(848.2Mrad/s)(0.88pF)\frac{2}{3}(1\mu m)^2 C_{ox}}{(1.8pF)\mu_n C_{ox}(0.18V)}} = 71uA$$

5.4.4 Power/Area Comparison

To approximate the total power consumption for the two filter topologies, we add the input and output branch currents and multiply by two due to the differential nature of the opamps while also estimating very roughly the opamp bias currents. One item of note is that the output stage currents for the DCT filters are so low that they are less than the sum of the input stage currents. This means that the external slew rate $SR_{ext} = \frac{I_7 - 2I_1}{C_{Load}}$ will be negative. In order to guarantee a positive slew rate and to guarantee that the opamps never slew, the output currents must be made only slightly higher than the input currents as per the discussion on slew rates earlier in this chapter. Thus, the numbers below make the output currents 25% larger than double the total input stage input current for the DCT filter only. In addition, the bias current in each of the opamps is approximated to be 1/3 of the total input stage tail current plus 1/4 of the total output stage current.

Thus, the total current for the biquad is given by: **921μA**

and the total current for the DCT filter is approximately given by: **565μA**

When calculating the area due to capacitors in the circuit, the conversion factor between capacitance and area is: **0.001017mm^2/pF**. Also note that from past projects, a dummy capacitor ratio has been determined from the ratio of nominal capacitor area to actual layout capacitor area. This number is **1.486**.

The capacitive area of the Biquad is given by: $2 \cdot 1.486 \cdot 0.001017 mm^2/pF(C_{c1} + C_{c2} + C_g(2 + \frac{1}{k_6}) + C_a(1 + \frac{k_6}{k_5} + \frac{1}{k_6})$= **0.218mm^2**

The capacitive area of the DCT filter is given by: $2 \cdot 1.486 \cdot 0.001017 mm^2/pF(C_{c1} + C_{c2} + C_1(1 + 25) + C_2(1 + 25))$=**0.125mm^2**

The power area product of the biquad is hence: $\mathbf{4.97 \cdot 10^{-10} W/m^2}$

The power area product of the DCT filter is hence: $\mathbf{1.77 \cdot 10^{-10} W/m^2}$

Even if the Biquad topology achieved a 20% area reduction due to clever choice of the filter coefficients, its power-area product would still be greater than twice that of the DCT filter topology. Thus, the DCT filter will be designed using the preliminary design derived above as a starting point.

Chapter 6

Analog Postfilter Implementation and Simulation Results

The Direct Charge Transfer filter designed using the methods described in the previous chapter was implemented and simulated in a 0.25μm CMOS process in the Cadence/Spectre design environment.

6.1   Analog Implementation

The full implementation of the postfilter, shown in Fig. 6-1, contains a number of details not discussed in the previous chapter that are considered below. A hand drawing of the schematic, with opamp and switch designations, is shown in Fig. 6-2 for clarity.

6.1.1   Architectural Considerations

Voltage References

For maximum voltage swing, the 2.5V supply rail can be used as the analog reference voltage and is so used in this implementation. Since opamps in general have a good
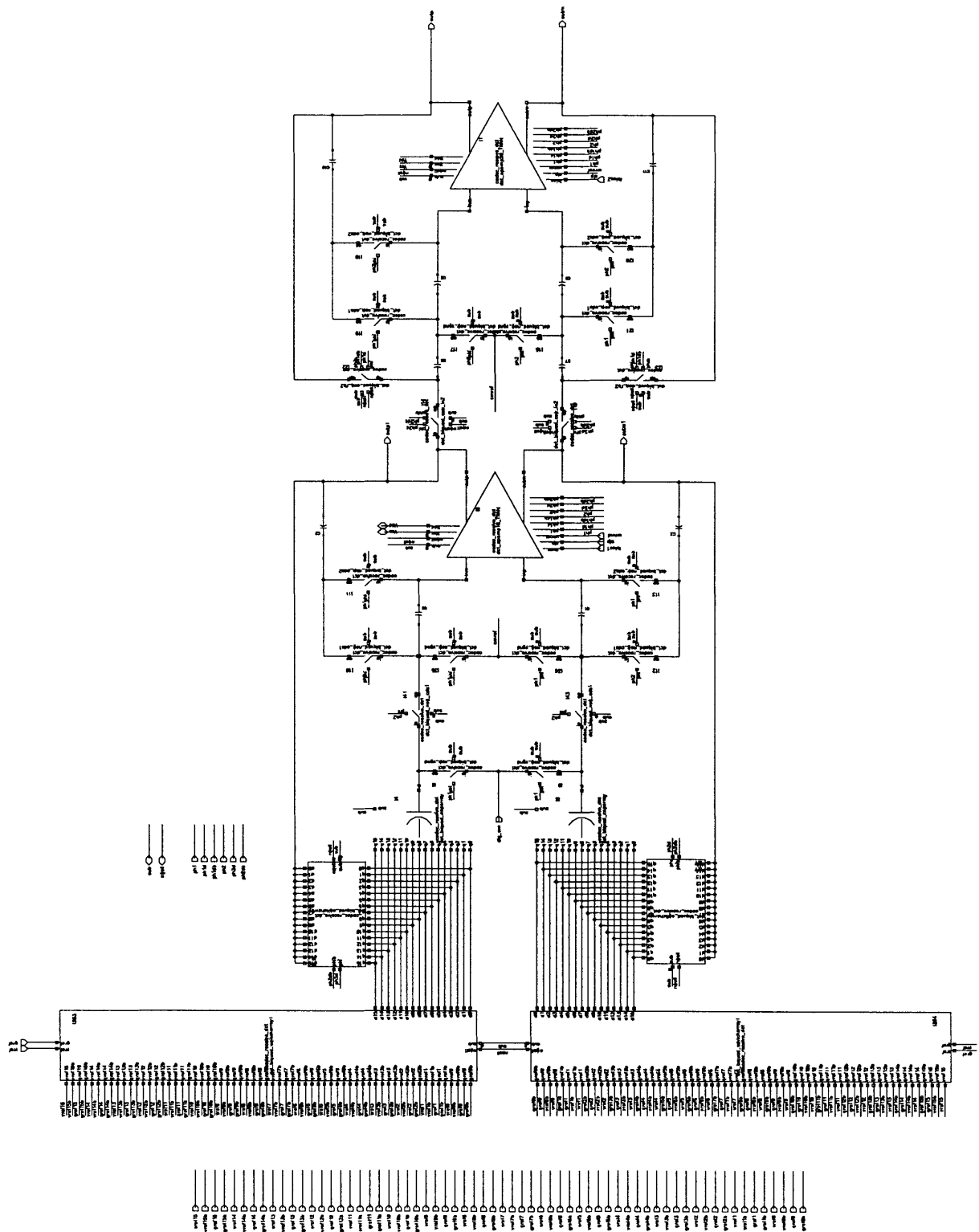
Figure 6-1: Cadence Schematic of DCT Postfilter

176

Figure 6-2: Hand Drawn Schematic of DCT Postfilter

177
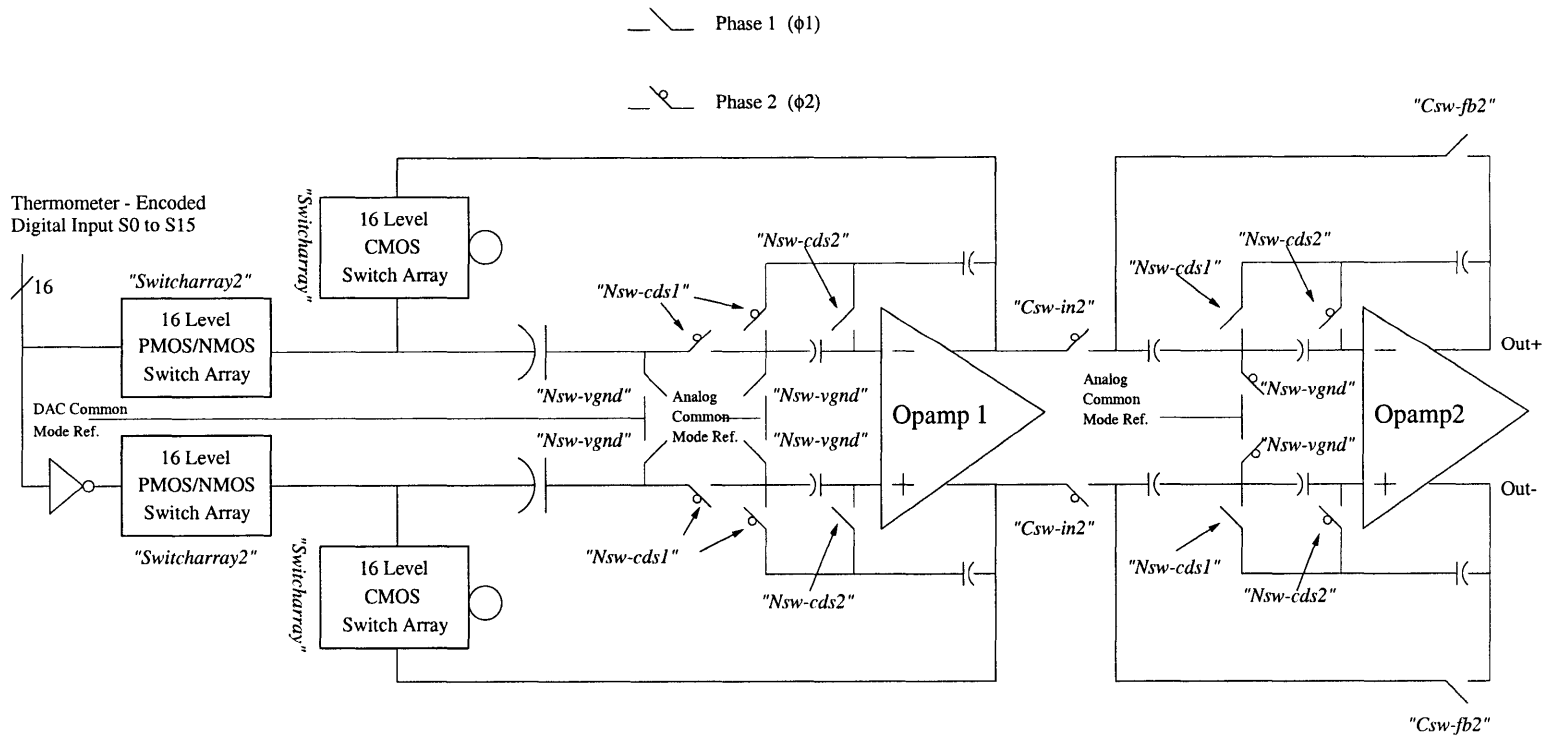
power supply rejection ratio (PSRR), noise on this supply line generally has negligible effect on the circuit. However, the same cannot be said of the reference for the D/A converter. Any noise or spurious signals on the D/A reference couple directly into the signal path, giving an effective PSRR of unity.

While previous DCT postfilter implementations solved this problem by bringing a voltage reference from off-chip [17], such a strategy is disadvantageous for a fully monolithic solution. Thus, an on-chip reference is used. Although the design of this voltage reference is beyond the scope of this thesis, it can be said that in general, the lower the value of the on-chip reference voltage, the greater amount of buffering can be applied and the lower the noise on this line can be achieved. It was found from previous implementations that an acceptable value for the digital reference voltage was 2V, which resulted in a supply noise power of $8.55 \cdot 10^{-6} V_{rms}$.

Since the postfilter implementation is fully differential, common mode reference voltages are necessary to act as differential ground voltages. The digital common mode reference is thus 1V and the analog common mode reference is 1.25V.

Dual Reference Switching Scheme

The astute reader will note that the switching scheme for the first DCT filter block is somewhat different than that described in the previous chapter. The situation requiring this switching setup is unique to the differential CDS-enhanced DCT filter. Assume for a moment that the D/A capacitor array shared a common mode reference voltage with the CDS capacitor. The common mode reference at this point would have to be the digital reference, otherwise a voltage offset would exist between the two differential signal paths. For the sake of argument, also assume that a DC input of 1V is introduced to the D/A sampling array (that is, 8 capacitors sample 2V, while the other 8 sample 0V). If this is the case, then the feedback capacitor must

have approximately no charge on it at DC. Also note that the opamp common mode feedback constrains the output voltage at both opamps to be 1.25V in this condition. Thus, on the first stage sampling clock phase Φ_1, the opposite terminal of the feedback capacitor is also at 1.25V and the CDS capacitors sample 0.25V plus any error voltage at the opamp inputs. This represents a problem in that on the integrating phase of operation, Φ_2, the voltage across the feedback capacitor is still 0V. When its bottommost terminal (as drawn) connects to the bottommost terminal of the CDS capacitor, the DC voltages at the input terminals jump abruptly to 1.5V due to the 0.25V offset stored on the CDS capacitor. Such a jump at the input terminals causes a temporary slewing in the common mode response of the opamp and must be avoided. The solution is to split the two references with a switch that is open on Φ_1 and closed on the integrating phase Φ_2, at which time it is only the voltages across the CDS and sampling capacitors that are of import.

Although not apparently obvious, the input terminals of the opamp start at 0V from circuit power up and eventually must reach 1.25V. This happens relatively quickly through the same mechanism as described above. The initial voltage on the feedback capacitor is 1.25V, since the common mode feedback holds the opamp outputs at this level for a differential input of 0V. Assuming for a moment that the input voltage ramps of the opamps ramps up much faster than the filter input signal, a DC differential input voltage to the D/A converter will result in that differential voltage being stored across the sampling capacitors. After enough charge sharing operations, this voltage appears across the feedback capacitor as well. As long as the common mode feedback is working, this compels the bottommost terminals of the capacitors to sit at 1.25V, as the differential output voltage appears on the topmost capacitor terminals. Likewise, the opamp input terminals must also sit at 1.25V.

D/A Converter

The oversize capacitors and large switches at the bottom of Fig. 6-1 and Fig. 6-2 are high-level representations of the 16-capacitor array and its associated switches that comprise the 4-bit D/A converter. At the very bottom of the figure are the switch signals from the DWA circuitry. The timing diagram for these signals is shown in Fig. 6-5. The switches in the bottommost blocks are comprised of single PMOS and NMOS transistors in parallel. The PMOS transistors connect to the high digital voltage reference of 2V, while the NMOS transistors connect to the low voltage reference of 0V. These switches were sized only as large as they needed to be to guarantee complete settling of the reference voltage onto the sampling capacitor/ D/A element. The smaller blocks represent the arrays of switches that connect the 16 capacitors in parallel with the feedback capacitor. Since the voltages seen by these switches are not binary, CMOS switches must be used and sized only large enough to not affect the settling behavior of the opamp.

Common Mode Feedback

The common mode output of a differential opamp is not inherently set by the internal biasing. Hence, an external common mode feedback circuit is required to keep the output common mode voltage with an analog common mode voltage reference. The process begins by averaging the two output voltages using a circuit as shown in Fig. 6-3.

When using switched-capacitors to implement a filter, the clocking infrastructure is already present to implement a switched-capacitor common mode feedback circuit. The switched capacitor common mode feedback presented in [46] and shown in Fig. 6-3 realizes an RC-equivalent averaging circuit with a very large time constant, thus removing all but the lowest frequency components of the output common mode voltage.
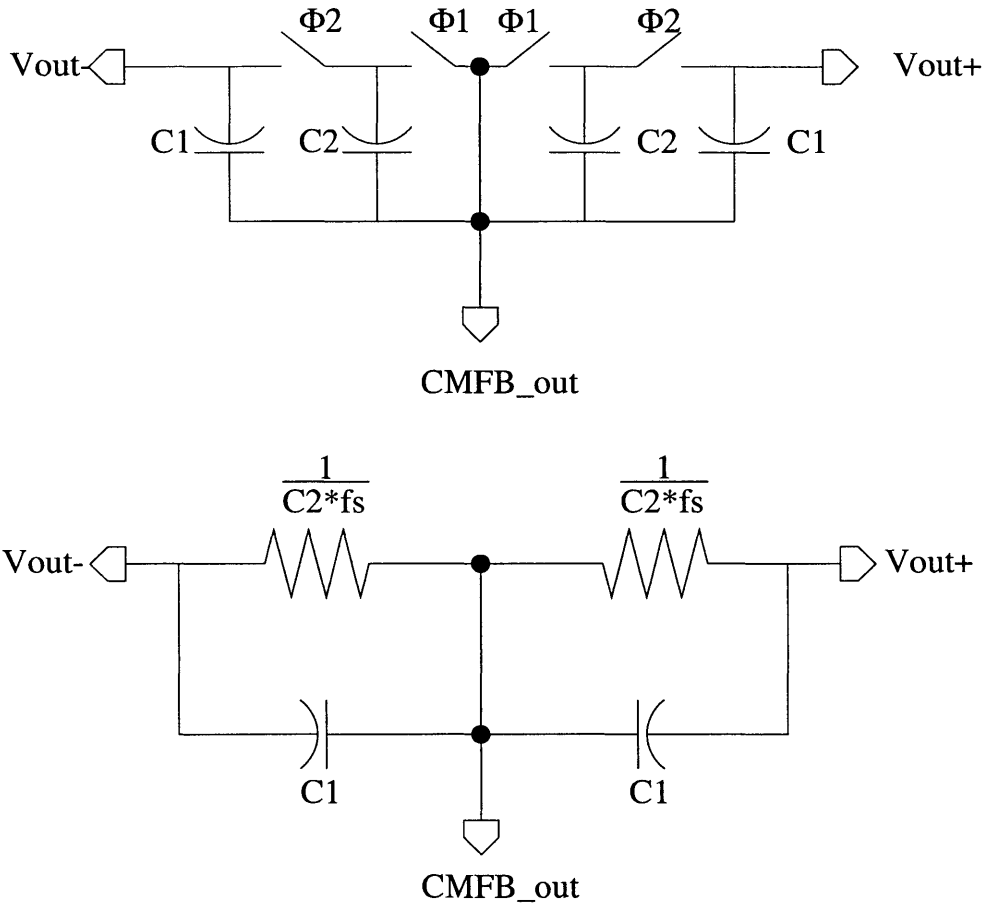
Figure 6-3: Switched-Capacitor Common Mode Feedback Averaging Circuit

The resulting averaged voltage is then taken to a differential buffer comprised of transistors M15-M20 in Fig.5-14. This buffer has a gain on the order of unity and serves as a comparator between the common mode voltage and the analog common mode reference. For example, of the output common mode is greater than the analog common mode, more current flows through the branch containing M17. This increases the current flowing through transistor M5, which in turn increases the voltage at the gates of M7 and M9, increasing the DC current flowing through the bottom halves of the output branches, lowering the common mode output voltage. This differential

buffer is used to increase the common mode feedback loop gain and to prevent capacitive loading of the switched-capacitor averaging circuit with the gate of M5. This topology for a common mode feedback circuit also allows for greater design flexibility and a larger output swing than other CMFB averaging circuits. [47]

6.1.2 Opamp Device Sizing and DC Operating Point

As shown in Table 6.1 and Table 6.2, the sizing of the key transistors (M1-M9) of the opamp follows from the analysis given in Chapter 5. Some of the device sizes have been changed slightly such that the simulated overdrive voltages match those given in the aforementioned analysis. The output stage current in opamp 1 was also increased slightly in order to doubly ensure that the external slew rate was of reasonable magnitude. The compensation capacitor for opamp 1 was 0.8pF, while the compensation capacitor for opamp 2 was 1.5pF.

Two-stage amplifiers such as the ones used in this design typically utilize lead compensation in order to avoid a right-half plane zero resulting from the feedforward path of a lone capacitor. Transistors M11 and M10 realize the resistors in the lead network and were sized such that optimal settling occurred for the cold, slow process corners. In general, a good starting point for iterating the resistance of this transistor is to first size and bias it such that $R = \frac{1}{1.2g_{m1}}$ [3]. This transistor was biased using the temperature and process independent biasing scheme of M12-M14 that is described in the Johns & Martin textbook [3].

The common mode feedback buffer transistors and the capacitors of the common mode feedback circuit are designed to give an open loop gain of about 100, with sufficient bandwidth and phase margin to allow the common mode to settle to an error value of 1/100 before the end of the switching phase. The goal here is not extreme

Device	W(μm)/L(μm)	Device	W(μm)/L(μm)	Device	W(μm)/L(μm)
M1	30/1	M10	6.25/1	M19	14/8
M2	30/1	M11	6.25/1	M20	7/8
M3	14/8	M12	6/1	M21	6/1
M4	14/8	M13	3/1	M22	2/0.5
M5	16/0.5	M14	3/1	M23	2/0.5
M6	36/1	M15	10/0.5	M24	2/0.5
M7	18/1	M16	10/0.5	M25	14/8
M8	36/1	M17	4/0.5	M26	4.70/0.25
M9	18/1	M18	4/0.5	M27	1/0.25

Table 6.1: Opamp 1 Device Sizes

accuracy, since the signal of interest is in the differential mode, but rather to avoid large common mode output transient excursions.

The input transistors of the common mode feedback buffer should be sized very small such that they do not capacitively load the common mode feedback circuit, which itself needs to be composed of very small capacitors so as to not inadvertently load down the opamp, whose outputs must drive the cmfb circuit. However, a reasonable W/L ratio is required for good DC gain and unity gain frequency. Transistor M5 should also be sized with a reasonable W/L ratio with its size kept in mind, as the capacitance on its gate node forms a non-dominant pole.

DC operating point simulations were performed over several corners to confirm that all devices were operating in the constant current region.

6.1.3 CMOS Switch Sizes

The transistor switches in the circuit were designed to be as small as possible without affecting the settling time of the opamps and while permitting 20-bit sampling on all sampling capacitors. The resultant switch lengths are shown in Table 6.3. The

Device	W(μm)/L(μm)	Device	W(μm)/L(μm)	Device	W(μm)/L(μm)
M1	60/1	M10	18/1	M19	21/8
M2	60/1	M11	18/1	M20	7/8
M3	28/8	M12	6/1	M21	6/1
M4	28/8	M13	3.2/1	M22	2/0.5
M5	30/0.5	M14	3.2/1	M23	2/0.5
M6	60/1	M15	10/0.5	M24	2/0.5
M7	32/1	M16	10/0.5	M25	14/8
M8	60/1	M17	5/0.5	M26	4.70/0.25
M9	32/1	M18	5/0.5	M27	1/0.25

Table 6.2: Opamp 2 Device Sizes

Switch	W_n(μm)	W_p(μm)	Switch	W_n(μm)	W_p(μm)
Switcharray	0.50	2.0	Switcharray2(split)	0.30	1.30
Csw-in2	2.5	10	Csw-fb2	2.5	10
Nsw-vgnd	4	N/A	Nsw-cds1	20	N/A
Nsw-cds2	10	N/A	Csw-cmfb	2	2

Table 6.3: Switch Sizes

switches were designed using the formula given in Rabaey [32] with the caveat in the paper by Chilakapati [42] in mind, while using a DC simulation on each switch to confirm its on resistance. In some cases, especially those seeing the CDS capacitor as a feedback load on the sampling phase of operation, the switch sizes needed to be increased over the sizes predicted by simple time constant analysis.

6.1.4 Clock Generator

The nonoverlapping clock generation circuitry, shown in Fig. 6-4 is designed to generate a nonoverlapping clock with waveforms as shown in Fig. 5-5. The clock generation circuitry takes as its input a clock waveform with a 50% duty cycle and outputs a series of nonoverlapping clock waveforms and their complements, when CMOS switches are to be driven. The logic gates buffering the clock signals were designed to drive

the gate loads seeing the particular waveforms such that the rise and fall times were kept sharp. The on-times and rise/fall times of the waveforms generated by the clock generator for an input clock running at 6.144MHz are shown in Table 6.4.
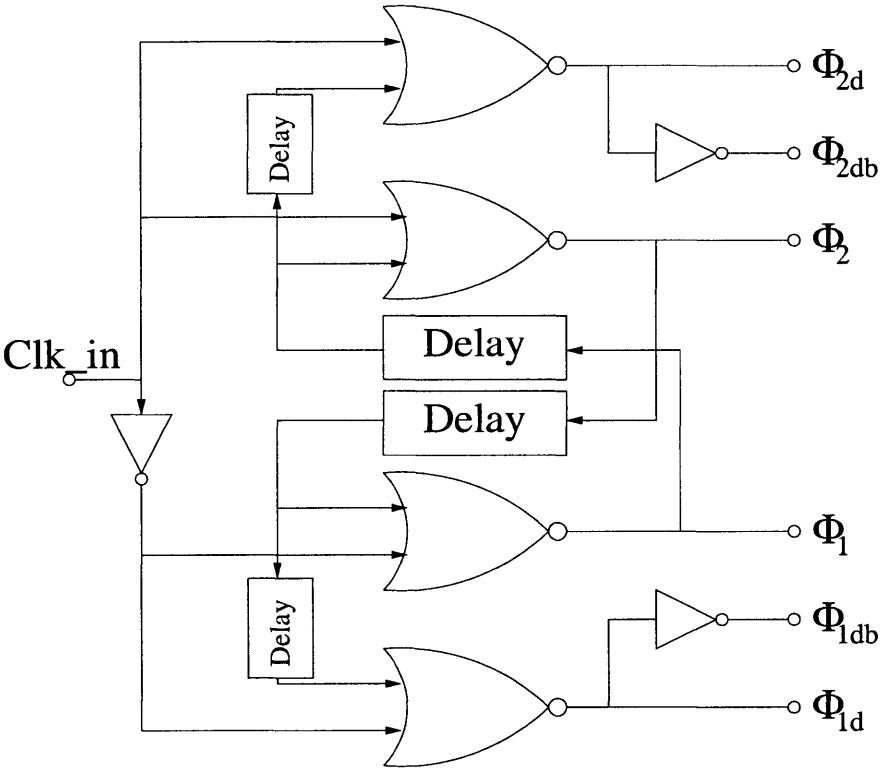
Figure 6-4: Clock Generation Circuitry Schematic

The switches to the D/A converter are controlled by the DWA circuitry and Φ_{1d}. Logic gates perform AND and OR operations on these signals to produce the switching waveforms for the arbitrary DAC element XX shown in Fig. 6-5, where XX is a number from 00 to 15. The power dissipated by the clock generation circuitry is **0.129mW** for the input clock waveform of 6.144MHz and its area is negligible for the overall design.

185

Clock Waveform	Rise/Fall Time(ns)	"On" Time (ns)	Offset from Clk_in(ns)
Φ_1	0.254	78.91	83.87
Φ_{1d}	0.327	79.79	83.89
Φ_{1db}	0.160	79.95	83.89
Φ_2	0.296	79.37	0.13
Φ_{2d}	0.248	80.45	0.13
Φ_{2db}	0.096	80.47	0.13

Table 6.4: Waveform Metrics for Clock Generation Circuitry

6.2 Circuit Simulation

6.2.1 Differential AC Performance

The AC performance of the two opamps was determined by breaking the feedback loop of the opamp at the opamp inputs and applying a test AC voltage to the opamp inputs. Dummy opamps were used as loads for the other broken end of the loop. Although the AC output voltage was taken at the output of the opamp, not accounting for the nonunity β feedback factor on the integrating phases of operation, the measurements were referred to the open loop output by the following calculations:

Gain Calculation to account for beta:

$$\text{DC Gain(dB)}_{real} = 20 \log_{10} \left(\beta 10^{\frac{\text{DC Gain(dB)}_{meas}}{20}} \right) \tag{6.1}$$

Conversion between opamp open loop unity gain frequency and closed loop -3 dB frequency.

$$f_{-3dB} = \beta f_{ug} \tag{6.2}$$

Phase margin calculation to account for beta:
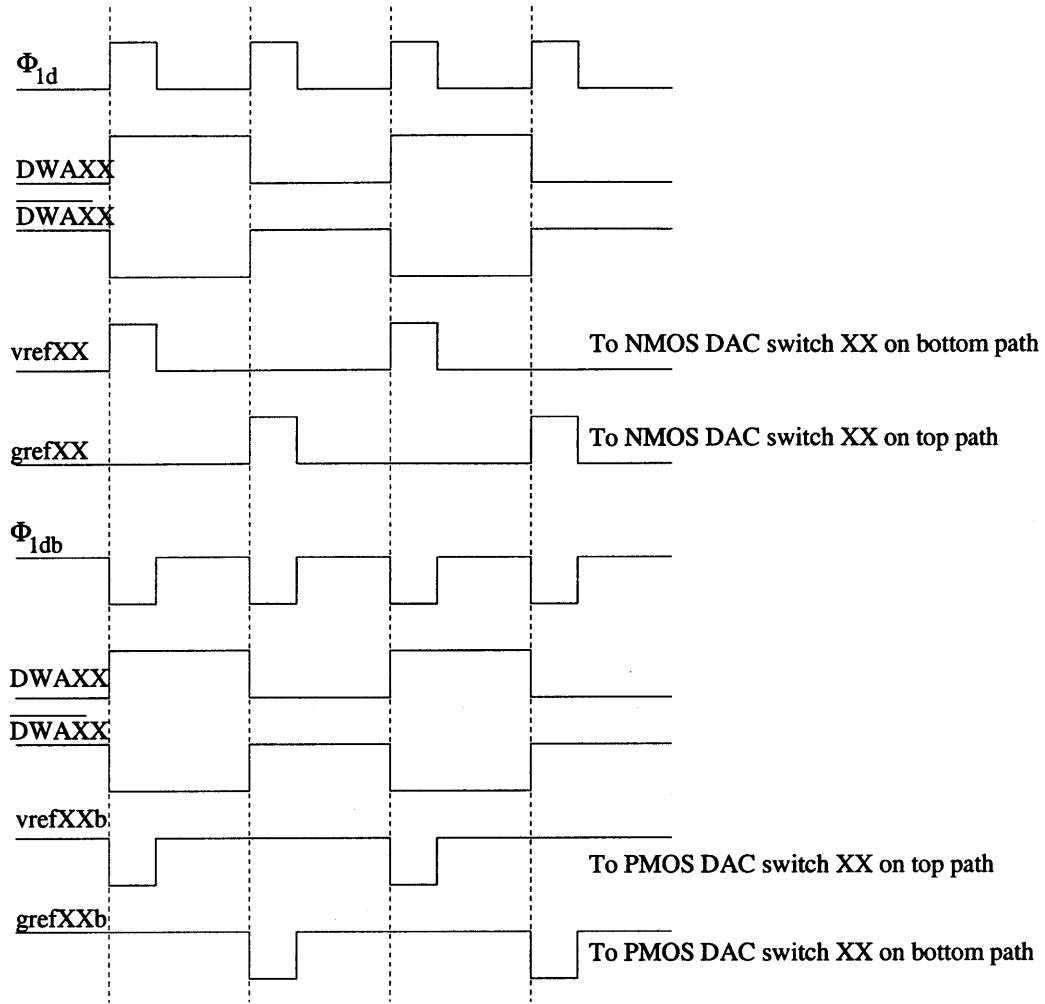
Figure 6-5: D/A Converter Capacitor Array Switch Timing Diagram

$$\Phi_{m,meas} = \tan^{-1}\left(\frac{f_{nd}}{f_{ug}}\right) \qquad (6.3)$$

$$f_{nd} = f_{ug}\tan(\Phi_{m,meas}) \qquad (6.4)$$

$$\Phi_{m,real} = \tan^{-1}\left(\frac{f_{nd}}{f_{-3dB}}\right) \qquad (6.5)$$

$$\Phi_{m,real} = \tan^{-1}\left(\frac{f_{ug}\tan(\Phi_{m,meas})}{\beta f_{ug}}\right) \qquad (6.6)$$

Clock Phase/Process Corner	f_{-3dB}(MHz)	Φ_m(degrees)	DC Gain(dB)
Φ_1, Typical	45.37	78.11	89.85
Φ_2, Typical	29.18	78.20	86.75
Φ_1, Slow, -40°C	34.48	82.54	91.58
Φ_2, Slow, -40°C	22.65	81.49	88.47
Φ_1, Slow, 110°C	34.67	81.54	89.66
Φ_2, Slow, 110°C	22.34	80.57	86.56
Φ_1, Fast, 110°C	59.38	72.37	81.20
Φ_2, Fast, 110°C	37.59	73.60	78.10

Table 6.5: AC Performance for Opamp 1, Beta=0.7 for Phase 2

Clock Phase/Process Corner	f_{-3dB}(MHz)	Φ_m(degrees)	DC Gain(dB)
Φ_1, Typical	29.97	82.08	86.30
Φ_2, Typical	43.47	71.59	89.91
Φ_1, Slow, -40°C	22.76	85.06	88.04
Φ_2, Slow, -40°C	33.11	75.69	91.65
Φ_1, Slow, 110°C	22.66	84.39	86.09
Φ_2, Slow, 110°C	32.72	75.00	89.70
Φ_1, Fast, 110°C	39.34	78.15	77.08
Φ_2, Fast, 110°C	56.69	66.33	80.69

Table 6.6: AC Performance for Opamp 2, Beta=0.66 for Phase 1

$$\Phi_{m,real} = \tan^{-1}\left(\frac{\tan(\Phi_{m,meas})}{\beta}\right) \tag{6.7}$$

Note that although the unity gain frequency of the opamps is slightly lower than that called for by the analysis given in Chapter 4 for the worst-case corners, the settling specifications were still met. In addition, it was found that a phase margin slightly higher than 75° produced an optimal settling time for this implementation.

AC performance was also determined while sweeping the DC output differential mode voltage to ensure that key AC parameters do not deviate into unacceptable values as the filter signal waveform approaches its extremes. The results of these

simulations are shown in Figs. 6-6 and 6-7. Note that these plots are for the integrating phases of both opamps, measured at the opamp outputs, and thus the plots should be viewed with the β conversions described above in mind. However, the key impetus behind the simulation is not lost, that is, the measurements still show minimal deviation of phase margin and -3 dB frequency (related to GBW plot by $1/\beta$) over the output differential mode range. DC Gain drop across the maximum differential output mode range (0V to 0.8125V) in Figs. 6-6 and 6-7 is 3.59dB for opamp 1 and 3.86dB for opamp 2 for the typical process corner. These numbers are viewed as good indicators that the total harmonic distortion of the filter will be lower than -60dB. Although the deviation for the hot, fast process corner is greater, this is viewed as acceptable as the total harmonic distortion is specified only for the nominal case. Note that in Fig. 6-6, the y-axis of the top graph in is units of **Hz** and the y-axis of the center graph is in units of **Degrees**. In Fig. 6-7, the y-axis of the center graph in is units of **Degrees** and the y-axis of the bottom graph is in units of **Hz**.
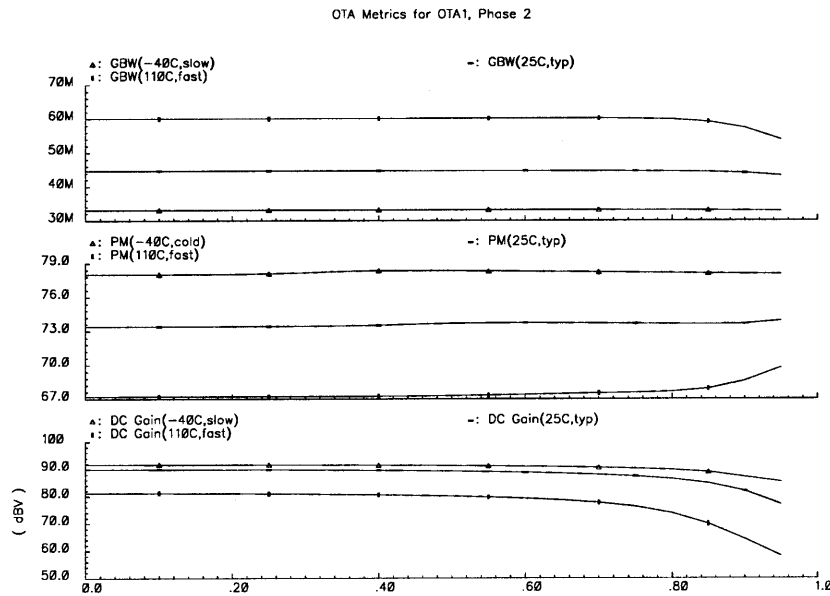
Figure 6-6: AC Performance for Opamp 1 Swept Over Differential Output Swing
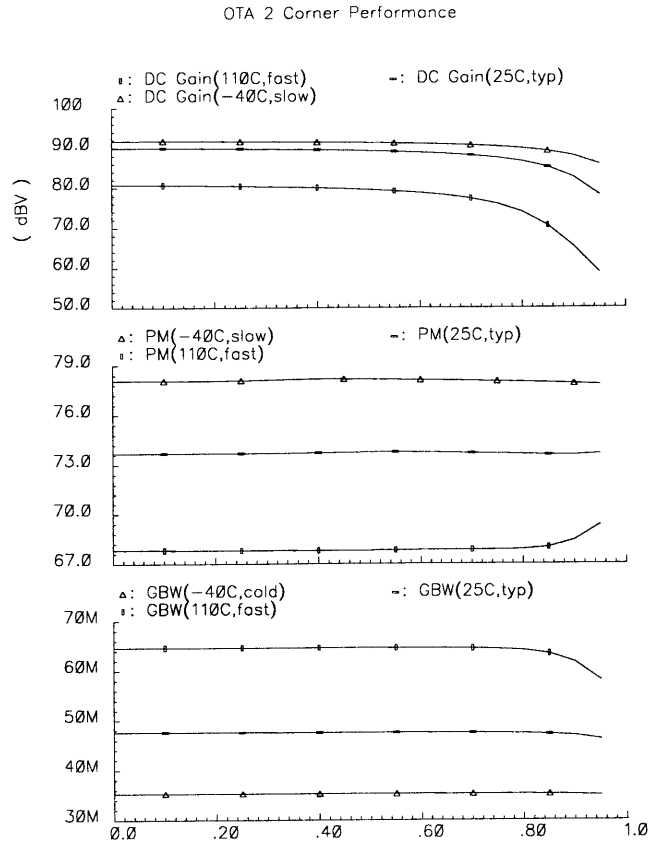
Figure 6-7: AC Performance for Opamp 2 Swept Over Differential Output Swing

6.2.2   Common Mode Feedback Loop AC Performance

The AC Performance of the common mode feedback loop was determined by breaking the feedback loop between the CMFB switched-capacitor averaging circuit and the CMFB buffer inside the opamp. Since the CMFB circuit cannot maintain the common mode output voltage during an AC simulation during which the CMFB loop is broken, the output voltages of the opamps were set by ideal CMFB circuits outside of the test schematic. A non-functional opamp serves as a dummy load here as in the differential AC performance tests.

190

Clock Phase/Process Corner	GBW(MHz)	Φ_m(degrees)	DC Gain(dB)
Φ_1, Typical	42.39	71.92	38.16
Φ_2, Typical	35.89	65.60	40.19
Φ_1, Slow, -40°C	28.59	80.32	37.57
Φ_2, Slow, -40°C	25.58	73.67	39.30
Φ_1, Slow, 110°C	30.76	79.36	33.03
Φ_2, Slow, 110°C	26.77	72.42	34.73
Φ_1, Fast, 110°C	60.93	60.36	37.87
Φ_2, Fast, 110°C	49.45	55.69	40.31

Table 6.7: AC-CMFB Performance for Opamp 1

Clock Phase/Process Corner	GBW(MHz)	Φ_m(degrees)	DC Gain(dB)
Φ_1, Typical	39.25	61.27	39.98
Φ_2, Typical	36.90	59.05	38.6
Φ_1, Slow, -40°C	28.18	68.37	39.41
Φ_2, Slow, -40°C	26.59	65.81	38.23
Φ_1, Slow, 110°C	27.94	68.44	34.13
Φ_2, Slow, 110°C	26.20	65.74	32.97
Φ_1, Fast, 110°C	53.41	52.53	39.80
Φ_2, Fast, 110°C	50.25	51.01	38.12

Table 6.8: AC-CMFB Performance for Opamp 2

6.2.3 Transient Simulation Results

The effectiveness of the correlated double sampling circuitry was simulated by applying a sizing offset of 10% to the input transistor pair (M1-M2) and observing the differential error voltage at the output of the filter for a DC filter input.

Output Differential Offset Without CDS: 10.7561mV
Output Differential Offset With CDS: 0.288mV

This represents an attenuation of **-31.45dB** at DC, enough to justify neglecting input-referred 1/f noise from opamp 1. Note that this case was concocted purely for test purposes and such a large sizing offset between the two input devices is not expected over a typical process run.

The transient settling behavior of the opamps was determined for a worst-case output voltage step. Since a simple observation of the sigma-delta modulator transfer function shows at worst case, the input of the filter is incremented by only one D/A converter level per clock cycle, the test was set up by generating both an increment and a decrement of one level at the input of the filter. Note that this voltage step is seen at the opamp outputs on the integrating phase of operation for both opamps (Φ_2 for opamp 1 and Φ_1 for opamp 2). The input clock was slowed by a factor of 4 so that the true output voltage could be determined, then the difference between this voltage and the actual output voltage at the end of the true time interval of Φ_2 (or Φ_1) was taken and divided by the magnitude of the voltage step to ascertain the error. The settling test results enumerated in Table 6.9 are for the worst case (high or low) transition.

Although the settling resolution was slightly lower than 18 bits for the worst case corner, it was decided that these results were acceptable for appropriate operation of

192

Opamp	Corner	Settling Error	Bits Settling Resolution(Bits)
1	Typical	Sim. Numerical Res.	20+
2	Typical	Sim. Numerical Res.	20+
1	Slow, -40°C	Sim. Numerical Res.	20+
2	Slow, -40°C	$5.4 \cdot 10^{-6}$	17.5
1	Fast, 110°	Sim. Numerical Res.	20+
2	Fast, 110°	$2.7 \cdot 10^{-6}$	18.5

Table 6.9: Settling Performance for DCT/CDS Postfilter

the opamp, resulting in negligible distortion due to settling errors.

6.2.4 Final Noise Calculations

Using the noise equations given in the previous chapter, along with the final transistor design values, the component noise contribution of the analog postfilter was determined. Note that a typical AC noise simulation cannot be performed on a switched-capacitor circuit and is instead performed on the RC-equivalent version of the postfilter. Since the DCT technique has no direct RC analogue, the noise contribution of the filter must be calculated.

$$\overline{V_{n,T}}^2 = 2 \cdot \left(\frac{2 \cdot 45.37MHz}{6.144MHz} \cdot \frac{4kT \cdot (20000Hz)}{\sqrt{2\mu_p C_{ox} \frac{30\mu m}{1\mu m} (22.27\mu A)}} \left[1 + \sqrt{\frac{\mu_n \frac{14\mu m}{8\mu m}}{\mu_p \frac{30\mu m}{1\mu m}}} \right] \cdots \right.$$

$$\left. + \frac{2 \cdot 43.47MHz}{6.144MHz} \cdot \frac{4kT \cdot (20000Hz)}{\sqrt{2\mu_p C_{ox} \frac{60\mu m}{1\mu m} (44.53\mu A)}} \left[1 + \sqrt{\frac{\mu_n \frac{28\mu m}{8\mu m}}{\mu_p \frac{60\mu m}{1\mu m}}} \right] \right) = 1.481 \cdot 10^{-10} V^2 \quad (6.8)$$

$$\overline{V_{n,1/f}}^2 = \frac{2k_p \int_{20}^{20000} \frac{1}{f^{1.2828}} \delta f}{4 \cdot (60\mu m)(1\mu m)C_{ox}} + \frac{2k_n \int_{20}^{20000} \frac{1}{f^{0.8824}} \delta f}{4 \cdot (28\mu m)(8\mu m)C_{ox}} \cdot \frac{(246 \cdot 10^{-6})^2}{(458 \cdot 10^{-6})^2} = 0.253 \cdot 10^{-10} V^2 \tag{6.9}$$

where $k_p = 1.184 \cdot 10^{-23} V^2 F$, $k_n = 3.454 \cdot 10^{-24}$

Recalling the result for switched capacitor noise from the previous chapter, which remains the same:

$$\overline{V_{n,kT/C}}^2 = 4.492 \cdot 10^{-10} V^2 \tag{6.10}$$

Bringing the total component noise power to:

$$\overline{V_{n,Total}}^2 = 6.226 \cdot 10^{-10} V^2 \tag{6.11}$$

The quantization noise power from the digital circuitry is:

$$\overline{V_{n,\Sigma\Delta}}^2 = \left(\frac{\frac{3.25V}{2\sqrt{2}}}{10^{\frac{98.36}{20}}} \right)^2 = 1.93 \cdot 10^{-10} V^2 \tag{6.12}$$

Despite the derivation done in Chapter 3, the jitter noise is assumed to be negligible, considering that the 1ns rms clock period variation was a worst case figure over many process runs.

The noise from the digital voltage reference is known and is given by:

$$\overline{V_{n,Reference}}^2 = 0.73 \cdot 10^{-10} V^2$$

The total noise of the circuit is thus:

$$\overline{V_{n,Circuit}}^2 = 8.886 \cdot 10^{-10} V^2$$

194

For a signal swing of 3.25Vpp, this results in **SNR=91.72dB**

6.2.5   Final Power and Area Calculation Results

In order to obtain the total power and area consumption of the circuit on the analog die, the contributions of the individual sections described in this report are summed:

Power

Sigma Delta: 0.3572mW

DWA: 0.1397mW

Clock Circuitry: 0.1290mW

Analog Postfilter: 1.600mW (as implemented)

Total: **2.223mW**

Area

Sigma Delta: $0.0363mm^2$

DWA: $0.0257mm^2$

Clock Circuitry: Negligible

Analog Postfilter: $0.125mm^2$

Total: $\mathbf{0.187mm^2}$

Chapter 7

Conclusion

7.1 Summary

A low-power, low area oversampling converter for audio bandwidth applications has been designed in a $0.25\mu m$ CMOS process. The previous discussion in this paper centered on strategies and techniques to maximize the noise budget available to the analog postfilter, where the area-power-noise tradeoff is severe. First, it was shown that it was important to place major gain blocks in the D/A converter towards the beginning of the chain. Second, it was shown that the number of stages in the digital upsampling filter scheme must be minimized in order to avoid introducing in-band quantization noise. Third, it was shown that a multibit sigma delta modulator running at a high oversampling ratio was necessary in order to guarantee the removal of noise shaper quantization noise from the signal band.

A survey of several D/A converter topologies was then presented, describing the merits and demerits for each. A brief analysis for each candidate architecture showed that, given the objectives and requirements of this project, a switched-capacitor D/A converter using dynamic element matching was best suited to achieve the noise specification with low power and area consumption. A brief summary of DEM techniques

was presented and the data weighted averaging (DWA) technique, a simple DEM algorithm that also provides first-order mismatch noise shaping, was introduced.

The switched-capacitor technique known as Direct Charge Transfer was introduced and examined, showing its robustness, parasitic insensitivity, noise performance, and compatibility with autozeroing techniques that significantly reduce the 1/f opamp noise. A hand design was performed in parallel on both a traditional biquad switched-capacitor filter and a switched-capacitor DCT filter. It was shown that the for the same noise performance, the DCT filter achieved a power-area product under half of what a biquad filter could achieve.

Finally, transistor-level implementations of both the digital and analog circuitry were designed and were shown to function properly over a range of process and temperature corners.

7.2 Recommendations for Further Investigation

This section discusses a few areas of interest that are of relevance to this project, but because of time constraints were left outside the scope of this document.

One item that deserves particular attention is the lack of an analog equivalent of the DCT switched-capacitor technique. Whereas traditional switched-capacitor structures are well approximated as continuous-time resistors (either positive or negative) provided that the oversampling ratio of the circuit is high enough, no such convenient approximation exists for a DCT switching structure. As described previously, this would simplify noise and AC transfer function analysis for the switched-capacitor postfilter.

The DCT postfilter was also implemented as a cascade of two first-order sections, resulting in two key disadvantages. First, such a cascade results in considerable pass-band droop that must be compensated for elsewhere in the D/A converter chain, most likely in the digital interpolation filters. Second, the filter does not have a high pass transfer function from the inputs of the second opamp to the filter output. Since the output of the second opamp cannot be sampled (it is the DT-CT interface), the effectiveness of the correlated double sampling technique in rejecting opamp 1/f noise is effectively halved. If a multiple-order DCT filter could be made to feed back to previous stages, perhaps these two problems could be avoided while also enjoying the power and area advantage provided by the DCT technique.

Bibliography

[1] H. Nyquist, "Certain Topics in Telegraph Transmission Theory," in *AIEE Trans.*, pp. 617-644, 1928.

[2] M. Gustavsson, J. J. Wikner, and N. N. Tan, *CMOS Data Converters for Communications*, Kluwer Academic Publishers, Boston, MA, 2000.

[3] D. A. Johns, K. Martin, *Analog Integrated Circuit Design*, John Wiley and Sons, New York, 1997.

[4] A. V. Oppenheim, R. W. Schafer, and J. R. Buck, *Discrete-Time Signal Processing*, 2nd Edition, Prentice Hall, Englewood Cliffs, NJ, 1998.

[5] K. Falakshahi, C-K.K.Yang, B.Wooley, "A 14-bit, 10-Msamples/s D/A Converter Using Multibit Sigma-Delta Modulation," in *IEEE J. of Solid State Circuits*, vol. 34, pp. 607-615, May 1999.

[6] J. L. Gonzalez and E. L. Alarcon, "Clock-Jitter Induced Distortion in High Speed CMOS Switched-Current Segmented Digital to Analog Converters," in *IEEE Symp. Circuits Systems*, vol. 1, pp. 512-515, 2001.

[7] M. Shinagawa, Y. Azakawa, and T. Wakimoto, "Jitter Analysis of High-Speed Sampling Systems," in *IEEE J. of Solid State Circuits*, vol. 25, pp. 220-224, Feb. 1990.

[8] M. Pelgrom, A. Duimmaijer, and A. Welbers, "Matching Properties of MOS transistors," in *IEEE J. Solid State Circuits,* vol. 24, pp. 1433-1439, October 1989.

[9] B. Blesser, "Digitization of audio: A comprehensive examination of theory, implementation, and current practice," in *J. Audio Eng. Society,* vol. 26, no. 10, pp. 739-771, October 1978.

[10] W. Sansen and K. Laker, UC Berkeley Extension Class Notes, Fall 2001.

[11] W.R. Bennett, "Spectra of Quantized Signals," in *Bell System Technical J. ,* vol.27, pp. 446-472, 1948.

[12] K. Nguyen, R. Adams, and K. Sweetland, "A 113dB SNR Oversampling Sigma-Delta DAC for CD/DVD Application," in *IEEE Trans. Consumer Electronics,* vol. 44, pp. 1019-1023, August 1998.

[13] S. Norsworthy, R. Schreier, and G. Temes, *Delta-Sigma Data Converters*, IEEE Press, Piscataway, NJ, 1997.

[14] R.M. Gray, "Quantization Noise Spectra," in *IEEE Trans. Information Theory,* vol.36, issue 6, pp. 1220-1244, November 1990.

[15] W.L. Lee and C. Sodini, "A Topology for Higher Order Interpolative Coders," in *ISCAS Digest,* pp. 459-462, 1987.

[16] D. Anastassiou, "Error Diffusion Coding for A/D Conversion," in *IEEE Trans. Circuits Systems,* vol. 36, no. 9, pp. 1175-1186, September 1989.

[17] I. Fujimori and T. Sugimoto, "A Multibit Delta-Sigma Audio DAC with 120-dB Dynamic Range," in *IEEE J. Solid State Circuits,* vol. 35, pp. 1066-1073, August 2000

[18] H.W. Paik and T.W. Grablander, "FIR Compensation Filter for the Zero Order Hold D/A Converter Using the Frequency Sampling Method", in *Proceedings of the 37th Midwest Symposium on Circuits and Systems*, vol. 2, pp. 1006-1009, 1994.

[19] T.W. Parks and J.H. McClellan, "A program for the Design of Linear Phase Finite Impulse Response Filters," in *IEEE Trans. Audio Electroacoustics,* vol. AU-20, no. 3, pp. 195-199, August 1972.

[20] J.F. Kaiser, "Nonrecursive Digital Filter Design Using the I_0-Sinh Window Function," in *IEEE Symp. on Circuits and Systems,* vol. 1, pp. 20-23, April 1974.

[21] D. Wouter, J. Groeneveld, H.J. Schouwenaars, H.A.H. Termeer, and C.A.A. Bastiaansen, "A Self-Calibration Technique for Monolithic High-Resolution D/A Converters," in *IEEE J. Solid State Circuits,* vol. 24, pp. 1517-1522, December 1989.

[22] R. Baird and T. Fiez, "Linearity Enhancement of Multibit Delta-Sigma A/D and D/A Converters Using Data Weighted Averaging," in *IEEE Trans. on Circuits and Systems - II Analog and digital Signal Processing,* vol. 42, pp. 753-762 , December 1995.

[23] T. Kwan, R. Adams, and R. Liebert, "A Stereo Multibit $\Sigma\Delta$ DAC with Asynchronous Master-Clock Interface," in *IEEE J. Solid-State Circuits,* vol. 31, pp. 1881-1887, December 1996.

[24] P. Rombouts and L. Weyten, "A Study of Dynamic Element-Matching Techniques for 3-Level Unit Elements," in *IEEE Trans. on Circuits and Systems - II: Analog and Digital Signal Processing,* vol. 47, pp. 1177-1187, no. 11, November 2000.

[25] R.W.Gregor, "On the Relationship Between Topography and Transistor Matching in an Analog CMOS Technology," in *IEEE Trans. on Electron Devices* vol. 39, no. 2, pp. 275-282, February 1992.

[26] D.K. Su and B.A. Wooley, "A CMOS Oversampling D/A Converter with a Current-Mode Semidigital Reconstruction Filter," in *IEEE J. Solid State Circuits,* vol. 28, pp. 1224-1233, December 1993.

[27] L. Jackson, *Digital Filters and Signal Processing*, 2nd ed. Boston: Kluwer 1990.

[28] C.C. Enz and G.C. Temes, "Circuit Techniques for Reducing the Effects of Op-amp Imperfections: Autozeroing, Correlated Double Sampling, and Chopper Stabilization," in *Proc. IEEE,* vol. 84, pp. 1584-1614, November 1996.

[29] J.H. Fischer, "Noise Sources and Calculation Techniques for Switched Capacitor Filters," *IEEE J. Solid State Circuits*, vol. SC-17, no. 1, pp. 742-752, August 1982.

[30] U-K.Moon, J.Silva, J.Steensgaard, and G.Temes, "A Switched-Capacitor DAC with Analog Mismatch Correction," *IEEE Symp. Circuits Systems,* vol. 1, pp. 421-424, 2000.

[31] J. Steensgaard, U-K. Moon, G. Temes, "Mismatch-Shaped Pseudo-Passive Two-Capacitor DAC," in *Conference Proceedings for the 1999 IEEE Alessandro Volta Workshop on Low Power Design (VOLTA '99), held March 4-5, 1999 in Como, Italy*

[32] J. Rabaey, *Digital Integrated Circuits: A Design Perspective*, 1st ed.,New Jersey: Prentice Hall 1996.

[33] I. Fujimori and T. Sugimoto, "A 1.5V, 4.1mW dual-channel audio delta-sigma D/A converter,"in *IEEE J. Solid State Circuits,* vol. 32, pp. 933-942, July 1997.

[34] P.W. Bosshart, "A Multiplexed Switched Capacitor Filter Bank," in *IEEE J. Solid State Circuits,* vol. 15, pp. 939-945, December 1980.

[35] N.S. Sooch, J.W. Scott, T. Tanaka, T. Sugimoto, C. Kubomura, "18-b stereo D/A Converter with Integrated Digital and Analog Filters," presented at the 91st AES Convention, October 1991.

[36] O.J.A.P. Nys and R.K. Henderson, "An Analysis of Dynamic Element Matching Techniques in Sigma-Delta Modulation,"in *IEEE Symp. Circuits Systems,* vol. 1, pp. 231-234, 1996.

[37] R. Radke, A. Eshraghi, and T. Fiez, "A 14-bit Current-Mode Sigma-Delta DAC Based Upon Rotated Data Weighted Averaging," in *IEEE J. of Solid State Circuits*, vol. 35, pp. 1074-1084, August 2000.

[38] M. Vadipour, "Techniques for Preventing Tonal Behavior of Data Weighted Averaging Algorithm in Sigma Delta Modulators," in *IEEE Trans. on Circuits and Systems II: Analog and Digital Signal Processing*, vol. 47, no. 11, pp. 1137-1144, November 2000.

[39] T. Shui, R. Schreier, and F. Hudson, "Mismatch Shaping for a Current-Mode Multibit Delta-Sigma DAC,"in *IEEE J. of Solid State Circuits*, vol. 34, pp. 331-338, March 1999.

[40] D. Su, "Oversampling Digital-to-Analog Conversion," Ph.D dissertation, Stanford Univ., August 1994.

[41] C.C. Enz and G. Temes, "Circuit Techniques for Reducing the Effects of Op-Amp Imperfections," *Proceedings of the IEEE*, vol. 84, no. 11, pp. 1584-1614, November 1996.

[42] U. Chilakapati, T.S. Fiez, "Effect of Switch Resistance on the SC Integrator Settling Time," in *IEEE Trans. Circuits Systems-II Analog and Digital Signal Processing*, vol. 46, no. 6, pp. 810-816, June 1999.

[43] K. Martin, A.S.Sedra, "Effects of the Op Amp Finite Gain and Bandwidth on the Performance of Switched-Capacitor Filters," in *IEEE Trans. Circuits Systems*, Vol. CAS-28, pp. 822-829, August 1981.

[44] Y. Huang, G.C.Temes, P.F.Ferguson, "Reduced Nonlinear Distortion in Circuits with Correlated Double Sampling," in *IEEE Symp. Circuits and Systems*, vol.1, pp. 159-162, 1996.

[45] F. Wang, R. Harjani, "Power Analysis and Optimal Design of Opamps for Over-sampled Converters," in *IEEE Trans. Circuits Systems,* vol. 46, pp. 359-369, April 1999.

[46] M. Sarhang-Nejad, G.C.Temes, "A High Resolution Multibit $\Sigma\Delta$ ADC with Digital Correction and Relaxed Amplifier Requirements,"in *IEEE J. Solid-State Circuits,* vol. 28, no. 6, pp. 648-660, June 1993.

[47] H. Recoules, R. Bouchakour, P. Lourneau, "A Comparative Study of two SC-CMFB networks used in fully differential OTA," in *IEEE Int'l Conference on Electronics, Circuits, and Systems,* vol. 2, pp. 291-294, 1998.

[48] D.G.Haigh and B.Singh, "A Switching Scheme for Switched-Capacitor Filters which Reduced the Effect of Parasitic Capacitances Associated with Switch Control Terminals, in *IEEE Symp. Circuits Systems,* vol. 1, pp. 586-589, May 1993.

[49] K. Laker and W. Sansen, *Design of Analog Integrated Circuits and Systems,* McGraw Hill Publishers, 1994.